POLITECNICO DI MILANO

Scuola di Ingegneria Industriale e dell'Informazione

Tesi di Laurea Magistrale in Ingegneria Chimica

Dipartimento di Chimica, Materiali e Ingegneria Chimica

"Giulio Natta"

HYDROGELS SYNTHESIS FROM NANOPARTICLES AGGREGATION

Relatore: Prof. Davide MOSCATELLI

Correlatori: Ing. Filippo ROSSI

Ing. Claudio COLOMBO

Tesi di laurea di:

Laura GALLETTI Matr. 799488

Maddalena LEPRI Matr. 798724

Anno accademico 2013 – 2014

Index

Figure index

Equation index

Table index

Sommario

L'ingegneria tissutale rappresenta una valida prospettiva nel campo della medicina, in quanto consente la rigenerazione di organi e tessuti malati laddove la medicina tradizionale si limiterebbe alla semplice riparazione o sostituzione. Essa realizza sostituti biologici tramite l'utilizzo di cellule in grado di formare tessuti di diversa natura, seminate su una matrice, naturale o sintetica, che funga da supporto per la crescita, la proliferazione e/o il differenziamento delle stesse. La componente cellulare è prelevata dal soggetto, espansa e fatta differenziare *ex vivo,* ed inserita in una matrice tridimensionale, che prende il nome di scaffold, con la funzione di sostituire temporaneamente la matrice extracellulare naturale (ECM).

Lo scaffold deve permettere la creazione di un microambiente che contribuisca alla sopravvivenza e allo sviluppo del fenotipo cellulare. Recenti studi hanno dimostrato, infatti, che l'identità della cellula non è determinata soltanto dal suo genoma ma è anche influenzata dalla matrice extracellulare, da fattori di crescita, ormoni e altre molecole che regolano la formazione e la funzionalità dei tessuti. E' infatti l'ambiente extracellulare che, permettendo la trasmissione di segnali intracellulari a cascata, influenza il fenotipo cellulare, regolandone l'espressione genica e proteica [1]. È stato dimostrato che soltanto una struttura tridimensionale permette la riproduzione di un microambiente che presenti le proprietà meccaniche e biochimiche peculiari dell'ECM.

In questo contesto, una delle principali sfide dell'ingegneria tissutale, e obiettivo di questo lavoro, è quella di ricercare un materiale che soddisfi specifici requisiti. Esso deve necessariamente essere biocompatibile, in quanto la sua azione deve essere svincolata da qualsiasi effetto collaterale indesiderato. Deve inoltre essere biodegradabile in modo da lasciare spazio alla matrice extracellulare neo sintetizzata dopo l'impianto *in vivo*.

Deve consentire, infine, il trasporto per via diffusiva di nutrienti, ossigeno, metaboliti e altre molecole indispensabili alla sopravvivenza delle cellule.

Quest'ultimo requisito rappresenta una delle principali limitazioni nella realizzazione di matrici di supporto, ma recenti sviluppi nel campo del drug delivery hanno portato alla formulazione di nuove tecnologie con alte potenzialità di rilascio del principio attivo al sito d'azione in modo mirato e controllato, minimizzando gli effetti collaterali. In questa ottica nanoparticelle (NPs) e idrogeli rappresentano materiali di grande interesse.

Il presente studio propone l'utilizzo di idrogeli sintetizzati per aggregazione di nanoparticelle come biomateriali destinati alla formazione di tessuti ingegnerizzati per cell housing e rilascio controllato di farmaci. Gli idrogeli presentano un network tridimensionale strutturato in grado di assorbire grandi quantità di acqua e soluti idrofilici. Inoltre, un equilibrio ottimale tra proprietà meccaniche, indispensabili per la migrazione e differenziazione delle cellule, e biodegradabilità, necessaria per lasciare spazio alla crescita delle cellule e all'infiltrazione di vasi sanguigni, contraddistingue questi materiali. La sintesi a partire da nanoparticelle allarga la gamma di potenziali applicazioni, infatti, le molecole idrofobe, tendenzialmente incompatibili con la matrice idrofilica degli idrogeli, possono essere caricate sulle particelle che sono successivamente aggregate in macrostrutture [2].

Al fine di ottenere le proprietà sopra citate, sono stati indagati idrogeli a partire da due diversi monomeri: il metilmetacrilato e l'ε-caprolattone.

Nella prima parte dello studio, lattici di nanoparticelle di polimetilmetacrilato (PMMA) sono stati sintetizzati sfruttando l'azione di tre agenti stabilizzanti: sodio dodecilsolfato (SDS), sale 3-sulfopropilmetacrilato di potassio (HEMA-SO_3-) e Polisorbato 80 (Tween 80). È inoltre stato analizzato il processo di aggregazione di nanoparticelle per gelazione DLCA (Diffusion Limited Cluster Aggregation) e l'influenza del tensioattivo su di esso.

La non biodegradabilità del PMMA è stata superata tramite l'utilizzo, nella seconda parte del lavoro, di nanoparticelle biodegradabili di poli-HEMA-poli-ε-caprolattone (HEMA-PCL_3).

Tali nanoparticelle sono state sintetizzate utilizzando agenti stabilizzanti ionici che, grazie alla loro capacità di co-polimerizzare con il macromonomero di HEMA-poli-ε-caprolattone, conferiscono cariche fisse superficiali. Due agenti stabilizzanti con cariche opposte sono stati utilizzati: cloruro di 2-metacrilossietiltrimetilammonio (HEMA-Ch+), carico positivamente, e sale 3-sulfopropilmetacrilato di potassio (HEMA-SO_3-), carico negativamente. La carica superficiale opposta ha permesso di ottenere un gel per aggregazione elettrostatica di nanoparticelle, senza la formazione di legami covalenti, ritenuti troppo forti per le cellule.

Gli idrogeli di HEMA-PCL_3 sono stati caratterizzati al fine di valutarne le proprietà di swelling, degrado, citocompatibilità e rilascio controllato. In prospettiva delle applicazioni sopra menzionate, tali proprietà risultano indispensabili per la creazione di un materiale ingegnerizzato (Figure I) che non si limiti a essere tollerato dal corpo umano ma sia in grado di interagire dinamicamente con esso.

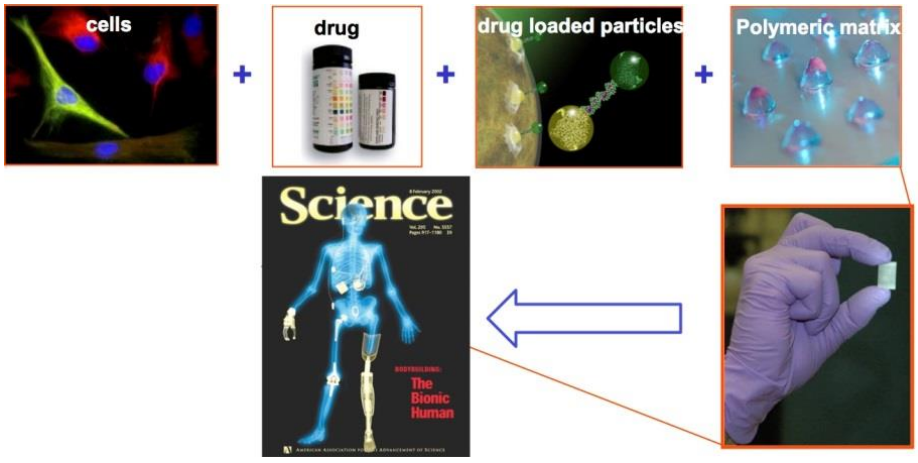

Figure I: Enginereed materials for tissue regeneration.

Abstract

Tissue engineering represents a valid perspective in medicine, since it allows organs and injured tissues regeneration, where traditional medicine would simply restore or substitute them. Tissue regeneration occurs thanks to biological substitutes realized by seeding cells on a matrix, natural or synthetic, that operates as a support for growth, proliferation and/or differentiation of the cell population. Cell component is collected from the patient, expanded and differentiated *ex vivo,* and inserted into a three-dimensional matrix, referred to as scaffold, that temporarily replaces the natural extracellular matrix (ECM).

The scaffold should be able to create a microenvironment that contributes to cells survival and phenotype development. Indeed, recent studies revealed that cell identity is not only determined from its genome but it is also influenced by the extracellular matrix, by soluble growth factors, hormones and other molecules that regulate tissues formation and functionality. The extracellular environment, orchestrating an intracellular signaling cascade, is responsible of gene and protein expression. A three-dimensional matrix has been proven as the only structure that allows the recreation of a microenvironment with the peculiar mechanical and biochemical properties of ECM.

In this frame, one of the main challenges of tissue engineering, and aim of this work, is to seek a material that can satisfy specific requirements. It must be biocompatible, indeed its action should prevent undesired side effects. Moreover, it must be biodegradable in order to leave sufficient space for the newly synthesized extracellular matrix after the *in vivo* implantation. Finally, it must allow the diffusive transport of nutrients, oxygen, metabolites and other molecules essential for cells survival.

The latter requirement represents one of the main obstacles to the fabrication of support matrixes, but recent developments in drug delivery brought to the formulation of new technologies with high potential in targeted and controlled delivery, in order to minimize the side effects. Therefore, nanoparticles (NPs) and hydrogels represent interesting materials for such purposes.

This work is focused on hydrogels synthesized from nanoparticles aggregation; they can be used as biomaterials to form engineered tissues for cell housing and controlled drug delivery. Hydrogels present a three-dimensional network able to absorb large amounts of water and hydrophilic solutes. Moreover, an optimal equilibrium between mechanical properties, needed for migration and differentiation of cells, and biodegradability, necessary for cells growth and blood vessels infiltration, distinguishes these materials. The synthesis from nanoparticles extends the potential applications range, indeed hydrophobic molecules, by nature not compatible with the hydrophilic matrix of hydrogels, can be loaded into the particles that are organized in macrostructures. Such peculiar property make the NPs-based hydrogels attractive materials also for drug delivery.

To obtain all the above-mentioned properties, hydrogels made of two different monomers have been investigated. The first monomer is methyl(methacrylate), and the second is ε-caprolactone.

In the first part of this work, nanoparticles latexes of poly-methyl(methacrylate) (PMMA) have been synthesized employing three different stabilizing agents: sodium dodecyl sulfate (SDS), 3-Sulfopropyl methacrylate potassium salt (HEMA-SO_3-) and Polysorbate 80 (Tween 80). Furthermore, the aggregation process from nanoparticles through DLCA (Diffusion Limited Cluster Aggregation) gelation has been analyzed, focusing on the influence of the stabilizing agents.

In the second part of the work, non-biodegradability of PMMA was overcome by using biodegradable nanoparticles of poly-HEMA-poly- ε-caprolactone (HEMA-PCL_3).

The synthesis of these nanoparticles was carried out with ionic stabilizing agents that were able to co-polymerize with HEMA-poly-ε-caprolactone macromonomer, thanks to their carbon double bond. Thus, they could provide stable superficial charges to the NPs.

Two oppositely charged stabilizers have been used: [2-(Methacryloyloxy)ethyl]trimethylammonium chloride (HEMA-Ch+), positively charged, and 3-Sulfopropyl methacrylate potassium salt (HEMA-SO_3-), negatively charged. The superficial opposite charge allows aggregation via electrostatic interaction of nanoparticles, avoiding covalent bonding, which is considered too strong for cells.

Afterwards, HEMA-PCL_3 hydrogels have been characterized in order to evaluate swelling, degradation, cytocompatibility and controlled release properties. In the outlook of the above-mentioned applications, those properties are essential for the fabrication of an engineered material able to interact dynamically with the human body.

Chapter 1

Introduction

Traumatic injuries, cancer treatment, and congenital abnormalities are often cause of total or partial loss of organs functionalities. Restoration of normal structure and function often requires surgical transfer of natural tissue from an uninjured location elsewhere in the body or transplantation [1].

Conventional therapies offered by traditional medicine, although remarkable developments have been made to improve the procedures, show significant limitations which reduce their applicability and efficacy. Surgical transfer, for example, is limited by availability, adequate blood supply, and secondary deformities at the donor site. Similarly, transplantation, despite the increased number of successful operations, still presents several problems that reduce its potential use. The ever-growing request cannot be satisfied, although the increasing availability of donors, as registered by UNOS data (United Network for Organ Sharing) that reveal a mortality rate among patients waiting for transplantation of about 15 per day (2009) [2]. Moreover, rejection risk can arise undesired side effects, which require further therapies with sometimes catastrophic consequences, such as immune deficiency, thromboembolism or hemorrhage, that may lead to the necessity of another transplantation.

Last but not least, the damage or injury of some tissues or organs, such as skin, cartilage and spinal cord [3], has proven to be too debilitating and difficult to repair effectively and permanently with conventional techniques [4].

Such limitations open the door to a radically new concept for the treatment of disease and injury, that is represented by tissue engineering. It involves multidisciplinary knowledge regarding molecular and cell biology, medicine and material science aimed to the regeneration of human body tissues made by its own cells.

New tissue formation is induced by activated cells seeded with growth factors and nutrients inside three-dimensional macrostructures that reproduce their natural environment, in order to favor their adhesion and proliferation and the creation, *ex vivo* or *in vivo*, of functional tissues or organs.

The introduction chapter deals with tissue engineering and drug delivery challenges and the role of nanoparticles-based hydrogels as promising materials in this perspective. Hydrogels and nanoparticles properties and the synthesis strategies used to obtain these materials are described in the following.

1.1 Tissue engineering

Tissue engineering is a branch of regenerative medicine whose aim is the substitution or regeneration of cells, tissues or organs, to restore or establish a normal function. More specifically, tissue engineering develops an integrated living tissue constituted by cells combined with biomaterials and growth factors.

The term “tissue engineering”, used for the first time in 1988 by the National Science Foundation, refers to a multidisciplinary field whose goal is to realize biological substitutes containing living and functional cells, for the regeneration, maintenance and improvement of tissues functions [5]. Generally, a tissue-engineered material consists of a cell component and a supporting matrix, which can be synthetic (polymeric) or natural.

The cell component is generally made of autologous cells for their characteristic of immuno-compatibility with the patient that should eliminate the risk of rejection. In particular, the scientific interest is focused on stem cells for their potential of differentiation and proliferation [6]. Cells, producing extra-cellular material, enhance the interaction with the target tissue and regenerate it.

Cells are collected from the patient, expanded and differentiated *ex vivo,* and then seeded inside a scaffold material which substitutes the mechanical functions of the extra-cellular matrix (ECM). After the implant of the engineered tissue in the patient, the scaffold gradually degrades, so newly synthesized ECM can take its place. The basic steps of a tissue engineering procedure are schematically represented in Figure 1.1.

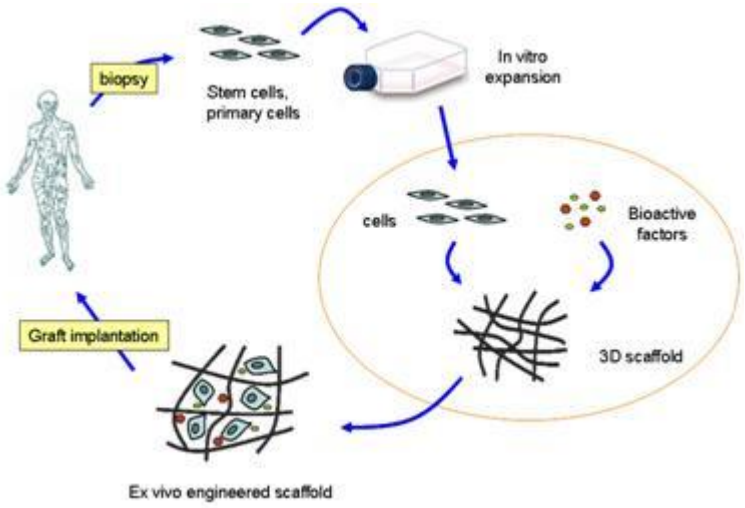

Figure 1. 1: Basic principles of tissue engineering.

The scaffold is a three-dimensional biomaterial that acts as mechanical supporting matrix for cell populations. It reproduces the extra-cellular environment to promote growth, proliferation and differentiation of cells.

The synthesis of a proper scaffold material is one of the main challenges of tissue engineering because of the numerous combined properties it must present.

Scaffold needs to be biocompatible, biodegradable and to promote a favourable environment for cells survival. Indeed, scaffold characteristics have to face diffusive transport limitations of nutrients and oxygen, that are necessary for cells life. Meanwhile, its three-dimensional structure should promote cell-cell and cell-ECM interactions reproducing *in vivo* environment, in contrast to 2D structure that cannot re-create it [7].

In practice, the addition of cells to porous scaffolds is often inadequate to obtain sufficient tissue functions. The attempts in this sense are focused on reproducing both the microarchitecture of the tissues and the microenvironment of the surroundings of the cells within the body.

The *in vivo* tissues are constituted of small repeating units on the scale of a hundred of microns. In this three-dimensional microarchitecture multicellular processes and integration with other organ systems are coordinated through a microcirculation network, while in the local microenvironment, the presence of biochemical, cellular and physical stimuli, contribute to regulate cellular fate processes such as differentiation, proliferation, migration and apoptosis [8].

Thus, a successful biomaterial synthesis should mimic an appropriate environment for cell viability and function at the micro-scale level, but it should also provide for those properties at the macro-scale level that favour the coordination of multicellular processes and guarantee an adequate nutrient supply and mechanical strength, similarly to what occurs in native cellular microenvironment.

In conclusion, engineered materials not only need to be tolerated by the human body, avoiding the risk of rejection, but they also need to interact dynamically and specifically with the site where they have been implanted.

Hydrogels, with their structural similarity to ECM, are promising alternative as tissue engineering materials. More details on this regard are explained in the following paragraphs.

1.2 Drug delivery

The aim of drug delivery systems is to deliver drugs to target sites that need pharmacological action. This field includes all the technologies involved in drug preparation, route of administration, site targeting, metabolism and toxicity. The challenge from a chemical engineering point of view is to design a material whose properties permit the controlled release of a drug in a target site.

Conventional formulations provide immediate release of the drug without controlling delivery rates. To maintain the concentration of drug in the plasma within the desired range that makes the therapy effective, most of the times several doses are needed every day. This arises the risk of under or over-dosage of the drug. Indeed, as can be observed from Figure 1.2, an immediate release results in fluctuations of drug plasma concentration and it can be below the minimum effective concentration (MEC) or above the minimum toxic concentration, thus invalidating the therapy or in worst cases compromising the health of the patient. Hence, the importance of controlled release systems arises [9].

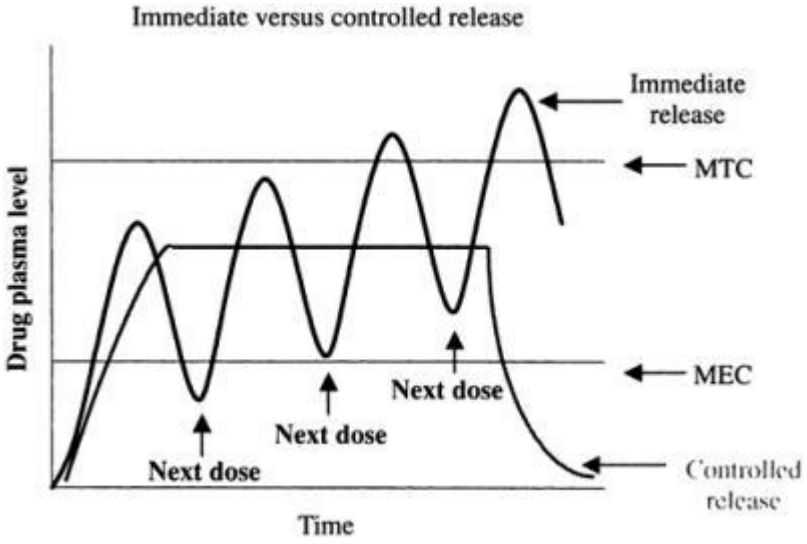

Figure 1. 2: Immediate versus controlled release. Drug plasma concentration in y-axis related to time in x-axis.

The following paragraphs explain why hydrogel, and specifically hydrogel made from nanoparticles, are a promising perspective for both tissue engineering and drug delivery applications.

1.3 Why hydrogels?

In recent years, hydrogels have been a challenging technology in human health care. Pharmaceutical industries are interested in tuning structure, shape and surface properties to improve their applicability in tissue engineering and drug delivery systems [10].

Hydrogels are semisolids materials (Figure 1.3), made of a matrix, constituted by hydrophilic cross-linked polymers, and a solvent, water, immobilized into the matrix.

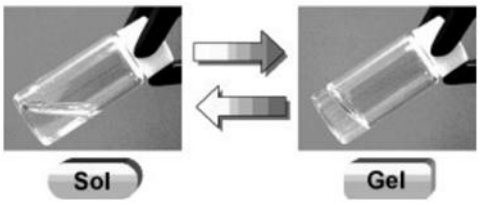

Figure 1. 3: Sol-gel transition.

Hydrogels are suitable materials for scaffold, indeed they can provide an appropriate environment for cells survival. Classic biomaterials, such as metals or ceramics, are widely used to replace the mechanical functions of tissues, but they are not able to re-create a suitable environment for cells. Hydrogels show many similar properties to the ECM and present fundamental properties to dynamically interact with cells. Cells identity is not only influenced by their own genome, but also by all the constituents, such as nutrients, hormones, proteins, present in the surrounding environment. Cell-ECM interactions are fundamental for cellular functions, such as adhesion, proliferation and differentiation.

Indeed, a proper extracellular environment should be able to transmit the intracellular signaling cascades that influence the phenotypic expression of cells.

Only a three-dimensional structure is able to provide and reproduce the typical biochemical and mechanical properties of ECM.

A stable cross-linked three-dimensional structure is essential to prevent polymeric chains dissolution in aqueous microenvironments. The solid reticulated matrix can be formed by chemical bonds or physical interactions (Figure 1.4). Chemical cross-linking creates covalent bonds between the reactive functional groups of polymeric chains, through different type of reactions: free chain polymerization, click reactions, reaction of Schiff bases and carbodiimide-mediated activation reactions. On the other hand, physical crosslinking exploits non-covalent interactions, such as ionic, van der Waals, electrostatic interactions, hydrogen bonding or hydrophobic interactions, to form a 3D structure. This work has been focused on physically cross-linked hydrogels since simple networks can be composed without the addition of chemical cross-linkers, usually toxic for cells. An optimal balance between mechanical strength and degradation should be present to provide both a structure able to resist to the mechanical stress of implantation and an efficient cellular microenvironment.

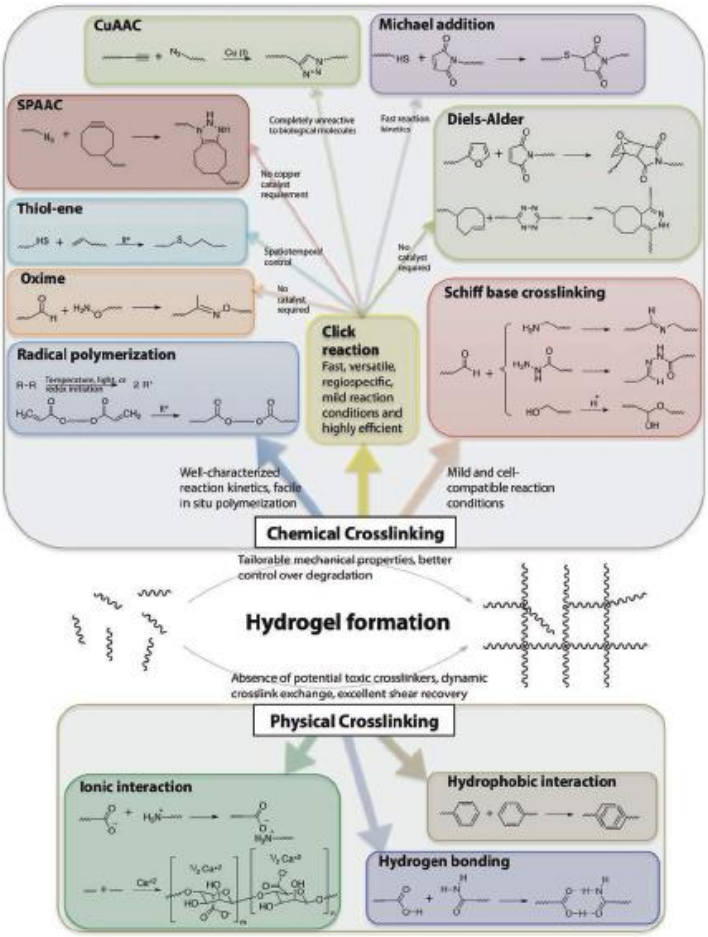

Figure 1. 4: Hydrogel formation techniques.

As stated by Flory-Rehner theory, the idealized network of a hydrogel is characterized by different structural parameters: mesh size, cross-linkage density, average molecular weight between two following crosslinked points and volume (Figure 1.5). The mesh size (ζ), the distance between sequential points of crosslink, is the open space accessible for drug or cell diffusion. The cross-linkage density (ν_e) represents the concentration of bonds between the chains and influences different properties of the hydrogels, such as elasticity, diffusivity, swelling behavior, mesh size and degradation. The effective molecular weight of the polymer chain between two following cross-linking points (Mc) depends on the degree of gel cross-linking and on the molecular weight of repeating monomer unit.

Hydrogels volume is highly variable, indeed they are able to retain water and to expand. The ability of enlarging their volume is correlated to hydrogels swelling capability.

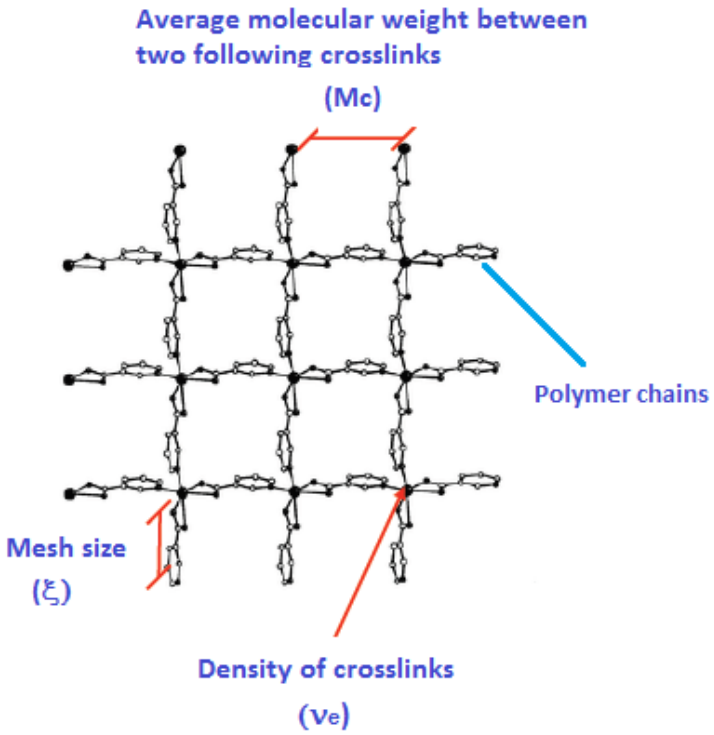

Figure 1. 5: Hydrogel reticulum.

The polymeric chains from which the hydrogels are synthetized highly influence this latter property. The hydrophilic nature of the functional groups present in the polymeric chains (-OH, -CONH, -$CONH_2$, -SO_3H) lends high swelling capability to the hydrogel, indeed it can retain large amounts of water (up to 90% of its original weight) increasing its volume. The water is able to fulfill the inner empty spaces of the gel and thanks to its mechanical and elastic properties the bonds can resist to the stress.

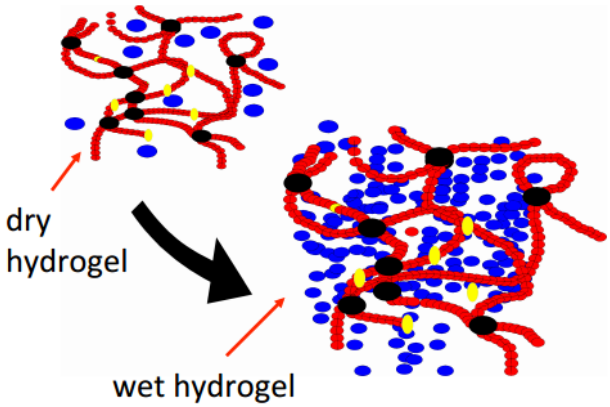

Figure 1. 6: Hydrogel swelling behaviour: dry to wet mass.

The hydration process of the dry hydrogel can be thermodynamically explained through the analysis of the chemical potential of the solvent, in this case water. When the dry gel is immersed, water presents a high tendency to enter inside the polymeric chains, since they are formed by hydrophilic groups. This behavior is caused by a drop of its chemical potential, indeed the fluid has a lower value of free energy than the pure liquid state.

Meanwhile, water's chemical potential inside the polymer is increased by the elastic response of the polymeric chains to the external fluid that is opposing to gel swelling. The swelling phase ends when the equilibrium between the chemical potential of the water inside and outside the hydrogel is reached: no more water is able to enter in it. If the cross-linking degree increases, the swelling capability of the gel decreases: a high density of bonds determines an enhancement of the elastic force applied on the fluid, so the equilibrium occurs at smaller quantities of absorbed water. The water inside the gel is not free to move but presents a reduced mobility due to the mechanical interaction with the polymeric structure and to the hydrogen bonds formed between water and hydrophilic groups [11].

Hydrogels can be classified as natural or synthetic. Natural hydrogels present a high biocompatibility degree and low toxicity and inflammation risks. They can provide a good cell adhesion, thanks to the superficial protein layers but they usually present insufficient mechanical properties and short degradation time. On the other hand, synthetic materials characteristics can be tuned and controlled. It is possible to design the material, changing its composition, chemical and mechanical properties, to increase cells transplantation and degradation capability. Functionalization of the hydrogel matrix is necessary to facilitate the integration with biological processes [7]. Biocompatibility is a key-property when hydrogels are used as cells scaffold or drug delivery systems. Indeed, the material has to maintain an appropriate cellular activity. Biocompatibility degree is associated to polymer's nature but also to the gelation technique, that can introduce cytotoxicity factors.

Another important property of hydrogels is biodegradability, that is their capability to degrade into physiological environment. If placed in a human tissue, hydrogels are able to degrade, so the growing tissue is able to replace the scaffold site. Hydrogels can degrade via ester hydrolysis, enzymatic hydrolysis and photolytic cleavage. Resorbable hydrogels are the ones that can dissolve in water, instead of stable hydrogels that do not present this property and should be stimulated to start the degradation process. Degradation is an essential parameter for drug release, indeed delivery kinetics are dictated by surface erosion or bulk degradation rates.

All the properties above-mentioned make hydrogels good materials also for Drug Delivery Systems (DDSs), indeed they are able to store and to release different substances, like nutrients or drugs, that are water soluble. Hydrogels capability of drug storage is important even if they are applied as cell scaffolds, indeed cells need nutrients to survive (Figure 1.7).

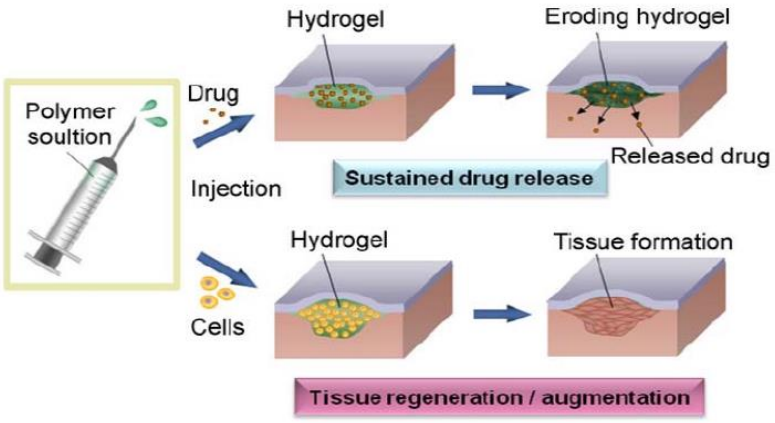

Figure 1. 7: Hydrogels for sustained drug release and tissue regeneration.

The molecular transport of substances is regulated by passive diffusion phenomena and explained by local concentration gradients (Fick Law). Indeed, molecules of small size can easily flow inside or outside hydrogels, respectively in storage or release periods.

Delivery studies divided drug release mechanisms from hydrogel as:

- Diffusion-controlled;
- Swelling-controlled;
- Chemically controlled.

Diffusion-controlled mechanism is influenced by elastic properties, porosity and density of the internal cross-links, so by the mesh sizes within the hydrogel matrix. Typical sizes of the internal canals of the hydrogel are larger than few nanometers, so they can easily contain almost all small-molecule drugs. Small molecules can be easily released: the process is diffusion-controlled because the flow of the particles is not retarded by hydrogel swelling. Thus, the swelling rate is faster than diffusion one.

Drug release is swelling-controlled when drug molecules diffusion is faster than hydrogel bonds elongation, that retard the diffusion process. In this case diffusion rate is faster.

Chemically-controlled release is due to chemical reactions occurring between the polymeric matrix and the loaded drug or to bonds breakage via degradation processes.

On the contrary, if molecules loaded in the hydrogel are larger than mesh sizes, they will accumulate mainly in the outer region of the structure so, at the beginning, drug release is very fast, but when the superficial drug is consumed, the delivery becomes extremely slow.

DDSs should release drugs in a targeted tissues or part of the human body, following a specific temporal and spatial manner. Hydrogel-based DDSs can be categorized as:

- Time-controlled systems;
- Stimuli-induced systems.

Time-controlled release is influenced by the own typical properties of the hydrogel, such as type of material, mechanical behavior, swelling and degradation capability. Otherwise the release mechanism is stimuli-induced, so the hydrogel delivers its content in response to physical or chemical conditions. These conditions should correspond to physiological requirements. Temperature, electricity, light, pressure, sound and magnetic field are physical stimuli, while pH, solvent composition and ions are chemical stimuli [12].

Moreover, hydrogels are usually easily deformable and can adapt to the shape of the surface where they are applied. Due to their dimensions, in the range of mm, they can remain *in loco*, minimizing the quantity of released drug that is spread around. Recent studies work to reduce some of their disadvantages: hydrogels are not always injectable, needing surgical implantation, and, due to their hydrophilic nature, have limited drug loading for hydrophobic molecules.
Hydrogels made by polymeric nanoparticles can overcome the latter limitation, as it will explained in the following paragraph [13].

1.4 Why hydrogels from nanoparticles?

Polymeric nanoparticles are colloidal systems of polymers, with at least one dimension in the nano-range, dispersed in water. Nanoparticles can carry a wide range of pharmaceutical active ingredients and they are able to retain big quantities of them, due to their high specific surface area (ratio between particle area and volume). The main purpose of the usage of nanomaterials is to promote the "targeted drug delivery", so to decrease the overall drug dose that is necessary to obtain the desired effect by maximizing the drug content in the target tissue.

Polymeric nanoparticles present appropriate prerequisites as drug delivery systems, indeed they show good properties of:

- Biocompatibility;
- Biodegradability;
- Drug incorporation and release;
- Biodistribution and targeting.

The choice between the polymeric matrix is made depending on therapeutic application, active ingredient characteristics, mechanical properties and biocompatibility. Biodegradable polymers are usually preferred because they are naturally expelled from the body. Polylactic acid (PLA), polyglicolic acid (PGA) or polycaprolactone (PCL) are the biodegradable polymers that typically constitute polymeric nanoparticles. All these three polymers are also biocompatible.

To be applied in the human body nanoparticles dimensions should be in a range between 30 and 250 nm.

Particles with a diameter bigger than 250 nm are opsonized by the immune system, on the contrary if the diameter is smaller than 30 nm particles are filtrated by the kidneys. Nanometric dimensions lend to the particles ease of application, indeed they can be injected with no need of medical surgery.

This advantage can be seen also as a limitation because nanoparticles can diffuse in non-diseased organs and tissues with potential side effects. Moreover, an overdosage raise the economic costs of therapies. Functionalization of nanoparticles surface can enhance targeting features, providing interactions with tissues and cells [14].

Drug delivery effectiveness is strictly influenced by the above-mentioned characteristics of the polymeric nanoparticles.

Drug has to be entrapped in nanoparticles and released preferentially in the targeted area. So the drug must be loaded in the nanoparticles and then delivered in a specific organ or tissue, increasing local drug concentration, and minimizing drug loss.

Release process can occur for different mechanisms:

- Diffusion-controlled: the diffusion process occurs faster than the degradation. The active ingredient is diffused through the macromolecular structure, then the polymeric matrix starts degrading decreasing its dimensions.

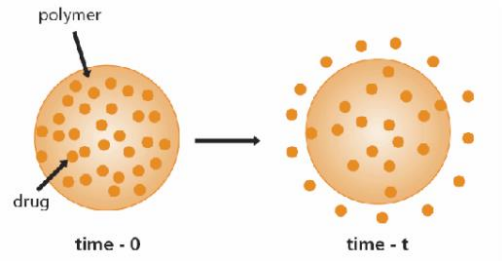

Figure 1. 8: Diffusion-controlled NPs drug release

- Swelling-controlled: this process is influenced by water concentration gradient, polymer stress gradient and osmotic forces.

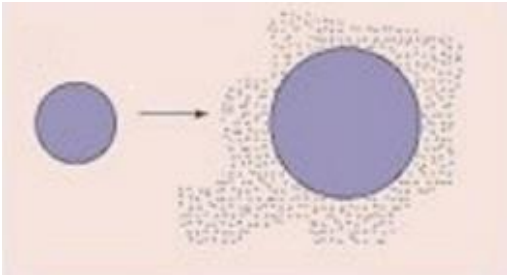

Figure 1. 9: Swelling-controlled NPs drug release.

- Degradation-controlled: the polymeric material starts the degradation process through bulk hydrolysis and meanwhile the drug is released.

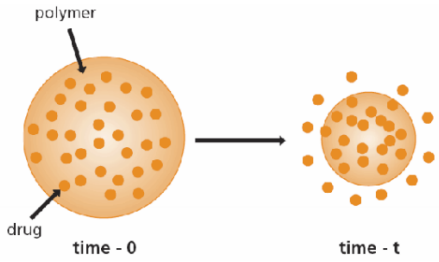

Figure 1. 10: Degradation-controlled NPs drug release.

All the properties of the nanoparticles mentioned above can be retained even in "macrostructures" obtained by aggregation of polymeric nanoparticles. Nanoparticles can be joined by covalent (chemical cross-linking) or non-covalent bonds, so short-range weak interactions such as hydrogen bonding, van der Waals forces, electrostatic forces etc. (physical cross-linking).

In this work, nanoparticles have been used to synthetized hydrogels for tissue engineering and drug delivery applications.

Indeed, hydrogel's three-dimensional structure, with a high void degree, hydrophilic tendency, swelling properties, biodegradability and biocompatibility make it suitable materials as scaffold for cell housing.

However, hydrogels from nanoparticles present interesting properties even if employed as DDSs. They are targeting materials, thus they face the problems relative to nanoparticles and drug leakage by being applied in a specific area. Furthermore, for their macroscopic size, they will not be able to move unless they degrade.

Hydrophilic nature of hydrogels makes the loading of a large variety of water soluble drugs possible. An interesting property of hydrogels formed by nanoparticles is also the opportunity to load even hydrophobic compounds. Hydrophobic molecules can be entrapped in nanoparticles, so the macrostructure formed can carry both hydrophilic and hydrophobic drugs. Such loaded hydrogels can simultaneously release the hydrophobic compound contained in the nanoparticles, and the hydrophilic solution retained in the matrix.

For all these reasons the work has been focused on nanoparticles-based hydrogels, that provide a high range of applicability and suitable properties in tissue engineering and drug delivery fields. Such structured materials are quite unexplored technologies in literature, due to the difficulty of synthesizing nanomaterials and combining them into macrostructure with peculiar characteristics.

The first part of this work deals with the synthesis of poly-methyl-methacrylate nanoparticles and their gelation methods.

The second part of the work is focused on the synthesis of opposite charged nanoparticles of PCL_3 and on the aggregation process between them to obtain a stable hydrogel for cell housing and drug delivery.

Characterization of both types of nanoparticles and hydrogels are developed.

1.5 Aggregation of nanoparticles overview

As mentioned above, nanoparticles specific characteristics make them promising materials in many fields. However, their dimension is sometimes a limiting factor. Thereby, their scalability remains the key roadblock to wide applications.

Indeed, nanoparticles can be assembled into superstructures which can reach final dimensions greater than the nanometric scale, without losing the typical properties of nanoscale structures; e.g., NPs assemblies retain the optical, magnetic, electrical, biological, and mechanical properties, typical of nanoparticles. Moreover, these assemblies are non-chaotic, i.e. organized according to a predetermined pattern, besides involving large numbers of NPs [15]. These superstructures can be obtained by simple, inexpensive, fault tolerant, and controllable processes, as a consequence, their application fields widens much more.

The assembly process is originated by a variety of interparticle interactions, mainly van der Waals forces, dipole-dipole, London, hydrogen bonding, electrostatic forces and entropic effects, or other interactions. Alternatively, it can be driven by external fields, such as electrical, magnetic, gravitational.

A schematic overview of the assembly processes is summarized in Figure 1.11.

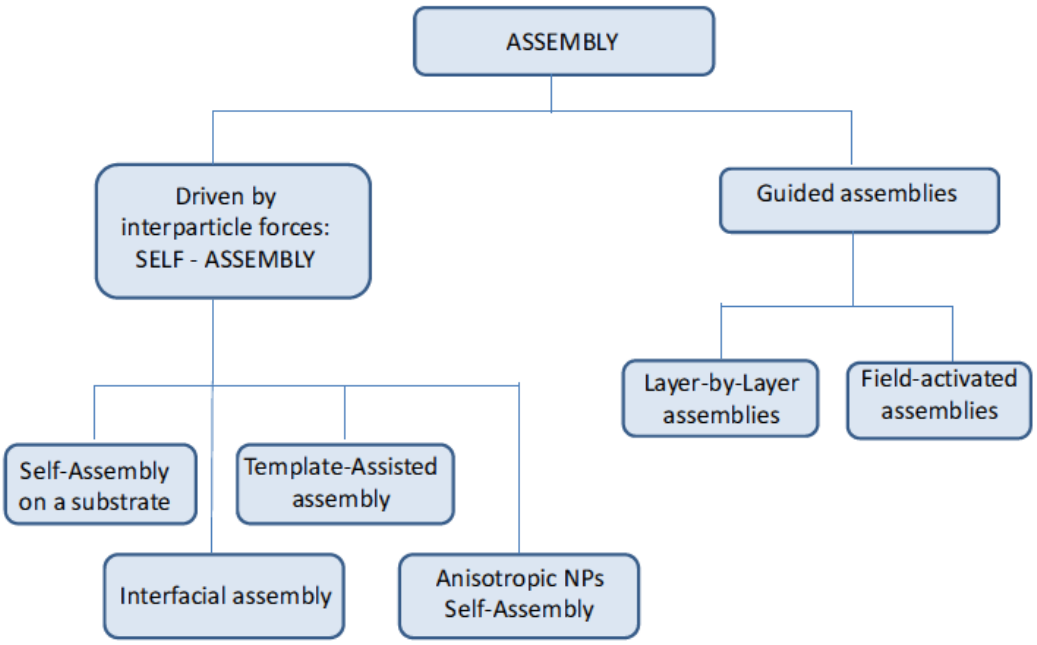

Figure 1. 11: Overview of NPs aggregation techniques.

If the particle organized pattern is driven by interparticle forces, it is known as "self-assembly". It consists of the spontaneous association and autonomous organization of components into stable and structurally defined patterns or aggregates without human interventions.

Self-assembly processes consist of several techniques. It is possible to use a substrate, typically carbon or silicon oxide copper grids, to provide support to organize 2D and 3D superstructures. Solvent evaporation from the dispersed solution leads to crystals formation, indeed a drying front, that induces deposition and organization of nanoparticle, is created thanks to solvent removal [16]. Otherwise, template-assisted self-assembly (Figure 1.12) uses functionalized surfaces or templates that introduce covalent/non-covalent interactions providing the necessary attractive forces between the surface and the nanoparticles to form 3D structures [17]. Recent studies are focused on functionalized polymers as template for highly ordered metallic NPs assemblies [18].

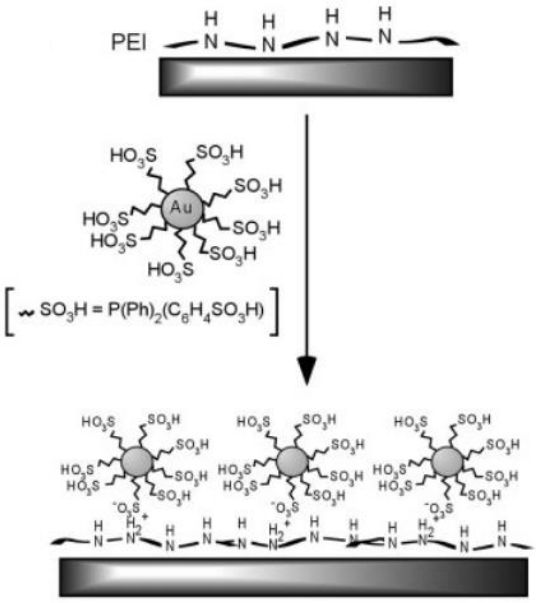

Figure 1. 12: A schematic diagram depicting self-assembly of sulfonated Au NPs on polythileneimine-template.

Another kind of nanoparticles self-assembly technique occurs at air-liquid or liquid-liquid interface (Figure 1.13), using lateral compression at controlled speed as driving force [19] .

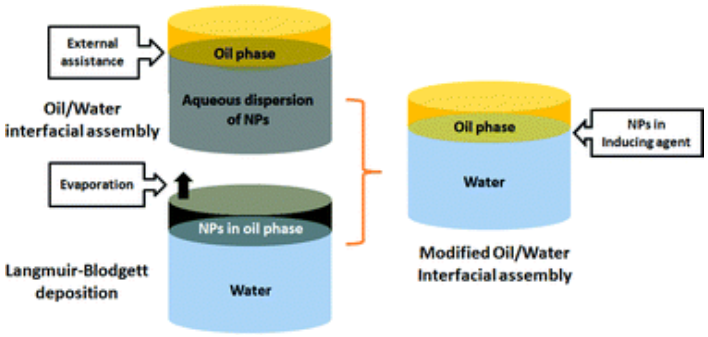

Figure 1. 13: Ultrathin graphene films based on interfacial assembling techniques.

As regard to non-spherical NPs, they present strongly anisotropic interactions, due to the mutual orientation of their crystalline faces and to the presence of intrinsic electrical and magnetic dipoles associated with a non-uniform charge distribution and a specific shape.

Successful realization of non-chaotic assemblies of non-spherical particles relies on making the system globally neutral; this can be achieved by partial removal of stabilizers from the NPs surface. When an approximate balance condition of attractive and repulsive interactions is reached, the anisotropy interactions between particles become significant and assembly occurs [20].

The process of NPs organization can also be driven by external inputs toward desirable geometries. External electric and magnetic fields can replace the intrinsic field between the individual NPs.

Light-sensitized NPs self-assembly relies on optical confinement or irradiation-induced changes in photoactive ligands. The induced isomerization determines the formation of dipoles. Dipolar interactions between NPs (together with solvophobic effect) triggers NP assembly in ordered 3D arrays. Electric field driven assemblies occur from induced polarization of NPs. Adjacent NPs interact through dipole-dipole interactions and form chains aligned parallel to the field lines. Finally, magnetic field-driven assemblies originate from NPs association via magnetic dipoles when torque exerted by a magnetic field exceeds NPs thermal excitation energy. Magnetic NPs can form chains or 3D superlattices.

Moreover, layer-by-layer technique is based on the alternate adsorption of solutions that contain complementary charges or functional groups to form integrated ultrathin films, as can be observed in Figure 1.14 [21].

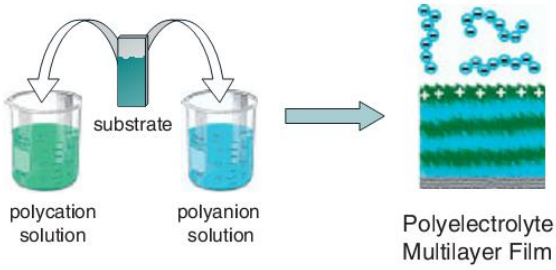

Figure 1. 14: Polyelectrolyte multilayer film made with layer-by-layer technique

1.6 Gelation methods

Polymers produced through emulsion polymerization are in form of colloidal nanoparticles dispersed in water, which take the name of latex. If properly destabilized, colloidal suspensions may aggregate in form of clusters that are typically mass fractal objects [22]. During aggregation, clusters' size grows. As a parameter of growth, one can consider the cumulative volume fraction occupied by all clusters (Φ). Φ is a function of time and it increases up to values larger than one. It means that the system is becoming progressively more crowded. This characteristic impede clusters movements and diffusion, enhancing the creation of strong interactions among them. This originates the transition from a liquid-like colloidal dispersion to a solid-like material, the gel.

In Figure 1.15 is shown the formation of clusters until the cumulative volume fraction of clusters is equal to one, and then the growing interconnection among clusters. Meanwhile, the cumulative volume fraction of clusters increases furtherly. The whole volume is going to be occupied by this new open solid-like phase. The time the process ends, is referred to as gelation time.

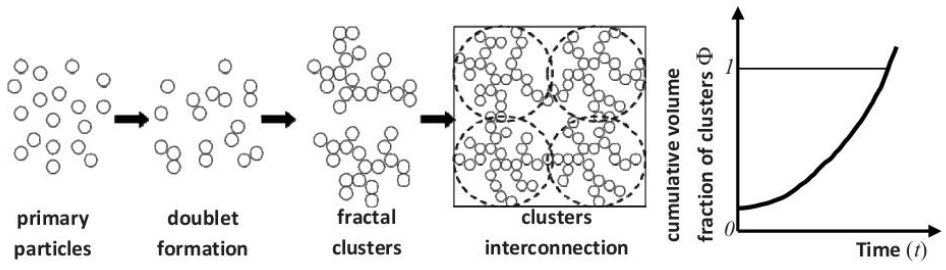

Figure 1. 15: Cluster formation and interconnection. Cumulative volume fraction of clusters increase with time.

Gels present completely different rheological properties from the original colloidal dispersion. This broadens its application field to many areas as medicine, food, detergency, etc.

The above-mentioned properties can be easily tuned by controlling the degree of coalescence. Indeed, different degree of coalescence, together with different polymeric nanoparticles nature, lead to different compactness of the clusters forming the gels.

The most common techniques of gelation starting from polymeric nanoparticles are:

- Brownian-motion induced gelation;
- Intense shear-induced gelation;

They will be briefly explained in the following paragraph, focusing on the technique used in this work [23].

1.6.1 Brownian motion- induced gelation

Polymeric nanoparticles in a latex follow Brownian motion because of their thermal energy, so they frequently collide. The interactions among the particles are governed by two different forces: van Der Waals attraction and electrostatic repulsion, due to the charges typically present on the surface. The combination of these forces, explained by the so-called DLVO (Derjaguin-Landau-Verwey-Overbeek) theory, generate an interaction barrier between the nanoparticles that make them repel each other when they collide.

Figure 1.16 shows how the repulsive effect is influenced by the presence of the so-called electrical double layer (EDL), which typically develops near charged surfaces in solution. The first layer corresponds to the charged surface, whose charges may come from adsorbed ions or ionic surfactants, dissociated surface groups or substituted ions within the lattice. The charged surface of the particle attracts counter-ions from the surrounding solution and repels co-ions. Thus, the formation of a diffusive second layer is enhanced. The EDL can be approximately divided into two regions.

Near the charged wall surface, ions are strongly bound to the surface; this region is the immobile layer (Stern or Helmholtz layer). The region beside the Helmholtz layer is called the diffuse layer, because it contains poorly associated ions and it is considered mobile.

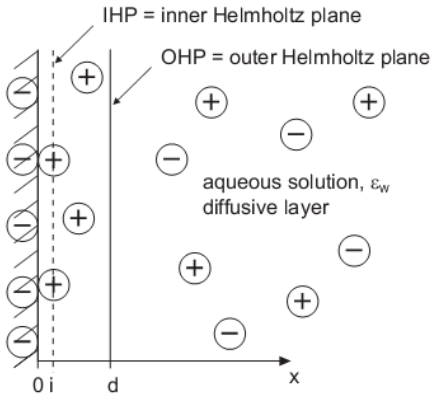

Figure 1. 16: Electrical Double Layer (EDL)

The combination between electrical double layer forces and van der Waals attractions, together with other weak interactions, all depending on the distance, can be synthesized in the total potential energy of interaction (V_T), whose trend is plotted in Figure 1.17.

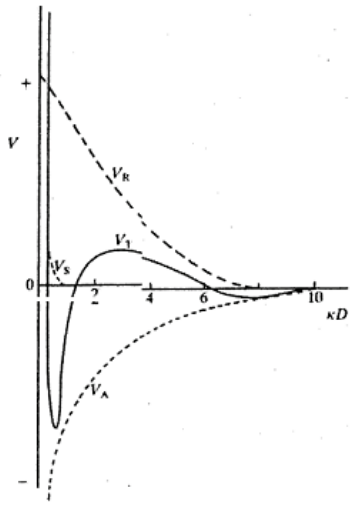

Figure 1. 17: Total potential energy of interaction (V) as sum of attractive forces (VA), repulsive forces (VR) and steric forces (VS).

Analyzing Figure 1.17 , it is evident how van der Waals forces prevail at low distances, but V_T does not go to -∞ because of the presence of very short-range repulsive forces acting when two particles are approaching each other. This determines the increase of V_T and gives rise to a primary minimum. There, in that deep attractive well, the bonding between nanoparticles occurs, thus, in most cases, it is irreversible. The presence of a secondary minimum is due to the fact that at greater distances, van der Waals forces dominate again.

From the shape of the total interaction potential curve as function of distance depicted above, it is possible to investigate upon the stability of the colloid and the possibility of its destabilization to let it aggregate.

It is possible to induce aggregation acting on the indifferent ions (Figure 1.18), that stands for double layer compression by introducing additional electrolytes (salts) into the latex. Thus, screening and counter-ion effects due to the salts reduce the interaction barrier as shown in Figure 1.19.

Brownian motions become stronger than the barrier because it is progressively reduced, until it can be overcome. By that time, there is no opposition to aggregation, which becomes very fast and controlled by Brownian diffusion. A doublet is formed first, and then the aggregation continues leading to fractal clusters. The smallest electrolyte concentration leading to such a fast coagulation is called critical coagulation concentration.

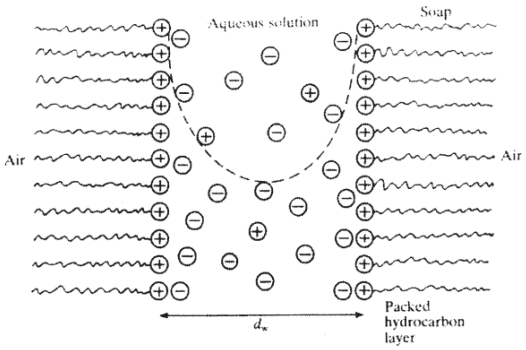

Figure 1. 18: Ions in aqueous solution close to a charged surface.

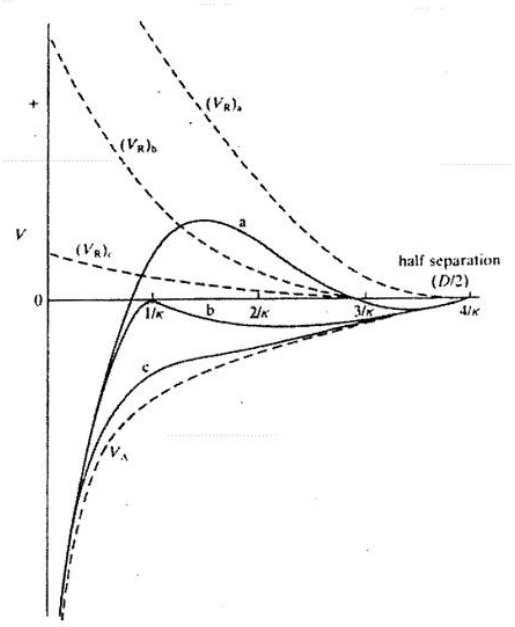

Figure 1. 19: As the concentration of the indifferent electrolyte increases, the energy barrier decreases and eventually becomes zero.

Depending on whether a small interaction barrier is present, two aggregation regimes are possible:

- Reaction-limited cluster aggregation (RLCA) when a small interaction barrier is present;
- Diffusion-limited cluster aggregation (DLCA) in the absence of any interaction barrier.

1.6.1.1 RLCA

If a small interaction barrier is present RLCA regime dominates. Brownian motion-induced gelation is usually carried out under this conditions because aggregation rate can be easily controlled, ensuring homogeneity of the gel structure. The average clusters size increases with time and open structures, with void greater than 90%, are usually obtained.

1.6.1.2 DLCA

In absence of any interaction barrier DLCA regime dominates. The standard procedure, based on mixing a salt solution and a latex, cannot be used because gelation occurs on a time scale of few milliseconds that is not enough to have a homogeneous mixing. Thus, mixing is the controlling process and the gel obtained is not uniform.

To avoid the mixing problem, two alternative techniques have been developed:

- In situ destabilization: this mechanism is catalysed by an enzyme that destabilizes the low viscous liquid to form a rigid gel [24].
- Frontal gelation [25].

  This technique consists in three main steps:

  - A latex with a desired volume fraction is prepared in a small container.
  - The salt solution is slowly added on the top of the latex. Thanks to the high ionic strength and the high volume fraction, a layer of gel immediately forms at the interface.
  - More salt solution is added that remains in place due to the mechanical strength of the gel layer previously formed. Then, a gelation front starts moving further inside the solution owing to the salt solution diffusion.

  The presence of an initial gel layer prevents not only convection-driven mixing of the two solutions, but also the diffusion of polymer particles back into the salt solution. On the other hand, since the gel has a very open structure, salt ions are free to diffuse through the gel layer into the latex, where they induce almost instantaneous gelation (DLCA).

The gel layer increases with time and the gelation front moves toward the bottom of the container (frontal gelation).

A simple diffusion model is enough to predict the position of the front of gelation over time. The dimension of the container influences the critical initial mass to form a resistant gel layer from which the gelation process will start.

The most attractive advantage of Brownian motion-induced gelation is that the hydrogel, with its solid-like features, can be formed starting from lattices with particles volume fraction higher than 2%. Therefore, material obtained with this technique, present void greater than 90%.

1.6.2 Intense shear- induced gelation

Nanoparticles from a colloidal system can aggregate by intense shear-induced gelation when the repulsive interaction energy barrier is overcome by applying a sufficiently high shear rate. Such shear rate is applied by a device with a z-shaped microchannel (z-Mc) where a high turbulent shear flow converts a liquid-like particle dispersion to a liquid-like cluster dispersion. Only after withdrawing the imposed shear, the clusters are able to interconnect with each other.

This technique presents some advantages: the purity of the final product, indeed no additional electrolytes are needed, the continuity of gelation process, and the possibility of scale-up for industrial productions.

However, intense shear gelation is possible for colloidal solutions where only DLVO forces are present. For example, when a surfactant is added to the system, shear-induced gelation doesn't occur, due to a high value of surfactant surface density.

1.6.3 Aggregation of charged nanoparticles

The first part of this work is focused on gelation of poly-methyl methacrylate nanoparticles. Since the nanoparticles were synthesized by emulsion polymerization, the starting colloidal dispersion contained a surfactant. Thus, DLCA was used as gelation technique. However, only with SDS the gelation occurred.

Since the aim of the work is to obtain a cyto-compatible hydrogel for cell housing, PMMA nanoparticles made with SDS tenside, which is cyto-toxic, have been abandoned. The second part of the work deals with gelation of poly-HEMA-ε-caprolactone nanoparticles.

The idea was to exploit the electrostatic attractive forces between opposite-charged nanoparticles. Aggregation via electrostatic interactions avoid covalent bonds that might be too strong for cell housing materials.

During the synthesis, two oppositely charged and cyto-compatible stabilizing agents were used in order to enable physical cross-linking among charged nanoparticles. Indeed, thanks to the carbon double bond of the stabilizing agents used, they could attach to the particles, providing them with stable charges. The operative procedure will be explained in Chapter 2.

1.7 Ring-opening polymerization

Ring-opening polymerization is one of the three most important paths to synthetize polymers. ROP reactions are more complicated than chain polymerizations and involve activated monomers. It has been proved that ROP is very useful to obtain polymers with specific properties, to prepare synthetic variants of natural and biodegradable polymers for agricultural, medicinal and pharmaceutical applications. ROP is a good way to obtain high molecular weight polymers because one of the advantages is the absence of typical by-products of liner monomers polymerization, such as water; this leads also to high purity products.

All ROP reactions have in common that monomers are rings, so what changes is just the reason why these reactions occur. Ring chain equilibrium, influenced by monomer concentration and temperature, is an important parameter to take into account when analyzing ROP reactions. Cycloalkanes, for example, have a good reactivity if they are formed by maximum 3 or 4 carbon atoms, indeed, a six carbons ring is a very stable configuration. However, a catalyst and a co-catalyst are necessary to open the ring.

Synthesis of HEMA-poly(ε-polycaprolactone), referred to as HEMA-PCL_3, is an example of ROP; this compound has been used in this work as the main component for the synthesis of biodegradable nanoparticles. In this process the ε-caprolactone ring is opened thanks to a catalyst, stannous-octoate, and a co-catalyst, hydroxyethyl(methacrylate) (HEMA). Stannous-octoate and HEMA react together forming, in two following steps, stannous dialkoxyde, the effective catalyst of ROP. This compound is able to open the ring acting on oxygen double bond. In this way a linear structure is obtained from a cyclic monomer. HEMA remains attached to the polymeric chain and thanks to its terminal carbon double bond HEMA-PCL_3 can polymerize [26].

1.8 Emulsion polymerization

The following paragraph deals with the analysis of emulsion polymerization reaction in batch and starved mode.

1.8.1 Analysis of the process

Emulsion polymerization is a heterogeneous process based on a reaction occurring in small particles in an aqueous matrix. The ingredients of emulsion polymerization are water, monomer, initiator and stabilizer. Usually the monomer is dispersed in a solution of water and surfactants and, due to the fact that the monomer is not soluble in water, it forms large droplets. Surfactants are generally amphiphilic molecules thanks to their typical structure with a hydrophilic head and a hydrophobic tail, for this reason they have affinity for both polar and non-polar solvents. If these molecules are present at the interface of an emulsion, the hydrophilic head will enter in the water phase and specific space distributions will take place in the surface because this arrangement of the molecules is energetically more favorable than dissolution into the bulk phase. If tensides are added in such quantities that they can saturate the interfacial layer and also the bulk phase, they form organized aggregates, so-called micelles, due to water-water and HC-HC interactions. Micelles' formation can be observable at a minimum value of concentration, the so-called CMC, critical micelle concentration. Micelles are useful to minimize the contact between hydrocarbon and water, which are not soluble, and maximizing contact between hydrophilic groups and water; they are a proper location for polymerization to occur.

Analyzing the kinetic mechanism of the process it is possible to divide it in three steps (Figure 1.21).

The first step is nucleation. A monomer and an initiator, water soluble, are added in the solution and agitated. Emulsion polymerization is a radical process: the initiator reacts with the monomer forming radicals that enter inside the micelles.

The monomer can also form big droplets (M_p), fluctuating in water, or can dissolve in it (M_w).

Radicals preferentially enter the micelles because higher surface area is available. Micelle is a small "reactor" where polymeric chains are growing. The nucleated particles, so their surface, grow by taking the monomer from the solution, so they need to absorb more surfactants to be stable. Surfactant's concentration decreases below CMC: this is the end of nucleation step. From this point the number of micelles will remain constant and they will be referred to as particles (N_p) .

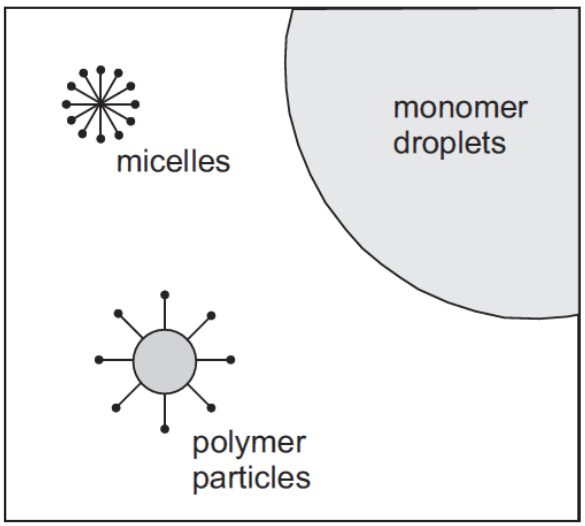

Figure 1. 20: Phases during emulsion polymerization: monomer droplets, micelles and polymeric particles.

The second step is the growth step. Monomer's activity is equal for the three different phases, so the monomer start flowing from the drops to the particles through the aqueous phase. The growth has constant rate until the end of the monomer.

The last step starts when the monomer drops are depleted. To balance monomer's activity between the particles and the aqueous phase, the monomer dissolved in water enters into the particles.

The polymerization ends when also aqueous monomer is completely consumed.

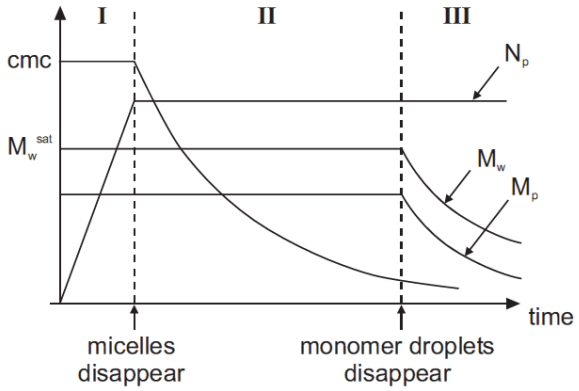

Figure 1. 21: Emulsion polymerization steps: nucleation (I), growth (II) and termination (III).

Emulsion polymerization is an attractive process because all the monomer can react and moreover it is possible to control the molecular weight of the obtained polymer and the process temperature.

The reaction rate is increased if there are more particles in solution, so if there are more micelles. The concentration of tenside obviously influences the number of micelles: if it is increased, also micelles number will increase. At the same time, analyzing the influence of initiator, it is observable that a smaller amount of it leads to a reduction of the number of radicals, therefore to a drop of the termination velocity. Thus, the polymerization keeps on going and this results in an increased molecular weight of the polymer.

As stated above, micelles can be considered as "small reactors" and temperature control is easier in these systems. A better temperature control makes the quality of the process higher because there is no formation of "hot spots" that lead to polymer degradation, to the enhancement of the molecular weight or to the increase of polymerization rate or in the worst case to explosion. The reason why these processes are made in water is because it can behave as a thermal diluent and it can make the process safer.

1.8.2 Starved procedure

Starved reaction procedure consists in a process characterized by a slow addition of the monomer. The slow addition of the monomer allows a better control on nanoparticles dimensions because the growth of the particles is influenced by the addition rate. The presence of monomer drops in the reaction mixture is decreased, because the monomer, as soon as it is injected, enters the particles and reacts. In this way, the pseudo-steady-state approximation (PSSA) is satisfied. The nucleation time is longer; under these conditions the number of particles will increase and they will have smaller dimensions. The quantity of emulsifier that has to be added to stabilize them can be smaller.

Chapter 2

Materials and methods

2.1 Materials

In this section we present an overview of all the compounds used for nanoparticle synthesis, aggregation and characterization: monomers, stabilizing agents, catalysts and co-catalysts, initiators and other chemicals. In addition we illustrate also the methodologies used together with analytical methods.

2.1.1 Monomers

2.1.1.1 Methyl methacrylate

Methyl methacrylate (MMA) is the ester coming from methacrylic acid and methanol.

Its formula is $CH_2 = C(CH_3)COOCH_3$.

Its properties and molecular structure are:

Molecular weight	100.12 g/mol
Density	0.94 g/cm^3
Melting point	-48 °C (225 K)
Boiling point	101 °C (374 K)
Solubility in water	1.5 g/100 ml
Viscosity	0.6 cP at 20 °C
CAS number	80-62-6

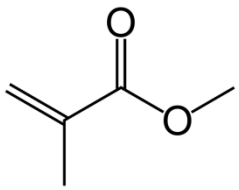

Figure 2. 1: Methyl methacrylate structural formula.

It is liquid at room temperature, colourless and volatile. It is produced in large quantity because it is used as monomer for poly methyl methacrylate, for the production of the co-polymer methyl methacrylate-butadiene-styrene (MBS) and as a modifier for PVC.

It is also the raw material for other methacrylates. MMA is also used as a chemical intermediate in many manufacture applications, such as coating polymers, construction chemicals and textile applications.

Commercial production is made by the reaction of acetone and hydrogen cyanide to form acetone cyanohydrin (ACH), which is further treated with sulfuric acid to produce methacrylamide sulfate. The sulfate is esterified with methanol to produce methyl methacrylate, with ammonium bisulfate as a byproduct.

Although this polymer is not biodegradable, it has been used for this work because it is approved by FDA and it has been widely studied, so a lot of information are available in this respect.

2.1.1.2 Methacrylic acid

Methacrylic acid (MAA) is the α-methylderivative of the acrylic acid. Its molecular formula is $C_4H_6O_2$.
Its characteristics and molecular structure are reported below:

Molecular weight	86.06 g/mol
Density	1.015 g/cm
Melting point	14 - 15 °C
Boiling point	161 °C
Solubility in water	Complete
CAS number	79-41-4

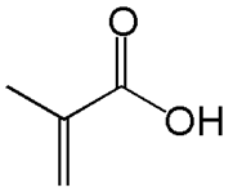

Figure 2. 2: Methacrylic acid structural formula.

It is a viscous liquid, it can dissolve in water and in most organic solvents. It is a carboxylic acid and commonly used as a precursor for its esters, especially methyl methacrylate (MMA) and poly methyl methacrylate (PMMA).

Every year, more than 3 million tons of methyl methacrylate (MMA) are produced. The most common approach to methacrylic acid synthesis is the hydrolysis of methacrylamide sulfate, obtained from acetone cyanohydrine.
It can be used as co-polymer for its stabilising effect and to increase the hydrophilic characteristics of the particles, in order to improve their swelling capacity. Indeed, the presence of COO- groups, negatively charged, amplify repulsions among particles and affinity with water, leading to greater stability of the system.

2.1.1.3 ε-Caprolactone

ε-Caprolactone is a cyclic ester with a seven-membered ring. It is part of the lactone family. Its IUPAC name is 2-oxepanone and its formula is $(CH_2)_5CO_2$.
Its properties and structure are:

Molecular weight	114.14 g/mol
Density	1.030 g/cm^3
Melting point	-1 °C (272 K)
Boiling point	253 °C (526 K)
Solubility in H_2O	miscible
CAS number	502-44-3

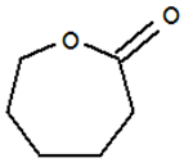

Figure 2. 3: ε-caprolactone structural formula.

This colourless liquid is miscible with most organic solvents and it is produced on a very large scale as a precursor to caprolactam. It is the reaction product of Bayer-Villiger oxidation of cyclohexanone with peracetic acid . It is mainly consumed as a precursor of caprolactam.
Its polymerization gives polycaprolactone via Ring-opening polymerization reaction or polyglecaprone, a high-specialised material used as suture material in surgery.

2.1.1.4 Hydroxyethyl methacrylate

Hydroxyethyl(methacrylate) or HEMA has molecular formula $C_{16}H_{10}O_3$. Its properties and skeleton structure are:

Molecular weight	130.14 g/mol
Density	1.073 g/cm^3
CAS number	868-77-9

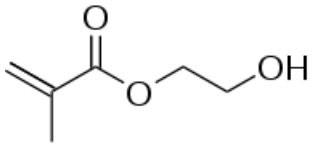

Figure 2. 4: HEMA structural formula.

It is obtained by esterification of methacrylic acid with diethylene glycol and it is mostly used for contact lens production for its large swelling behavior (from 10% to 600%).

Indeed, this basically hydrophobic molecule has the capability to swell when immersed in water thanks to its hydrophilic pendent group.

2.1.2 Stabilizing agents

2.1.2.1 Sodium dodecyl sulfate

Sodium dodecyl sulfate is an anionic surfactant with molecular formula:

$$NaC_{12}H_{25}SO_4$$

It consists in a sulfate group with a 12-carbon tail attached:

Molecular weight	288.38 g/mol
Density	1.1 g/cm^3
Melting point	204 °C (477 K)
Boiling point	380 °C (653 K)
Solubility in water	196 g/l at 20°C
CAS number	151-21-3

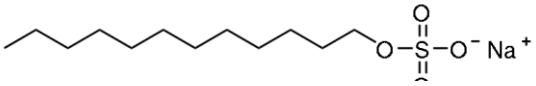

Figure 2. 5: SDS structural formula.

Thanks to this structure the molecule has amphiphilic properties, that are typical properties of all tensides.

SDS is an odorless white solid and it is used in lots of cleaning and hygiene products thanks to its derivation from coconut and palm oils, inexpensive raw materials. SDS is synthetized from sulfur trioxide gas, lauryl alcohol, derived from coconut or palm oil by hydrolysis, and sodium carbonate, used to neutralized the product.

Its critical micelle concentration (CMC) in water at 25°C is 8,2 mM and it presents a HLB equal to 40.

SDS can irritate for prolonged usage or in hypersensitive individuals, but in daily life applications it is not considered carcinogenic.

Experimental studies point out that SDS is cytotoxic: cells exposed to SDS shown, after a time, morphological changes, loss of membrane integrity, reduction of cell adhesion to substratum and reduction of mitotic cells.

2.1.2.2 3-Sulfopropyl methacrylate potassium salt

3-Sulfopropyl methacrylate potassium salt has molecular formula $C_7H_{11}KO_5S$ and skeleton structure.This compound will be hereinafter named HEMA-SO_3-.

Molecular weight	246.32 g/mol
Melting point	295 °C (568 K)
CAS number	31098-21-2

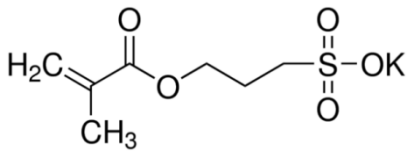

Figure 2. 6: HEMA-SO_3- structural formula.

It is a ionic tenside but the presence of a shorter carbon chain, that decrease its amphiphillic properties, makes it less effective than other ionic surfactants. However, its terminal carbon double bond offers a polymerization site. Therefore, it can attach to the macromonomer giving a stable charge to the nanopolymer.

2.1.2.3 Polysorbate 80

Polysorbate 80 (Sigma Aldrich), also called TWEEN 80, is a nonionic surfactant and emulsifier, whose molecular formula is $C_{64}H_{124}O_{26}$ and the chemical structure shown below.

Molecular weight	1310 g/mol
Density	1.06–1.09 g/cm^3, oily
Boiling point	> 100°C
Solubility in water	High
CAS number	9005-65-6

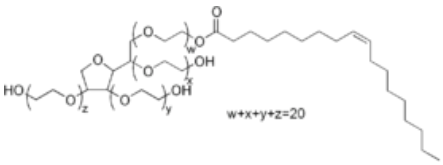

Figure 2. 7: Tween-80 structural formula.

It is used in biochemical applications and in medicinal and food products to emulsify and disperse substances. It is a clear yellow viscous liquid and it is soluble in water. It presents a critical micelle concentration (CMC) of 0,012 Mm and a HLB=15. Polysorbate 80 is extremely versatile and effective while also being non-toxic, non-mutagenic, non-carcinogenic, with very little potential for human skin irritation, sensitization, or phototoxicity.

2.1.2.4 [2-(Methacryloyloxy)ethyl]trimethylammonium chloride

[2-(Methacryloyloxy)ethyl]trimethylammonium chloride is a liquid compound, colorless to slightly yellowish with an ester-like odour. This compound will be hereinafter named HEMA-Ch+.

Molecular weight	206.5 g/mol
Density	1.1 g/cm^3
Boiling point	100 °C (578 K)
Water solubility	miscible
Viscosity	20 -50 mPa s
CAS number	5039-78-1

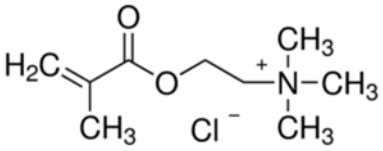

Figure 2. 8: HEMA-Ch+ structural formula.

It is used as an intermediate product for polymer synthesis in the chemical industry, it is commercially available as 75% solution in water.

It has no evident toxicity, but it can cause eye irritation and allergic skin reaction. So, exposure to this chemical substance is very limited. It is readily biodegradable.

As well as HEMA-SO_3-, HEMA-Ch+ is a charged molecule with a terminal carbon double bond, so it can give a stable charge to the synthesized nanoparticle when polymerized.

2.1.3 Initiators, catalysts and other chemicals

Next paragraphs introduce the initiators used during polymerization, potassium peroxidisulfate and α-α'-Azodiisobutyramidine dihydrochloride, the catalyst for ROP, stannous octoate, and the phosphate buffered saline. In addition, drugs used to drug release tests are presented: TO-PRO®-3 and fluorescein.

2.1.3.1 Potassium peroxodisulfate

KPS, also known as potassium persulfate or potassium peroxodisulfate, is an inorganic compound with formula $K_2S_2O_8$ and skeleton formula:

Molecular weight	270.32 g/mol
Density	2.477 g/cm^3
Melting point	< 100 °C (373 K) (decomposes)
Solubility in water:	4.49 g/100 ml (20 °C)
CAS number	7727-21-1

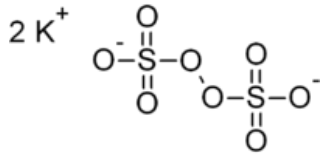

Figure 2. 9: KPS structural formula.

KPS is a white odorless powder, soluble in water. One of the most important characteristics of this salt is that potassium persulfate is a powerful oxidant and for this reason is mostly used to initiate polymerizations.

In solution, the dianion dissociates to give radicals:

$$[O_3SO - OSO_3]^{2-} \leftrightarrow 2\,[SO_4]^{-}$$

It can be prepared by electrolysis of a solution of potassium bisulfate in sulfuric acid at high current density.

2.1.3.2 α-α'-Azodiisobutyramidine dihydrochloride

α-α'-Azodiisobutyramidine dihydrochloride is a free radical initiator with chemical formula $C_8H_{20}Cl_2N_6$.

Its properties and skeleton formula are shown below.

Molar mass	271.19 g/mol
Melting point	178 °C (451 K)
Density	0.42 g/cm³
CAS number	2997-92-4

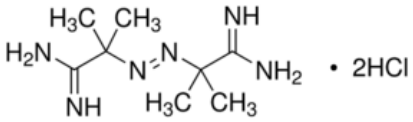

Figure 2. 10: α-α'-Azodiisobutyramidine dihydrochloride structural formula.

It is a water soluble white powder, sensitive to heat and light.

2.1.3.3 Stannous octoate

Stannous octoate is a yellow liquid catalyst used in ROP reactions. It is the only catalyst approved by FDA (Food and Drug Administration) for this type of reactions.

Molar mass	405.12 g/mol
Density	1.251 g/cm³ at 25 °C

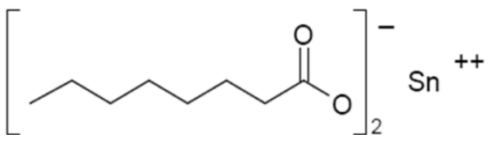

Figure 2. 11: Stannous octoate structural formula.

2.1.3.4 Phosphate buffered saline

Phosphate buffered saline (PBS) is a balanced salt solution commonly used as a buffer solution in chemical and biological laboratories. It contains sodium chloride, sodium phosphate and potassium phosphate. The buffer helps to keep constant the pH value at 7,4 which is the same as the human body. Since it is isotonic and non-toxic, it is widely used for cell culture applications, such as washing, transporting, diluting cells and reagents.

In this work, it has been used for many purposes: for the gelation of PMMA particles, to guarantee the complete dissociation of AMA which means the availability of negative charges necessary to form the hydrogel and to study the degradation of the hydrogel at human body pH.

The PBS- 10x used has the following composition:

- **NaCl** - Final concentration 1.37M;
- **KCl**- Final concentration 27mM;
- **$Na_2HPO_4*7H_2O$**- Final concentration 81mM;
- **KH_2PO_4**- Final concentration 19mM.

The steps of solution preparation are: the salts are added into water until the pH of 7,4 is reached, than everything is diluted with water MilliQ , sterilized and filtrated.

2.1.3.5 TO-PRO®-3

TO-PRO®-3 stain is a carbocyanine monomer nucleic acid stain with far-red fluorescence. TO-PRO®-3 and the other monomeric cyanine stains have wide applicability due to their low background and bright fluorescence.

Uses include staining of nucleic acids on solid supports, prestaining of samples for gel or capillary electrophoresis, viability detection and counterstaining in multiple-label experiments.

It is a hydrophobic molecule (Figure 2.12). For the purposes of this work, it was used to study drug loading and release from hydrogels. Its skeleton formula is below:

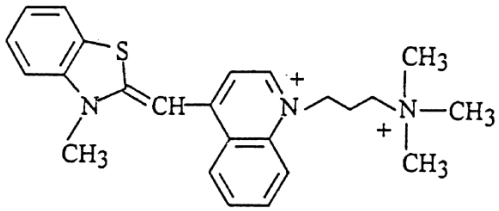

Figure 2. 12: To-Pro3 structural formula.

2.1.3.6 Sodium fluorescein

Fluorescein is a synthetic organic compound (Figure 2.13) available as a dark orange/red powder slightly soluble in water and alcohol. It is widely used as a fluorescent tracer for many applications. It is a hydrophilic molecule. It was used for drug loading and release tests.

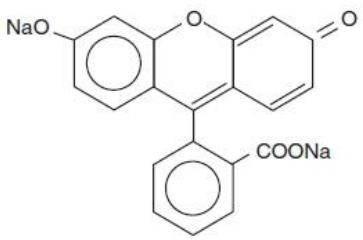

Figure 2. 13: Fluorescein skeleton formula.

2.2 Instrumentation

This section deals with instrumentation used to characterize NPs and hydrogels: dynamic light scattering, infrared spectroscopy, scanning and transmission electron microscopes and atomic force microscope. Their theoretical and operating principles are explained.

2.2.1 Dynamic Light Scattering

Light scattering technique has been used to analyze and characterize nanoparticles obtained by emulsion polymerization. This analysis method is one of the most important for colloidal systems because it is a non-invasive technique that can estimate various properties of nanoscaled particles . The diameter and polydispersity of particles can be obtained using the dynamic light scattering (DLS).

This process involves the diffusion of a light beam whose energy, interacting with matters, is scattered in all directions (Figure 2.14). When the light beam, that is nothing else than an electromagnetic wave, hits the matter ("diffuser center"), the electrons inside the molecule move from the original position and this change of position create a dipole. The dipole oscillates with the same frequency of the incident beam and radiates electromagnetic beams in all directions: the sum of all diffused beams is the scattered light. Dimension and shape of particles influence the intensity and the scattered angle of light.

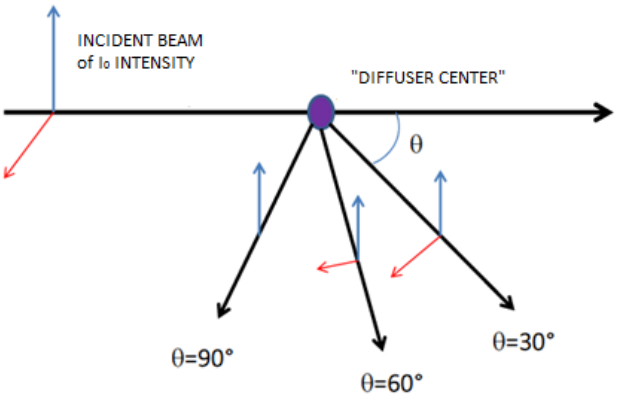

Figure 2. 14: Diffusion of a light beam.

The Rayleigh law, with the assumption of diffuser center's dimensions much smaller than the wavelength of incident light, describes the relationship between the intensity of diffused light and three main parameters: the angle of scattering (angle between the incident light beam and the diffused light beam), the particle's diameter and the incident beam wavelength. The assumption above is necessary because big particles in the system can obscure the smaller ones, so it is necessary to have a unimodal distribution.

$$\frac{i_\theta}{I_0} = \frac{8\pi^4}{\lambda^4 r^2}(1 + cos^2\theta) * \left(\frac{n^2 - 1}{n^2 + 2}\right)^2 * \left(\frac{d}{2}\right)^6$$

Equation 2. 1: Rayleigh law.

$i_\theta = intensity\ of\ diffused\ radiation\ for\ the\ single\ "diffusion\ center"$

$I_0 = intensity\ of\ the\ incident\ beam$

$\theta = angle\ between\ the\ incident\ beam\ and\ the\ diffused\ beam$

$n = refraction\ index\ of\ the\ particle$

$r = distance\ from\ the\ "diffusion\ center"$

$d = particle\ diameter$

$\lambda = incident\ beam\ wavelength$

From this equation it is possible to notice that the intensity of scattered light depends on the particle diameter and the incident beam wavelength.

DLS is a useful technique to obtain information about the particles' properties but it is necessary to avoid "multiple scattering" to get results with a high degree of accuracy. "Multiple scattering" occurs when a beam refracted by a particle hits another particle, before arriving to the detector, and it is refracted again: the information obtained is not a good representation of the own characteristics of the first particle. Diluting the analyzed samples and decreasing the optical contrast, the results obtained can be considered reliable. The Rayleigh-Debye-Gans theory neglects the "multiple scattering":

$$I = I_0 \cdot K_1 \cdot N \cdot V_p^2 \cdot p(q) \cdot S(q)$$

Equation 2. 2: Rayleigh-Debye-Gans theory.

Where K_1 is a typical constant of the instrument, N is the particles concentration, V_p is the particles volume, $p(q)$ is a shape factor and $S(q)$ is a structure factor.

DLS measures the intensity fluctuations of diffused light due to Brownian motion of particles. Brownian motion is the continuous disorganized motion of particles due to collisions with the solvent's molecules that surround them. Stokes-Einstein Law defines a translation diffusion coefficient D_T:

$$D_T = \frac{k_b T}{6\pi\eta R_H}$$

Equation 2. 3: Stokes-Einstein relation.

D_T (m^2/s) is a measure of particles dispersion rate through a concentration gradient.

Particles' dimension influences their movement and consequently the intensity of diffused light in time (Figure 2.15). Big particles move slowly instead of smaller ones that move faster.

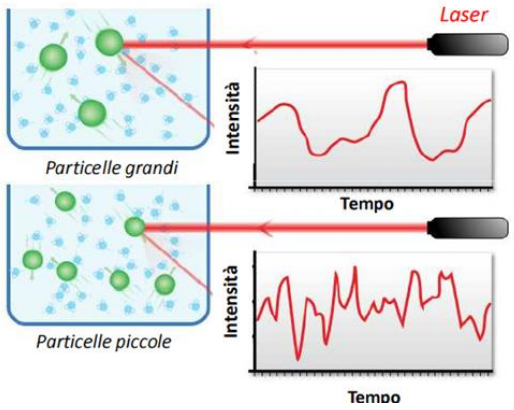

Figure 2. 15: NP dimension influence on intensity of diffused light.

A *correlator*, a digital component of the instrument, is used to derive the variations of diffused light in time and to transform them into a correlation function. The correlation function is the function that lies the particles' dynamics with the intensity of scattered light. If the analysis of signals is made in short periods of time a good correlation in the generated spectra is visible. A good correlation is lost if the time is increased.

$$G(\tau) = A[1 + Bexp(-2D_T q^2 \tau)]$$

Equation 2. 4: Correlation function.

From the correlation function it is possible to obtain D_T and then, from Stokes-Einstein equation, it is possible to calculate the particles' diameter. The diameter calculated by this equation is the hydrodynamic diameter of suspended particles and matches with the real diameter of particles for spherical ones.

In practice, the sample is placed in a cuvette and diluted with water, then it is inserted in the instrument where it can be hit by the light beam.

The instrument temperature is set at 25°C. An important step before the measure is to set the typical parameters of the colloidal dispersion. The scattered beam is then detected and analyzed as described above.

The instrumentation of DLS is presented in Fig 2.16:

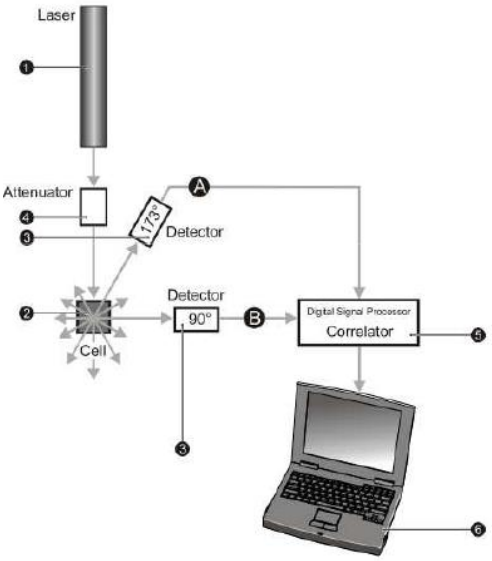

Figure 2. 16: Dynamic light scattering.

1. *Laser* : light source.
2. *Cell*: to contain the sample
3. *Detector*: measures the diffused light intensity
4. *Attenuator*: reduces the intensity of laser and scattering
5. *Correlator*: compare the scattering intensity in different periods of time
6. *Computer*: elaborates the signals obtained

The instrument used in this work is a Zetasizer-Nano by Malvern (Figure 2.17).

Figure 2. 17: Zetasizer-Nano by Malvern dynamic light scattering.

From DLS technique two main parameters are obtained: Z-average and polydispersity.

Z-average represents the average diameter of the dispersed nanoparticles. This parameter is not calculated as the average of the obtained diameters but it is the average of the intensity of diffused light.

Polydispersity (PDI) represents the difference, in terms of dimensions, between the particles contained in the sample.

$$PDI = \left(\frac{\sigma}{d}\right)^2$$

Equation 2. 5: PDI definition.

PDI is the ratio between the standard deviation (σ) of the population of nanoparticles from the average value of the diameter and the Z-average size. Smaller particles influence more the PDI value.

2.2.2 Infrared Spectroscopy

Infrared (IR) spectroscopy is one of the most common spectroscopic techniques used by organic and inorganic chemists. It is the absorption measurement of different IR frequencies by a sample positioned in the path of an IR beam. Infrared radiation spans a section of the electromagnetic spectrum having wavenumbers from roughly 13,000 to 10 cm^{-1}, or wavelengths from 0.78 to 1000 μm, but the present work will be focused on the most frequently used mid IR region, between 4000 and 400 cm^{-1} (2.5 to 25 μm). The far IR requires the use of specialized optical materials and sources.

The main goal of IR spectroscopic analysis is to determine chemical functional groups in the sample, in order to identify all types of organic and many types of inorganic compounds and to determine the molecular composition of mixtures, surfaces.

It is based on the principle that at temperatures above absolute zero, all the atoms in molecules are in continuous vibration with respect to each other.

When the frequency of a specific vibration is equal to the frequency of the IR radiation directed on the molecule, the molecule absorbs the radiation. The major types of molecular vibrations are stretching and bending. Infrared radiation is absorbed and the associated energy is converted into these type of motions. The absorption involves discrete, quantized energy levels. However, the individual vibrational motion is usually accompanied by other rotational motions.

In simple terms, IR spectra are obtained by detecting changes in transmittance (or absorption) intensity as a function of frequency. The spectra are then matched with reference spectrum to identify compounds or functional groups in unknown substances.

Most commercial instruments separate and measure IR radiation using dispersive spectrometers or Fourier transform spectrometers. Recently, Fourier transform spectrometers have replaced dispersive instruments due to their superior speed and sensitivity. Since they have been applied to many areas that are very difficult or nearly impossible to analyse by dispersive instruments, they have greatly extended the capabilities of infrared spectroscopy. In this kind of instruments, each component frequency is not viewed sequentially, but all frequencies are examined simultaneously.

In a FT system can be distinguished three main components: radiation source, interferometer and detector.

- Radiation source:

The radiation source is the same for both dispersive and FT systems: an inert solid heated electrically to 1000-1800°C, which can be Nernst glower (constructed of rare-earth oxides), Globar (constructed of silicon carbide), and Nichrome coil. They all produce continuous radiations, but with different energy profiles.

– Interferometer:

The radiant beams produced by the source are divided by the interferometer which generates an optical path difference between the beams, then it recombines them to produce repetitive interference signals, which contain infrared spectral information generated after passing through a sample. The most common interferometer is a Michelson interferometer. It consists of three active components: a moving mirror, a fixed mirror, perpendicular to the other, and a beamsplitter. The beamsplitter, usually made by depositing a film of germanium onto a KBr substrate, is a semireflecting device. Radiation from the broadband radiant source is collimated and directed to the interferometer, and impinges on the beamsplitter. At the beamsplitter, half the IR beam is transmitted to the fixed mirror and the remaining half is reflected to the moving mirror. After reflection on the two mirrors, they are recombined at the beamsplitter. After the changes in the relative position of the moving mirror to the fixed mirror, an interference pattern is generated. The resulting beam then passes through the sample and is eventually focused on the detector.

– Detector response:

The easiest case of a detector response is that of a single-frequency component from the IR source. As previously described, differences in the optical paths between the two split beams are created by varying the relative position of moving mirror to the fixed mirror. If the two arms of the interferometer are of equal length, the two split beams travel through the exact same path length. The two beams are totally in phase with each other; thus, they interfere constructively and lead to a maximum in the detector response. This position of the moving mirror is called the point of zero path difference (ZPD). When the moving mirror travels in either direction by the distance l/4, the optical path (beamsplitter–mirror–beamsplitter) is changed by 2 (l/4), or l/2.

The two beams are 180° out of phase with each other, and thus interfere destructively. As the moving mirror travels another l/4, the optical path difference is now 2 (l/2), or l. The two beams are again in phase with each other and result in another constructive interference.

When the mirror is moved at a constant velocity, the intensity of radiation reaching the detector varies in a sinusoidal manner to produce the interferogram output. The interferogram is the record of the interference signal. It is actually a time domain spectrum and records the detector response changes versus time within the mirror scan. If the sample happens to absorb at this frequency, the amplitude of the sinusoidal wave is reduced by an amount proportional to the amount of sample in the beam. Extension of the same process to three component frequencies results in a more complex interferogram, which is the summation of three individual modulated waves. It is a complex summation of superimposed sinusoidal waves, each wave corresponding to a single frequency. When this IR beam is directed through the sample, the amplitudes of a set of waves are reduced by absorption if the frequency of this set of waves is the same as one of the characteristic frequencies of the sample. The interferogram contains information over the entire IR region to which the detector is responsive.

A Fourier transformation, which is a mathematical operation, converts the interferogram (a time domain spectrum displaying intensity versus time within the mirror scan) to the final IR spectrum, which is the familiar frequency domain spectrum showing intensity versus frequency.

In Figure 2.18 the FT spectrometer structure and operation is schematically represented.

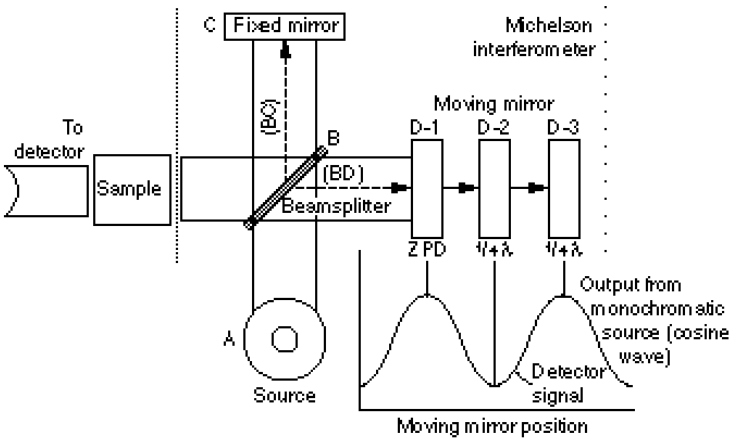

Figure 2. 18: FT spectrometer structure and operation scheme.

Because of complex interactions of atoms within the molecule, IR absorption of the functional groups may vary over a wide range. However, it has been found that many functional groups give characteristic IR absorption at specific, narrow frequency ranges regardless of their relationship with the rest of the molecule. Generalized tables of the positions and relative intensities of absorption bands have been established and used to determine the functional groups present or absent in a molecule. Moreover, multiple functional groups may absorb at one particular frequency range, but a functional group often gives rise to multiple-characteristic absorption. Thus, the spectral interpretations should not be confined to one or two bands and the whole spectrum should be examined.

For the purposes of this work, the samples have been prepared by placing a small amount of the hydrogel between two layers of compressed KBr. Then, hydrogel spectra have been compared to those of the original nanoparticles.

Figure 2. 19: Infrared spectroscope.

2.2.3 Scanning Electron Microscope

A Scanning Electron Microscope (SEM) is an instrument that uses an electron beam to analyze a sample, up to nano and micro-scale, and form an image . This technique reveals information about external morphology, chemical composition, crystalline structure and orientation of the molecules that form the sample.

SEM presents some advantages over the light microscope:

- *Resolution*, defined as the least distance between two close point at which they can be detected as two separate entities, is about 10 nm in a SEM instead of the 200 nm of a light microscope. Resolving power of the microscope is not only influences by the quality or number of the lenses but also by the wavelengths of the light that is between 400 and 700 nm. Electrons have shorter wavelengths that provide a better resolution.
- *Depth of field*, defined as the height of a sample that appears in focus in an image, is 300 times higher in a SEM than in a common light microscope.
- *Microanalysis*, so the analysis of the sample to obtain information about chemical composition and structure, is possible with a scanning electron microscope.

A scanning electron microscope presents electron optics systems, instead of normal glass lenses in a LM (light microscope), because the beam used to analyze the sample is made by electrons that cannot be focused by glass lenses. LM and SEM have a common structure and they present analogous devices but all electrons microscopes have more complex operation, such as electron detectors, voltage supplies, electron optics systems and a vacuum equipment, indeed SEM operates under vacuum.

Another difference between LM and electron microscopes is that the samples must be conductive to be viewed, this is possible by coating the samples with a thin layer of metal or carbon.

An electron beam, whose position is controlled by scan coils, is produced at the top of the instrument, electrons are accelerated downwards and a fine beam is produced by passing through a combination of lenses and apertures. The fine beam hits the sample contained in a apposite area. The vacuum is made thanks to the usage of pumps. A number of signals is produced after the beam interaction with the sample and they are detected by detectors.

Since SEM can focus also in depth, it provides 3D images of the samples even if it is not a tridimensional technique.

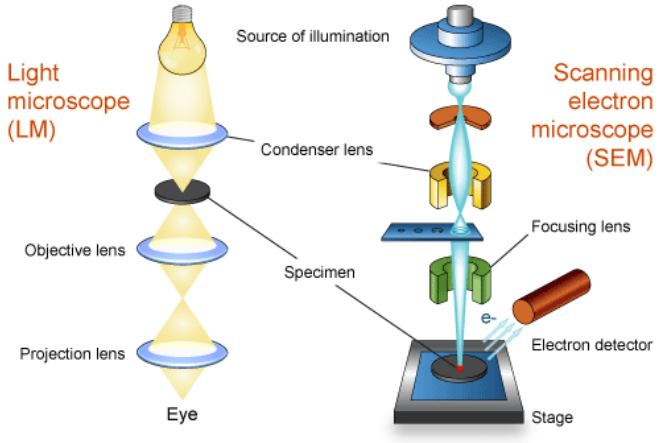

Figure 2. 20: Scanning electron microscope.

2.2.4 Transmission Electron Microscope

A Transmission Electron Microscope (TEM) has similar principles of a light microscope but uses electrons instead of light to provide information about morphology, composition and crystallographic characteristics of samples. TEMs are the most powerful microscopes, indeed they can reach a maximum magnification of 1 nanometer and they provide two-dimensional images, useful for a wide range of applications (life sciences, nanotechnology, medical, biological and material research). They can arrive on a molecular level to observe a nano-sized structure in depth and detail (Figure 2.21).

TEM consist of the following components:

- An electron source;
- Thermionic Gun;
- Electron beam;
- Electromagnetic lenses;
- Vacuum chamber;
- 2 Condensers;
- Sample stage;
- Phosphor or fluorescent screen;
- Computer.

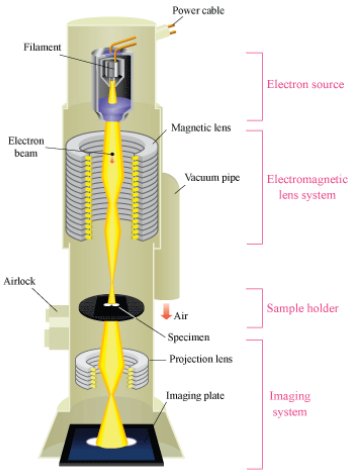

Figure 2. 21: Transmission electron microscope.

The two-dimensional images produced are high-resolution, black and white images made by the interaction between the samples that are investigated and the electron beam in the vacuum chamber. The instrument works under vacuum conditions because air has to be pumped out of the chamber to make it a suitable space where electrons can easily move. The beam passes through electromagnetic lenses to create a very thin electron beam. Then the beam passes through the specimen: depending on specimen density some electrons are scattered and cannot be collected, instead the unscattered electrons arrive at the bottom of the microscope where they hit a fluorescent screen and they are converted to a “shadow image” of the sample.

The sample need to have certain properties: to be sliced thin enough to let electrons to pass through, to be able to withstand the vacuum conditions of the chamber and to be prepared (dehydration, coating with conductive materials, sectioning, staining) before analysis.

The image presents zones with different darkness according to their density: the lighter areas are the ones where a larger number of electrons pass through the sample, the darker areas are the dense ones. Adjusting the voltage of the gun it is possible to manipulate the image because the speed of electrons is correlated to electron wavelength: if electrons move faster the wavelength is shorter and it is possible to obtain a better image.

As mentioned before, TEM images can provide information about structure, texture, shape and size of the sample.

This technique presents at the same time large advantages, such as high-quality images, wide-range applications and information, but also some disadvantages:

- TEMs are large and very expensive;
- Laborious sample preparation;
- Potential artifacts from sample preparation;
- Operation and analysis requires special training;
- Samples are limited to those that are electron transparent, able to tolerate the vacuum chamber and small enough to fit in the chamber;
- TEMs require special housing and maintenance;
- Images are black and white;
- TEMs are sensitive to vibration and electromagnetic fields, the need to be isolated;
- TEM is a high-cost technique.

2.2.5 Atomic Force Microscope

Atomic force microscope (Atomic Force Microscopy, AFM) permits the analysis of the structure, viscosity, elasticity, adhesion forces and friction and the dielectric characteristics of the sample.

A scanning force microscope is constituted by:

- *Piezoelectric scanner* which moves the sample in three directions;
- *A lever-type sensor*, said cantilever, with pyramidal tip which is sensible to interactions with the sample and to the possible movements of both vertical and horizontal directions;
- *A photodiode sensor* which records the movements of the laser beam in relation to those of the cantilever.

The technique involves various methods of operation that allow to study biostructures and to detect 3D profiles thanks to the scan made with a tip that is moved along x and y directions in two different operational modes: Contact Mode and Tapping Mode. The tip, located at the apex of a cantilever, is selected with an appropriate resonant frequency and elasticity depending on the operative mode and the characteristics of the analysed sample. The deflection of the cantilever moving on the surface of the sample is in the order of fractions of nm and it is due to forces acting on nanoNewton scale. To register and amplify these forces is used an optical system consisting of a laser beam that, hitting the upper part of the cantilever, is reflected on a photodiode that generates an output signal proportional to the position of the reflected beam on its surface. Through it, it is possible to detect the vertical and torsional movement of the tip.

The distance between the sample surface and the tip is kept constant thanks to a feedback circuit based on the signal from the photodiode and all movements are possible thanks to a piezoelectric that ensures movements precision along the three axes.

– Contact mode:

The tip is always maintained in contact with the surface of the sample. This mode is not recommended for the hydrogels which are too much sticky;

– Tapping mode:

The tip vibrates few nanometers far from the surface of the sample. It has only a transient contact with the surface of the sample. In non-contact mode, there is a reduction of the interference due to lateral forces and interactions that may damage soft samples, like micelles, gels etc. Tip vibration is close to its natural resonance frequency and the image reconstruction takes place by recording the variation of oscillation frequency. In these conditions Van der Waals attractive forces act. They are weakly dependent on distance, therefore it is not likely to obtain high lateral resolution.

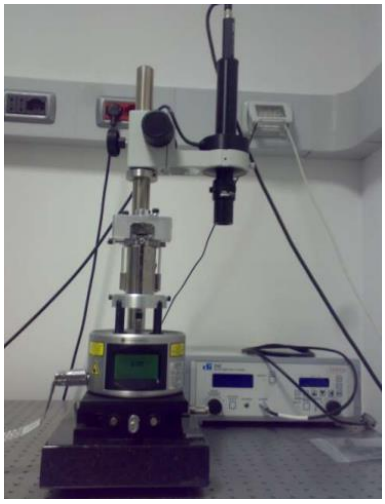

Figure 2. 22: Atomic force microscope.

2.3 Methods

The following paragraph is focused on the methods used to produce nanoparticles.

2.3.1 Synthesis of poly-(methyl-methacrylate)-based NPs

Poly-(methyl-methacrylate)-based nanoparticles (PMMA) are synthesized from MMA using MAA as co-monomer to improve their swelling properties. In this way, biocompatible NPs with high swelling ability can be obtained.

2.3.1.1 Batch reaction procedure

The experimental set-up used to synthetize nanoparticles of poly-methyl methacrylate consists of a 100 mL three necks glass flask where the reaction takes place under magnetic agitation and isothermal conditions.

Constant operating temperature of 80°C is guaranteed by an oil bath previously heated by a metallic hot plate. When the operating temperature is reached, the flask containing the reaction mixture is immersed in the oil bath.

The starting reaction mixture must contain monomer, co-monomer, if added, water and tenside. The quantity of tenside is expressed in percentage v/v of reactants. In poly-methyl methacrylate nanoparticles synthesis the principal monomer is MMA and the co-monomer is MAA. MAA is added in the reaction in order to confer to the final NPs the ability to swell if put in a basic environment.

The quantity of reactants depends on the desired concentration of nanoparticles dispersed in water, that represents latex concentration. In particular, to obtain a 20% concentrated latex, the reacting mixture must contain:

- 20 % v/v of reactants and eventually surfactants;
- 80 % v/v of water.

In this work the density of the materials is assumed to be 1 g/L, so the percentage v/v is considered approximately equal to w/w percentage. Different relative contents of the two monomers were employed in this work in order to obtain NPs of different composition.

In this work the percentage of MAA is fixed to 10%, except for the three proofs, while the percentage and the type of tenside change in each formulation.

The glass flask containing monomer, co-monomer, water and tenside is equipped with a reflux condenser and with a nitrogen flux for three times. When residual oxygen is removed, the initiator (KPS) can be injected through a syringe which perforates the rubber stopper which closes the flask. The initiator solution consists of 0.1 g of KPS dissolved in water.

The reaction is maintained under these conditions for 2 hours, then the obtained latex is filtered through a filter paper and placed in the fridge at 4°C.

Figure 2. 23: Emulsion polymerization set: batch mode.

2.3.1.2 Starved reaction procedure

Starved reaction procedure operates at the same conditions as batch procedure; the difference between the two modalities lie in the way the monomer are fed into the reactor.

The glass flask is filled with water, while the monomer, the co-monomer (MAA) and the tenside are added through two pumps to guarantee a constant flux in time. The first pump is loaded with MMA and MAA mixed together while the second pump is loaded with the tenside dissolved in water. The injection time is equal to one hour for both. The tenside is not added to the monomer because it is water-soluble while the monomer is not. The initiator is injected with a syringe when the first drop of monomer and tenside comes in contact with the aqueous phase. The initiator solution consists of 0.1 g of KPS dissolved in water.

The reaction is maintained under these conditions for 3 hours, then the obtained latex is filtered through a filter paper and placed in the fridge at 4°C.

A summary of all the tests is presented in Table 2.1 below:

	LATEX	MMA	MAA	Stabilizing agent	Stabilizing agent [%]	Reaction procedure
PMMA-1	5%	100%	0%	SDS	10%	BATCH
PMMA-2	5%	100%	0%	SDS	10%	STARVED
PMMA-3	20%	90%	10%	SDS	0.54%	BATCH
PMMA-4	20%	80%	20%	SDS	0.54%	BATCH
PMMA-5	20%	90%	10%	HEMA-SO_3-	1.08%	BATCH
PMMA-6	20%	90%	10%	HEMA-SO_3-	1.62%	BATCH
PMMA-7	20%	90%	10%	HEMA-SO_3-	5%	BATCH
PMMA-8	20%	90%	10%	HEMA-SO_3-	0.54%	STARVED
PMMA-9	20%	90%	10%	TWEEN80	10%	BATCH

Table 2. 1: PMMA tests with different composition.

2.3.2 Synthesis of HEMA-ε-polycaprolactone macromonomer

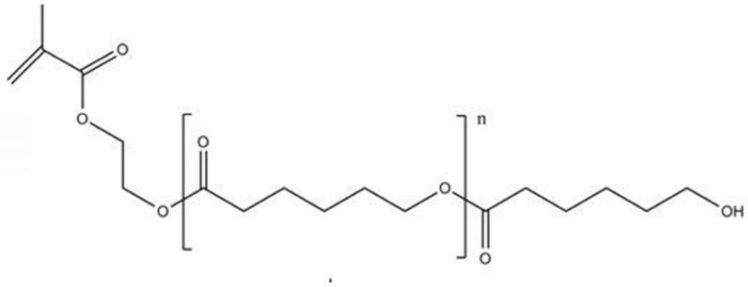

Figure 2. 24: HEMA-PCL_3 structural formula.

The synthesis of the macromonomer HEMA-poly(ε-polycaprolactone), hereinafter named HEMA-PCL_3, is carried out via a Ring Opening Polymerization (ROP) starting from two main components: ε-caprolactone, a cyclic ester, and 2-hydroxyethilmethacrylate (HEMA), a molecule bearing an –OH group and thus suitable as co-catalyst for a ROP process. Stannous octoate is the catalyst of the reaction that has the task to open the ring of ε-caprolactone; it is the only catalyst approved by FDA for this kind of reactions. Catalyst and co-catalyst react to form the alkoxyde that will be able to open the ring. HEMA can easily form the alkoxyde, and also be reactive for polymerization, thanks to its C=C bond, which is preserved at the end of the ROP procedure.

The HEMA-PCL_3 macromonomer obtained is shown in Figure 2.25. As it is evident it present in both ends of the structure groups that can easily react and polymerize.

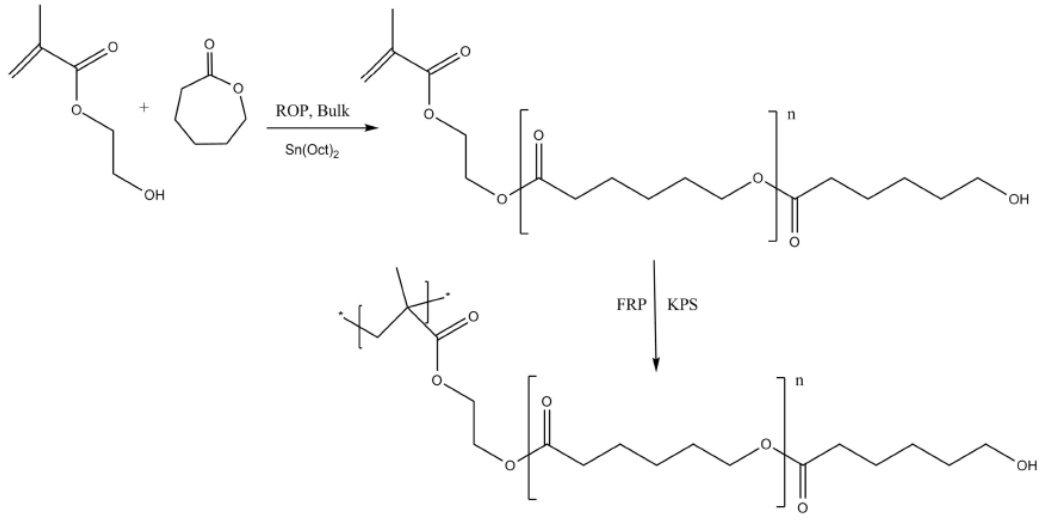

Figure 2. 25: HEMA-PCL$_3$ synthesis process.

The first step of the synthesis is the preparation of the alkoxyde that consists in mixing HEMA and stannous octoate in a 10 mL vial under specific molar ratios. At first stannous octoate is weighted in a range between 30 and 50 mg and the quantity of HEMA that is needed is calculated maintaining a ratio equal to 400 between HEMA and stannous octoate mass, as reported in the literature [citazione articolo di raffo]. The vial containing the catalyst and the co-catalyst is placed under magnetic agitation for 15 minutes at room temperature.

The ε-caprolactone quantity is arbitrarily chosen and the quantity of catalyst/co-catalyst mixture needed is calculated depending on the chain length required, in this case equal to 3. The ε-caprolactone is placed in a closed one-neck flask under magnetic agitation and heated with an oil bath at the temperature of 130°C. When the required temperature is reached, the proper amount of solution of HEMA and catalyst is added with a syringe. The system is maintained under these conditions for three hours to achieve complete conversion.

The obtained macromonomer is biocompatible and biodegradable.

2.3.3 Synthesis of HEMA-PCL3-based nanoparticles

HEMA-PCL_3-based nanoparticles are biodegradable materials synthesized with cyto-compatible stabilizing agents. Different compositions were varied in order to obtain the best-performing nanoparticles.

2.3.3.1 Batch reaction procedure

The experimental set-up used to synthetize nanoparticles of poly-caprolactone consists of a 100 mL glass flask where the reaction takes place under magnetic agitation and isothermal conditions.

Constant operating temperature of 80°C is guaranteed by an oil bath previously heated by a metallic hot plate. When the operating temperature is reached, the flask containing the reaction mixture is immersed in the oil bath.

The starting reaction mixture must contain water and tensides. The tensides used in this work are all water soluble. The quantity of tensides is expressed in percentage v/v of reactants.

Batch reaction procedure has been used to synthetize poly-HEMA-PCL_3 nanoparticles with different emulsifiers:

- HEMA-Ch+;
- HEMA-Ch+ + MAA;
- HEMA-SO_3- ;
- HEMA-SO_3- + MAA;

These condition were chosen with the aim of obtaining biodegradable NPs with negative (for the HEMA-SO3- case) or positive (for the HEMA-Ch+ case) charge with different dimension. MAA was added in some formulation to give to the final NPs the ability to swell if put in a basic environment. Different amount of stabilizing agents in respect to the HEMA-PCL macromonomer were used in order to obtain NPs of different dimensions.

The quantity of reactants depends on the desired concentration of nanoparticles dispersed in water, that represents latex concentration.

In particular, to obtain a 5% concentrated latex, the reacting mixture must contain:

- 5 % v/v of reactants;
- 95 % v/v of water.

The total amount of the mixture is 50 mL.

The 5% of reactants is divided into a certain percentage of tensides and the percentage referred to the macromonomer.

For example, if the nanoparticles are synthetized with the addition of 3% of choline and 5 % of MAA, the initial mixture will be divided as follow:

- 5% of reactants, which corresponds to 2.5 mL, that are subdivided into:
  - 3 % v/v of choline, so 0.075 mL;
  - 5 % v/v of MAA, so 0.125 mL;
  - 92% v/v of HEMA-PCL, so 2.3 mL.
- 95% of water, which corresponds to 47.5 mL.

The glass flask containing water and tensides is joined to a reflux condenser and inerted with a nitrogen flux for three times. When residual oxygen is removed, the HEMA-PCL_3 macromonomer is injected through a syringe which perforates the rubber stopper used to close the flask. Sometimes ethanol is added to HEMA-poly-caprolactone because its high density makes the injection difficult. After the addition of the macromonomer also the initiator is injected. The initiator consists of 0.04 g of α-α'-azodiisobutyramidine dihydrochloride for nanoparticles containing choline and 0.08 g of KPS for nanoparticles containing 3-Sulfopropyl methacrylate potassium salt or MAA. Since they are both solid powders they are dissolved in water before being injected.

The reaction is maintained under these conditions for 2 hours, then the obtained latex is filtered through a special filter paper and placed in the fridge for a good conservation.

2.3.3.2 Starved reaction procedure

Starved reaction procedure has been used to synthetize poly-HEMA-PCL_3 nanoparticles with different emulsifiers:

- HEMA-SO_3-;
- HEMA-SO_3- + MAA;
- MAA;
- HEMA-SO_3- + MAA + TWEEN 80.

Even in this case different quantities of stabilizing agents were used to obtain different dimension. It is worth to point out that positively charged NPs were synthetized only via batch emulsion polymerization because it was possible to obtain monodispersed positively charged NPs without having to employ starved polymerization.

The glass flask is filled with water and emulsifiers, while the macromonomer is added through a pump that guarantees a constant flux in time. The quantity of macromoner added is injected in 1 h. As mentioned in batch procedure, HEMA-poly-caprolactone is mixed with ethanol to make it less dense and to easily inject in the reactor. The initiator is injected with a syringe when the first drop of macromonomer comes in contact with the aqueous phase. The initiator solution consists of 0.08 g of KPS dissolved in water.

The reaction is maintained under these conditions for 3 hours, then the obtained latex is filtered through a filter paper and placed in the fridge for a good conservation.

Figure 2. 26: Pump for starved procedure.

Summary of the experiments:

	LATEX	HEMA-Ch+	MAA	HEMA-PCL_3	Reaction procedure
HEMA-Ch+ #1	5%	5%	0%	95%	BATCH
HEMA-Ch+ #2	5%	3%	5%	92%	BATCH
HEMA-Ch+ #3	5%	5%	5%	90%	BATCH
HEMA-Ch+ #4	5%	10%	5%	85%	BATCH
HEMA-Ch+ #5	5%	3%	10%	87%	BATCH
HEMA-Ch+ #6	5%	5%	10%	85%	BATCH
HEMA-Ch+ #7	3%	5%	15%	80%	BATCH

Table 2. 2: HEMA-Ch+ tests with different composition.

	LATEX	HEMA-SO_3-	MAA	Tween-80	HEMA-PCL_3	Reaction procedure
HEMA-SO_3- #1	5%	5%	0%	0%	95%	BATCH
HEMA-SO_3- #2	5%	5%	0%	0%	95%	STARVED
HEMA-SO_3- #3	5%	5%	10%	0%	85%	BATCH
HEMA-SO_3- #4	5%	5%	10%	0%	85%	STARVED
HEMA-SO_3- #5	5%	3%	5%	0%	92%	STARVED
HEMA-SO_3- #6	5%	3%	5%	10%	82%	STARVED

Table 2. 3: HEMA-SO_3- tests with different composition

2.3.4 Gelation methods

Synthesized nanoparticles are used to form biocompatible and biodegradable hydrogels for cell housing and drug delivery. Hereinafter, aggregation techniques and their theoretical principles are explained.

2.3.4.1 Diffusion Limited Cluster Aggregation Method

Gelation process for PMMA nanoparticles has been made following DLCA (Diffusion Limited Cluster Aggregation) approach. 1 mL of PMMA latex is placed in a small cuvette and an equal volume of PBS is inserted. The gelation effect can be seen at least after 2 hours when solid-like behavior can be observed. The aim of these experiment is to obtain biocompatible materials through the gelation of PMMA NPs in a slightly basic environment due to the presence of MAA. SDS was employed to stabilize the NPs; afterwards HEMA-SO_3- and TWEEN 80 were used in order to overcome the cytotoxicity issues related to the use of a ionic surfactant.

2.3.4.2 Aggregation of charged nanoparticles

In this paragraph hydrogel formation by aggregation of charged nanoparticles is described.

Choline-based PCL nanoparticles, containing MAA for its swelling properties, are positively charged, while 3-Sulfopropyl methacrylate potassium salt-based or MAA-based nanoparticles are negatively charged. Since the aggregation process occurs due to the electrostatic forces between the particles, the two different types of latex, oppositely charged, have to be mixed together.

Theoretically, complete and instantaneous precipitation of the produced NPs is obtained only at the isoelectric point, which means when all the charges of the starting latex (which can either be positive or negative) are balanced with the one coming from the other latex, which has to be added in the first one.

Therefore, in order to proceed rigorously, two selected amounts of latexes should be mixed together in order to reach the isoelectric point in the final solution. This approach however requires the knowledge of the precise density of charges present in a selected amount of latex. Such value is almost impossible to determine due to several reasons. First of all, no analytical technique can be applied to determine this value, at best only average and qualitative results can be obtained. Moreover, theoretical evaluation of this value is difficult due to the fact that is not possible to determine whether all the charges are located onto the NPs surface.

Therefore, a more qualitative and less rigorous approach was chosen. A certain volume of positively charged NPs latex is inserted in a 10 mL vial and the negative one is slowly dripped into it. The aggregation process is visible through the formation of a white sticky solid-like material and the dripping of the solution is stopped when it is evident a transition of the liquid from a white tone to an almost transparent one. The whole precipitation of the nanoparticles occurs after shaking manually the vial. In this way, a white aggregate is obtained (Figure 2.27) and the supernatant is totally transparent. Water is then removed and the hydrogel is examined with all techniques presented in paragraphs 2.4. Hydrogels are lyophilized to be preserved. Frames of the procedure are reported in Figure 2.28.

Figure 2. 27: Just formed hydrogel.

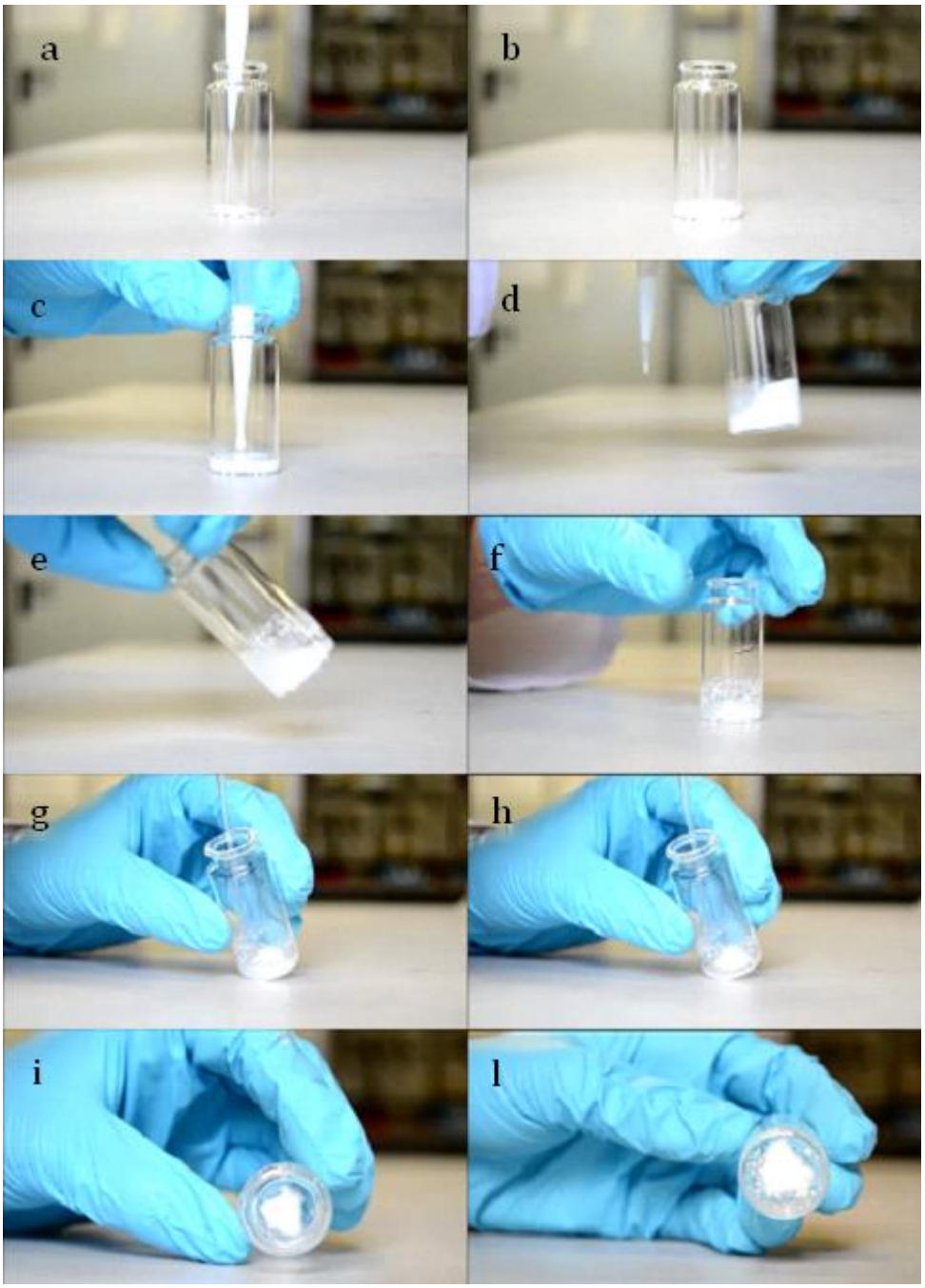

Figure 2. 28: Frames of gelation via electrostatic NPs aggregation: a) Positively-charged NPs addition and b) in the vial; c) Dripping of negatively-charged NPs; d) Agitation; e),f) Hydrogel formation; g),h) Clear water removal; i),l) Focus on hydrogel.

2.4 Characterization methods

In this section are reported the methodologies used for the characterization of both NPs and hydrogels.

2.4.1 Nanoparticles size

NPs are analysed by Dynamic light scattering to determine their dimension. Their dimensions should be in the nanometric range with small values of PDI (polydispersity index), as an index of monodispersed latexes.

Samples for DLS analysis consist of few drops of nanoparticles dispersion mixed with distilled water, useful to dilute the solution, inside a cuvette, as shown in Figure 2.29.

Figure 2. 29: Cuvette for DLS characterization.

Resulting size-distribution plots are discussed in Chapter 3.

2.4.2 Composition and structure of NPs and hydrogels

Composition and structure of the hydrogel have been investigated through different tests in order to gather as many information as possible about the newly synthetized material.

Information about functional groups present in the NPs ase taken from Infrared spectroscopy analysis. Different NPs and hydrogel spectra were compared to understand which kind of chemical transformation was taking place during the formation of hydrogels. For both materials, the samples have been prepared by sandwiching the liquid (in the case of NPs) or the gel between two plates of KBr which are transparent to the infrared light. The resulting spectra are discussed in Chapter 3.

Pictures about the structure of the hydrogel are obtained by TEM, SEM, AFM techniques. Since preparation of the hydrogel sample for TEM analysis was not possible, only NPs pictures have been captured.

2.4.3 Gelation yield

Starting from different composition of NP dispersions to obtain the hydrogel, different results can be achieved. Indeed, depending on the composition, NPs are differently charged, and this parameter influences the behaviour of the final material.

Gelation yield reveals how much hydrogel is formed starting from a certain amount of NPs dispersion. This kind of measure has been applied only to hydrogels obtained by opposite-charge gelation technique, so the yield was calculated as the ratio between the mass of the solid after lyophilization and the effective mass of the initial NPs, both the positive and negative ones, as reported in Formula 2.2.

$$y_{hydrogel} = \frac{m_{solid}}{m_{NPs+} + m_{NPs-}}$$

Equation 2. 6: Gelation yield.

Where m_{solid} is the mass of the solid formed after lyophilization, m_{NPs+} is the actual mass of the positive nanoparticles used for aggregation, so computed by concentration tests, and m_{NPs-} the mass of the negative nanoparticles.

2.4.4 Drug loading and release

Positively-charged NPs were loaded with a near infrared dye, To-Pro3, and were used to produce To-Pro loaded hydrogels with the same methodology described above. Hydrogels were than tested concerning the *in vitro* release of the dye.

To-Pro was loaded onto the NPs by exploiting its lipophilic nature. At first the compound itself was dissolved in DMSO at a concentration of 1 mM. Then, 40 µl of the solution were mixed with 1 mL of positively charged NPs latex (HEMA-Ch+ 3% + MAA 5%). After magnetic stirring, the solution was then diluted down to a concentration of 1% using water.

As discussed above, 2 mL of To-Pro3 loaded NPs were employed for the synthesis of To-Pro3 loaded hydrogels by contacting them with 2 mL of the unloaded negatively charged NPs. The obtained hydrogel was put in 4 mL vial with PBS at 37°C (Figure 2.30). The release was studied by evaluating the dye in the supernatant.

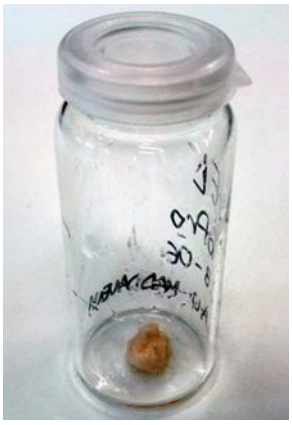

Figure 2. 30: To-Pro3 loaded hydrogel.

In order to determine whether the produced hydrogels are able to load and release also an hydrophilic compound the same procedure described for the case of To-Pro3 was applied also for Fluorescein. In this case, the dye was loaded in 2 mL of negatively charged NPs and then, the hydrogel was formed by dripping 2 mL of the positive ones (Figure 2.31).

Figure 2. 31: Fluorescein loaded hydrogel.

Small aliquots (100 µL) of the supernatant of both To-Pro3 and Fluorescein-loaded hydrogels were collected at certain time points and replaced by fresh PBS.

The amount of drug in the supernatant was measured by spectroscopy. Samples were withdrawn after: 6 h, 1, 2, 7, 14, 21 and 28 days. The amount of released drug was plotted for each time point. Resulting graphs are presented in Chapter 3.

2.4.5 Hydrogel swelling

The ability to absorb water is crucial for biomedical applications and for this reason the hydrogels were produced adopting NPs with different composition and different content of the swelling component (MAA) in order to optimize this parameter.

Swelling tests were done simultaneously for both fresh and lyophilized hydrogels. In general, a certain amount of hydrogel was put in 6 mL of water or PBS (Figure 2.32). At certain time points, water was removed from the samples and the hydrogel was weighed again. Chosen time points were: 0, 1, 4, 8, 24 and 120 hours.

The hydrogel swelling ratio was calculated as the difference between the swollen (m_s) and initial (m_i) mass divided by the initial mass.

$$q_{swelling} = \frac{m_s - m_i}{m_i} * 100$$

Equation 2. 7: Swelling ratio.

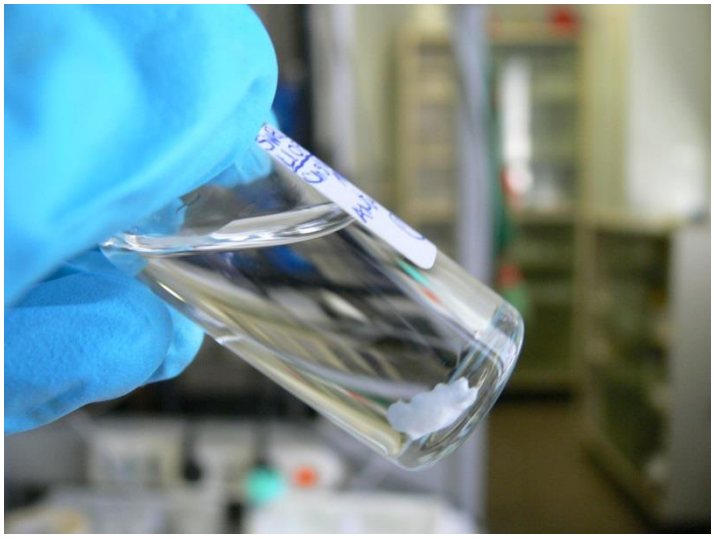

Figure 2. 32: Hydrogel swelling sample.

2.4.6 Hydrogel degradation

Degradation of hydrogel is an important parameter for the purposes of this work because it can be an index of biodegradability of the synthetized material. To make the environment of degradation more similar to the human tissues, PBS solution has been used.

After preparation of hydrogel samples, they have been weighed and inserted into 10 mL vials with the degradation liquid, PBS. They have been stored in two incubators: one operating at 37° C and one at 50° C. For each time point 6 samples were removed from the incubators: 3 at 37°C and 3 at 50° C. The initial weight was then compared to the weight of the hydrogel remained at those time points, previously frozen and lyophilized.

Degradation ratio was calculated as the difference between the degraded mass (m_d) and the initial mass (m_i) divided by the initial mass, as reported in Equation 2.8.

$$q_{degradation} = \frac{m_d - m_i}{m_i} * 100$$

Equation 2. 8: Degradation ratio.

The chosen time points were: 1, 7, 14, 28, 56 days. The trend of the degradation ratio with time is reported and examined in Chapter 3.

2.4.7 Cytocompatibility test

Cytocompatibility tests have been done at the "Istituto di ricerche farmacologiche Mario Negri".

The hydrogels were formed and extruded from the syringes into cell culture inserts (Falcon, 1.0 μm pore size). Murine fibroblasts (L929) were seeded in 24-well plates at concentration of 50000 cells/well in 1 mL complete medium and grown at 37 °C, 5% CO_2. After 24 h, the medium was changed and the inserts with 0.2 mL of the hydrogels were added in contact with the medium.

After 3 days of culturing, the cytotoxicity of hydrogels was evaluated by performing an MTS assay analogously to the cytotoxicity analysis of the individual gel components (Figure 2.33, 2.34).

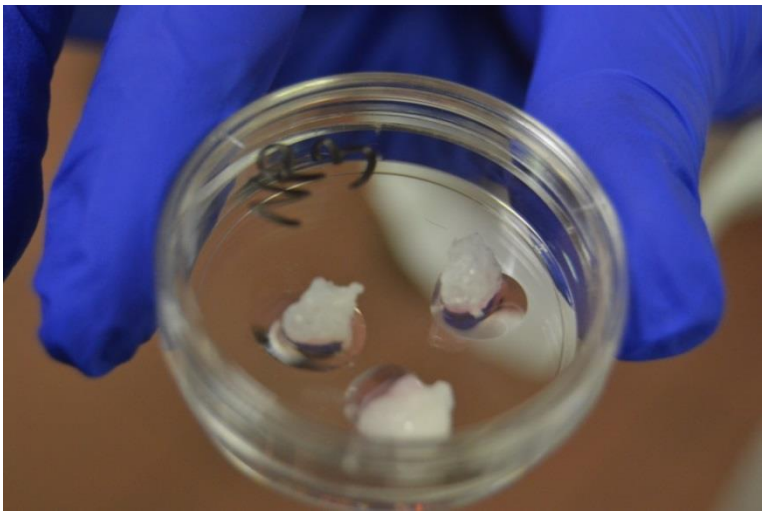

Figure 2. 33: Cell loaded hydrogel samples.

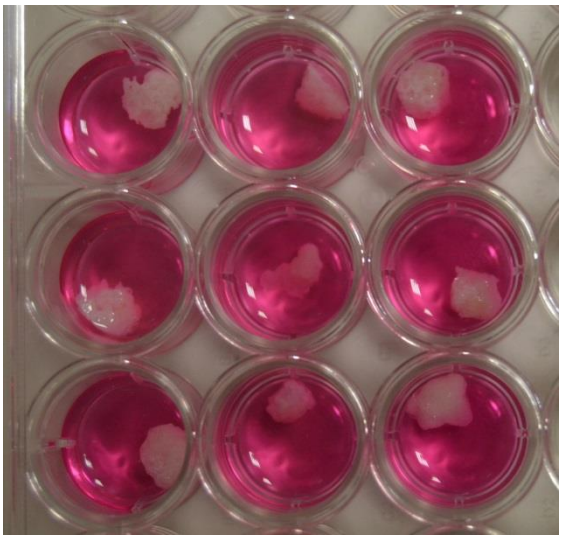

Figure 2. 34: Citocompatibility test samples.

Chapter 3

First part: MMA-MAA system

3.1 Results of MMA – MAA-based NPs and hydrogels

Nanoparticles of poly-(methyl-methacrylate) have been synthetized as described in paragraph 2.3.1 from methyl methacrylate and methacrylic acid as co-monomers. Different tests have been carried out in order to obtain hydrogels by diffusion-limited cluster aggregation technique (DLCA) using PBS solution, as described in Chapter 2. Surfactant type and percentage, reaction procedure have been modified to pursue this aim.

The tensides used are: SDS, HEMA-SO_3-, Tween 80. Their specific characteristics influence nanoparticles dimensions and, accordingly, their gelation capabilities, as will be explained in the following paragraphs. All the produced NPs have been summarized in Table 3.1.

	LATEX	MMA	MAA	Stabilizing agent	Stabilizing agent [%]	Reaction procedure
PMMA-1	25%	100%	0%	SDS	10%	BATCH
PMMA-2	25%	100%	0%	SDS	10%	STARVED
PMMA-3	20%	90%	10%	SDS	0.54%	BATCH
PMMA-4	20%	80%	20%	SDS	0.54%	BATCH
PMMA-5	20%	90%	10%	HEMA-SO_3-	1.08%	BATCH
PMMA-6	20%	90%	10%	HEMA-SO_3-	1.62%	BATCH
PMMA-7	20%	90%	10%	HEMA-SO_3-	5%	BATCH
PMMA-8	20%	90%	10%	HEMA-SO_3-	0.54%	STARVED
PMMA-9	20%	90%	10%	Tween 80	10%	BATCH

Table 3. 1: Table of the tests with different composition and surfactants.

The analysis of nanoparticles and hydrogel characteristics are divided for stabilizing agents in the following paragraphs.

3.1.2 Stabilizing agent: SDS

Previous works [1] proved that SDS was a good surface agent and the nanoparticles synthetized with it were able to form gels if put in a basic environment. As mentioned in paragraph 2.1.2.1, SDS is an ionic tenside. This characteristic makes it strongly effective in stabilizing the latex. As result, its quantity can be lowered up to the minimum quantity needed to form a stable hydrogel by addition of PBS.

Table 3.2 shows the quantities of co-monomers and stabilizing agent used for the experiments.

	LATEX	MMA [g]	MAA [g]	Stabilizing agent	Stabilizing agent [g]	Reaction procedure
PMMA-1	5%	2.542	0	SDS	0.253	BATCH
PMMA-2	5%	2.528	0	SDS	0.256	STARVED
PMMA-3	20%	9.089	1.024	SDS	0.054	BATCH
PMMA-4	20%	8.043	2.023	SDS	0.054	BATCH

Table 3. 2: Co-monomers and surfactant actual weights for nanoparticles with SDS.

PMMA-1 and PMMA-2 were first synthetized without using MAA as co-monomer, but its presence is essential for the swelling capability of the hydrogel.

Indeed, COOH groups increase the hydrophilic tendency, while its COO- groups amplify repulsive forces among particles, thus stabilizing the system. For all these reasons, MAA has been used as co-monomer for PMMA-3 using 0.54 % of SDS surface agent, which has been proven in previous works to be the minimum quantity to obtain a gel. Indeed, it has been the only sample which formed a stable hydrogel.

Trying to increase MAA content, PMMA-4 nanoparticles have been investigated, but the sample did not form a gel.

Nanoparticles dimensions, obtained by DLS measurements are reported in Table 3.3. It is evident how the diameter increases by decreasing SDS percentage.

	Diameter [nm]	**PDI**	**Stabilizing agent**	**Stabilizing agent [%]**	**Reaction procedure**
PMMA-1	38.9	0.073	SDS	10%	BATCH
PMMA-2	19.3	0.349	SDS	10%	STARVED
PMMA-3	122.3	0.192	SDS	0.54%	BATCH

Table 3. 3: NPs dimensions by DLS measurements for nanoparticles with SDS.

The dimensions of some samples which did not form a gel were not measured with DLS (i.e. PMMA-4).

The size distribution plot of PMMA-3, the only sample which did form a gel, is reported in Figure 3.1. It presented a mono-dispersed distribution.

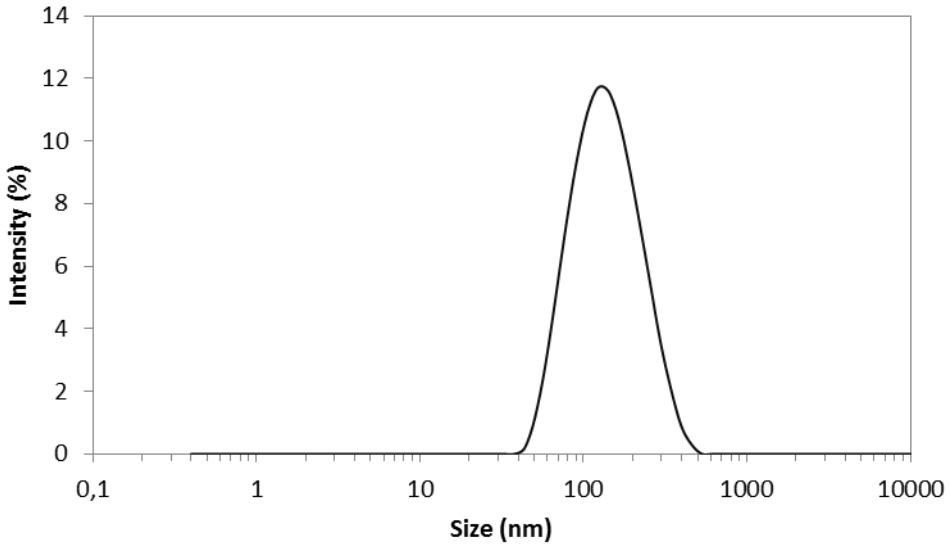

Figure 3. 1: Size distribution plot of PMMA-3. Size of the NPs in x-axis (nm) and intensity (%) in y-axis.

Although SDS was proven to be an effective tenside to form hydrogels by nanoparticles, because of its ionic nature it is cyto-toxic. For this reason, other cyto-compatible surface agents have been tested.

3.1.3 Stabilizing agent: HEMA-SO3-

HEMA-SO3- is an ionic compound. It has a shorter carbon chain than SDS, and this makes it less effective as tenside by lowering its amphiphilic nature. But, thanks to its terminal double bond, it can co-polymerize providing a fixed charge, that enhances repulsive forces among particles, thus stabilizing the system.

The nanoparticles, that were able to form a gel when stabilized with SDS, did not show the same behaviour with HEMA-SO_3-. Therefore, the percentage of surfactant has been increased gradually in PMMA-5, PMMA-6, up to 0.5 g in PMMA-7 without any result in terms of gel formation.

Finally, starved reaction procedure (PMMA-8) has been used to investigate whether if it could influence gelation process by varying nanoparticles characteristics.

Table 3.4 shows the quantities of co-monomers and stabilizer used for the experiments.

	LATEX [g]	MMA [g]	MAA [g]	Stabilizing agent	Stabilizing agent [g]	Reaction procedure
PMMA-5	20%	9.017	1.017	HEMA-SO_3-	0.111	BATCH
PMMA-6	20%	9.057	1.008	HEMA-SO_3-	0.162	BATCH
PMMA-7	20%	9.016	1.009	HEMA-SO_3-	0.500	BATCH
PMMA-8	20%	9.027	1.020	HEMA-SO_3-	0.055	STARVED

Table 3. 4: Co-monomers and surfactants actual weights for nanoparticles with HEMA-SO_3- .

Nanoparticles dimensions are reported below in Table 3.5. It is possible to observe that, as expected, with starved procedure resulting NPs are on average smaller. Since gelation did not occur for these kind of particles, not all the samples were measured.

	Diameter [nm]	PDI	Stabilizing agent	Stabilizing agent [%]	Reaction procedure
PMMA-5	426.3	0.014	HEMA-SO_3-	1.08%	BATCH
PMMA-8	250.5	0.057	HEMA-SO_3-	0.54%	STARVED

Table 3. 5: NPs dimensions by DLS measurements for nanoparticles with HEMA-SO_3- .

With this kind of stabilizing agent, not any gelification process has been observed, thus the tests have been focused on Tween 80.

3.1.4 Stabilizing agent: Tween 80

Tween 80 is a non-ionic, non-toxic, non-mutagenic and non-carcinogenic [30] surfactant used as emulsifier to synthetize PMMA nanoparticles. The stabilizing effect is due to steric hindrance of the surfactant branched structure. A high percentage of Tween 80 has been used in the experiment for its low effectiveness as surface agent. Just one test, PMMA-9, has been made with Tween 80 because even with a high percentage (10%) the nanoparticles where not able to form a hydrogel.

Table 3.6 shows the quantities of co-monomer and tenside used for the experiments:

	LATEX	MMA	MAA	Stabilizing agent	Stabilizing agent [%]	Reaction procedure
PMMA-9	20%	90%	10%	Tween 80	10%	BATCH

Table 3. 6: Co-monomer and surfactant used in the synthesis for nanoparticles with Tween 80.

3.1.5 Discussion

In conclusion, analyzing the results reported in the previous paragraphs, the PMMA-3 is the only system that presented a stable hydrogel after addition of PBS. The hydrogel formation for this system and not for the other ones was influenced by the type of surfactant added to the solution. As stated above, SDS is a strong ionic tenside that leads to smaller nanoparticles compared to HEMA-sulfate and Tween 80 systems. However, it is not cyto-compatible, as required for the desired applications.

The tests from PMMA-5 to PMMA-8 are all made with the addition HEMA-SO3- that is a weaker ionic surfactant: even varying the percentages of the tenside up to 5% there was no formation of a hydrogel. As mentioned above, it is a good stabilizing agent for its chemical structure, therefore aggregation by DLCA technique, adding a salt solution (PBS), is made harder.

The last experiment, PMMA-9, was carried on adding a steric tenside, Tween 80, to pursue the aim of this work to form a stable hydrogel made only by cyto-compatible and non-toxic compounds, but the hydrogel did not form.

It was not possible to achieve that goal by DLCA gelation of PMMA nanoparticles, so the work hereinafter was focused on synthesis and aggregation of charged HEMA-PCL3 nanoparticles; the results of this new investigated technique are presented in the following paragraphs.

Second part: HEMA-PCL$_3$ system

3.2 Results of HEMA-PCL$_3$-based NPs

The interest of the second part of the work has been focused on HEMA-PCL$_3$-based NPs. As explained in Chapter 1, using stabilizing agents, such as HEMA-Ch+ and HEMA-SO3-, it is possible to synthetize NPs that present fixed charges, respectively positive and negative. The presence of charges allows the hydrogel formation when the opposite charged NPs come in contact.

The following paragraphs are focused on the characterization of positively and negatively charged NPs. Dimensional and structural features are reported below. Nanoparticles composition is varied in order to analyze how it can influence hydrogel properties. So the choice of the best composition of nanoparticles is made considering hydrogel characteristics, as will be explained in paragraph 3.3.

3.2.1 Positively charged HEMA-PCL$_3$-based NPs

Positively charged nanoparticles are synthetized through emulsion polymerization of HEMA-PCL$_3$ with the use of HEMA-Ch+ as stabilizing agent. HEMA-Ch+, thanks to its terminal double bond, can polymerize with HEMA-PCL$_3$ and provide a positive charge with stabilizing effect. The reaction procedure is explained in paragraph 2.3.3.

The first synthesis of positively charged HEMA-PCL$_3$-based NPs was carried out with the composition indicated in table 3.7 :

	LATEX	**HEMA-PCL$_3$ [g]**	**HEMA-Ch+ [g]**	**Reaction procedure**
HEMA-Ch+ #0	5%	0.962	0.0635	BATCH

Table 3. 7: Actual composition of HEMA-Ch+ #0 NPs.

In order to improve the swelling property of the hydrogel, MAA has been used as co-monomer on further synthesis of the NPs. Varying the quantity of MAA used, its effect on the characteristics of the hydrogel has been investigated.

Also the amount of HEMA-Ch+ has been varied in order to examine the influence on NPs dimensions and hydrogel properties.

Table 3.8 summarizes the variation of MAA and HEMA-Ch+ content in the synthesis. Each combination presents a name used later on in the characterization part.

MAA / **HEMA-Ch+**	**5%**	**10%**	**15%**
3%	HEMA-Ch+ #1	HEMA-Ch+ #4	/
5%	HEMA-Ch+ #2	HEMA-Ch+ #5	HEMA-Ch+ #6
10%	HEMA-Ch+ #3	/	/

Table 3. 8: Nomenclature of HEMA-Ch+ NPs varying HEMA-Ch+ % in the column and MAA % in the raw.

Referring to the nomenclature above, Table 3.9 reports the actual weights of reactants used in the synthesis.

	LATEX	**HEMA-PCL_3 [g]**	**MAA [g]**	**HEMA-Ch+ [g]**	**Reaction procedure**
HEMA-Ch+ #1	5%	2.302	0.125	0.081	BATCH
HEMA-Ch+ #2	5%	2.251	0.128	0.172	BATCH
HEMA-Ch+ #3	5%	2.125	0.138	0.317	BATCH
HEMA-Ch+ #4	5%	2.186	0.254	0.121	BATCH
HEMA-Ch+ #5	5%	2.146	0.260	0.186	BATCH
HEMA-Ch+ #6	5%	2.043	0.385	0.157	BATCH

Table 3. 9: Actual composition of NPs with HEMA-Ch+ from #1 to #6.

Synthetized nanoparticles have been characterized in terms of dimensions and structure in the following paragraphs.

3.2.1.1 Nanoparticles size

Nanoparticles dimensions were investigated to confirm the presence of nanoparticles and to prove that their dimensions were in the nanometers range. Indeed, there was no necessity for the aggregation process to have a specific dimension of them.

DLS analysis, as previously explained, gives information about NPs dimensions through size distribution plots. Table 3.10 reports the average diameter and PDI (polydispersity index) values for all the compositions.

	Diameter [nm]	**PDI**
HEMA-Ch+ #1	143.48	0.087
HEMA-Ch+ #2	105.72	0.034
HEMA-Ch+ #3	77.58	0.034
HEMA-Ch+ #4	93.76	0.044
HEMA-Ch+ #5	74.26	0.119
HEMA-Ch+ #6	79.52	0.059

Table 3. 10: Dimensional characterization of NPs with HEMA-Ch+ through DLS measurements. Diameter and PDI are reported.

First of all, it is possible to observe how HEMA-Ch+ amount influences NPs diameter. Indeed, the higher the percentage of HEMA-Ch+, the smaller the particles. This is a peculiarity of emulsion polymerization reactions, because, increasing stabilizing agent amount, micelles size is reduced. Thus, resulting NPs are smaller as well.

This trend is remarked in Figure 3.2, where the diameter is plotted versus HEMA-Ch+ content (3%-5%-10%) at a fixed MAA concentration of 5 %.

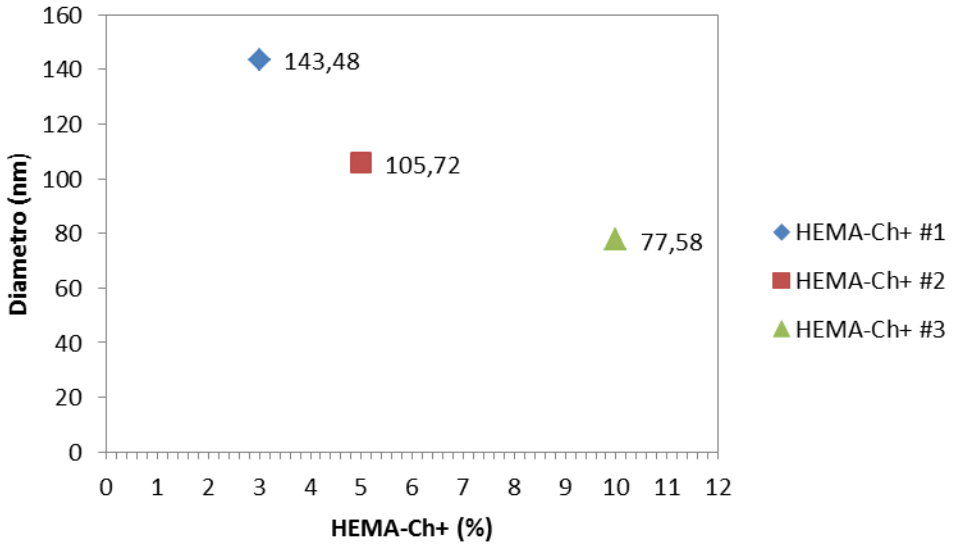

Figure 3. 2: NPs diameter versus different HEMA-Ch+ content. The HEMA-Ch+ increases in the x-axis.

The graph below (Figure 3.3) shows the size distribution of the NPs obtained by DLS measurements. In the x-axis, the average size values are reported in a logarithmic scale.

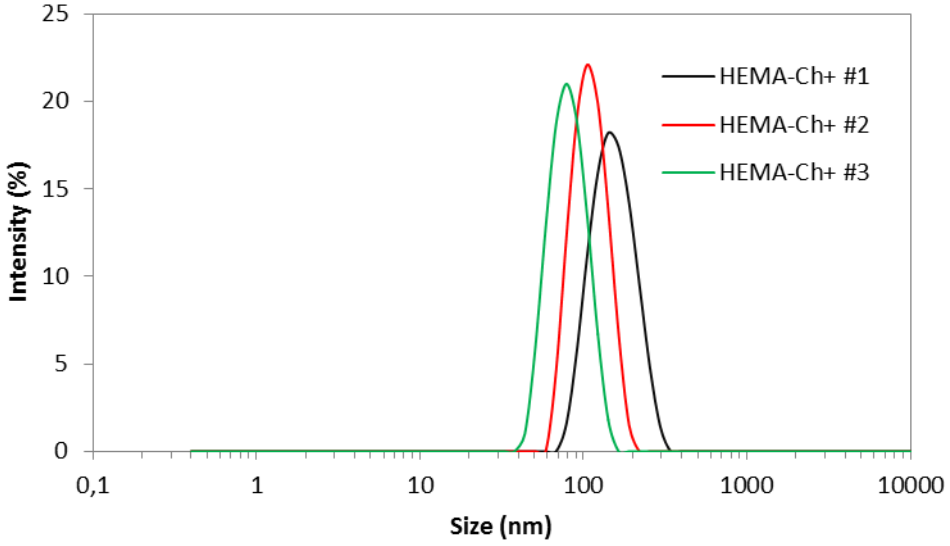

Figure 3. 3: Size distribution of HEMA-Ch+ #1, HEMA-Ch+ #2, HEMA-Ch+ #3 from DLS measurements. The peak intensity (y-axis) is related to the diameter (nm) in x-axis.

As observed above, increasing HEMA-Ch+ content, the peak mean intensity corresponds to a smaller size value (x-axis). PDI small values of the three measurements represent monodisperse distributions. Therefore HEMA-Ch+ was proven to be a good stabilizing agent with no necessity to use starved reaction procedure.

3.2.1.2 TEM characterization

The following pictures (Figure 3.4 and 3.5) are the images obtained by transmission electron microscope for HEMA-Ch+ #1 and HEMA-Ch+ #2.

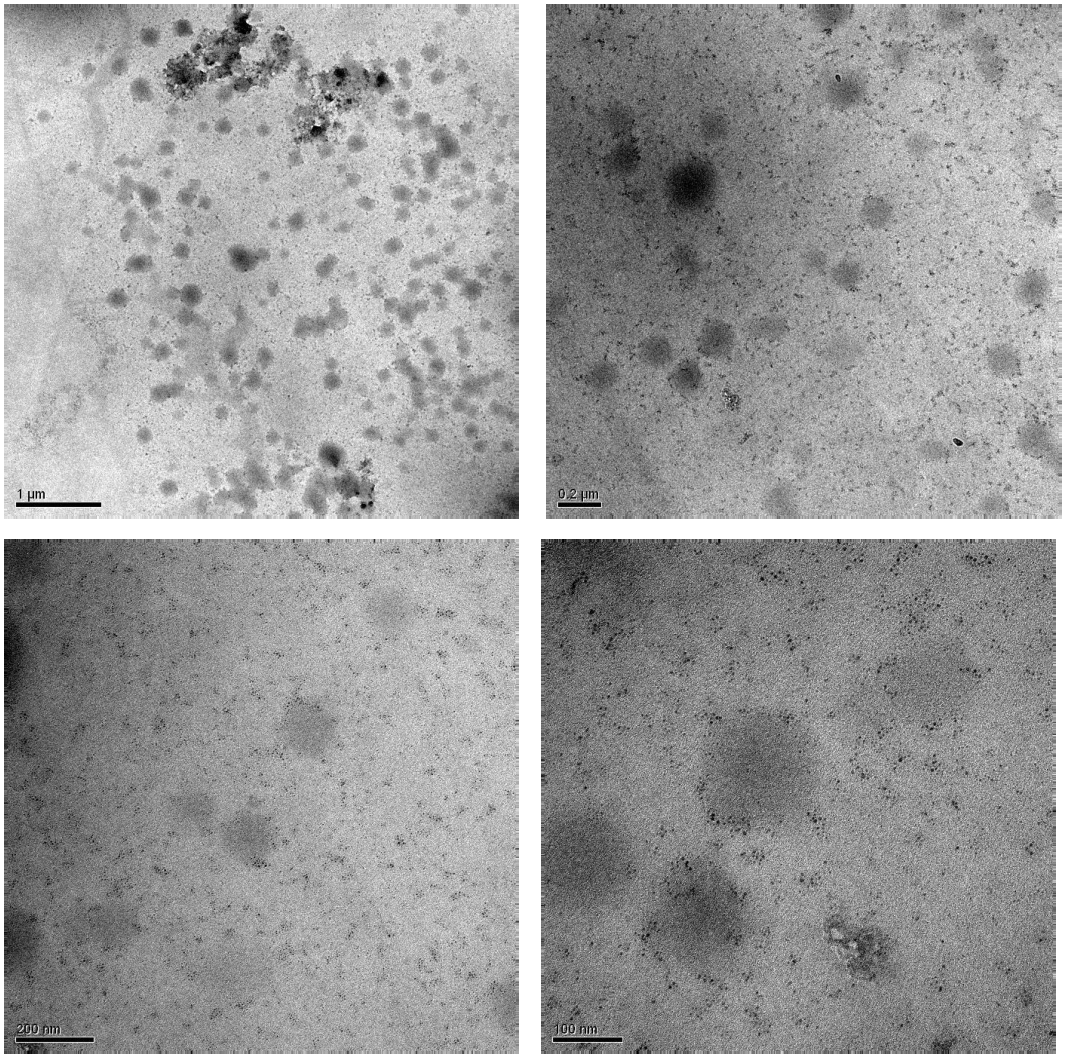

Figure 3. 4: TEM images of HEMA-Ch+ #1. Resolution of 1000 nm, 200 nm, and 100 nm. The NPs can be recognized as grey stains.

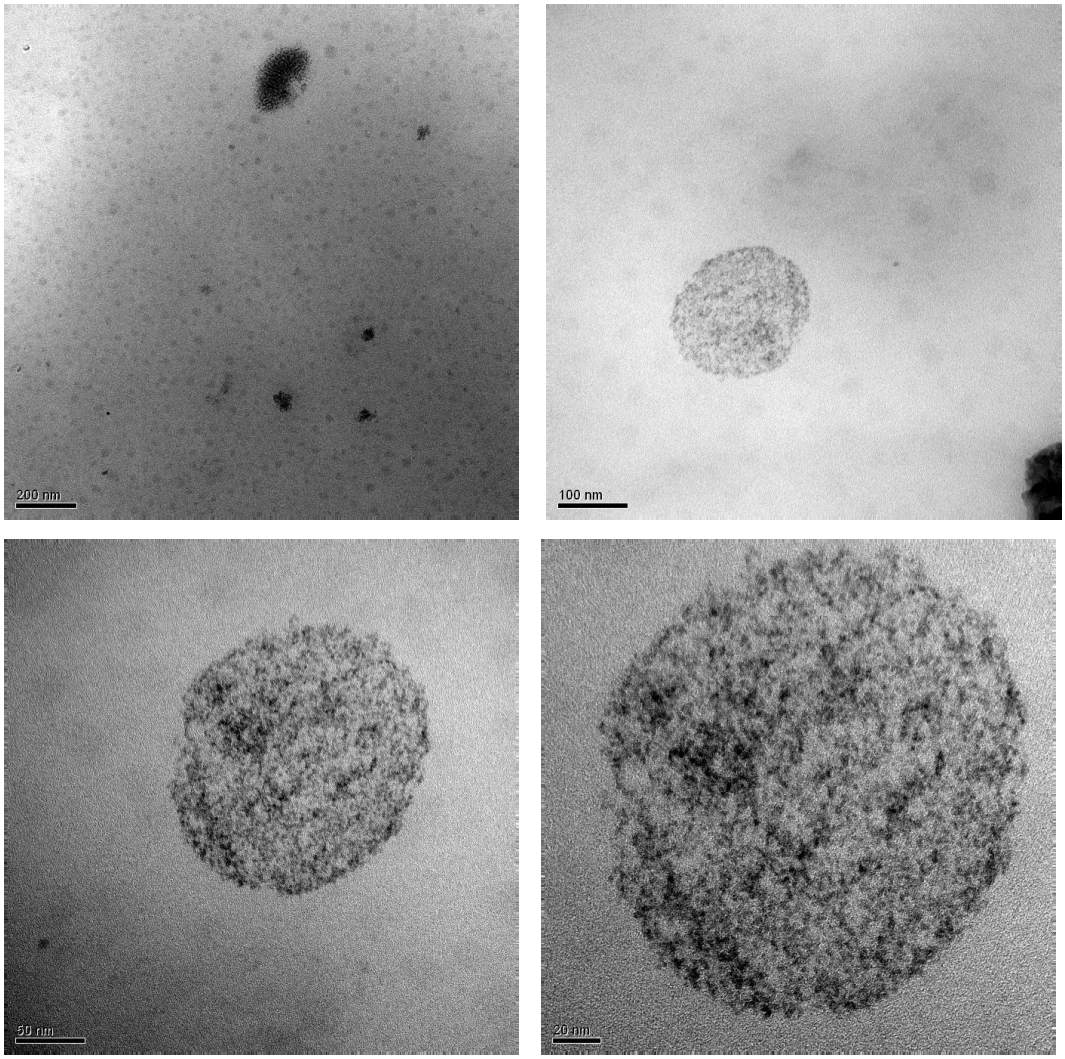

Figure 3. 5: TEM images of HEMA-Ch+ #2. Resolution of 200 nm, 100 nm, 50 nm, and 20 nm of the same NP.

The spherical and regular shape of the NPs is shown in the pictures above. The dimensions obtained by DLS technique are also confirmed by TEM images.

However, TEM characterization for polymeric materials is not the most advisable technique because the electron beam can damage the nanoparticles.

Other characterizations have been focused only on one kind of NPs, HEMA-Ch+ #1, those which demonstrated highest performances when used to form a hydrogel, as will be explained later on.

3.2.1.3 HEMA-Ch+ #1 nanoparticles: HEMA-Ch+ 3% - MAA 5%

The brief comparison among the different NPs characteristics, in order to choose which composition could be the best for the hydrogel, led to the choice of HEMA-Ch+ #1, which means 3 % of HEMA-Ch+ and 5 % of MAA.

First of all because the minimum quantity of HEMA-Ch+ (3 %) was proven to be enough to give a monodisperse stable colloidal dispersion with particles magnitude in the order of nanometers, so a higher amount of stabilizer was worthless.

Moreover, further investigations on the hydrogels formed from these NPs showed good properties in terms of swelling capability, degradation and mechanical behaviour.

Therefore, many samples of HEMA-Ch+ 3% and MAA 5% NPs have been prepared. The actual weights of the reactants are reported in Table 3.11. The name HEMA-Ch+ #1 followed by the progressive number indicates the same composition of the latexes.

	LATEX	HEMA-PCL_3 [g]	MAA [g]	HEMA-Ch+ [g]	Reaction procedure
HEMA-Ch+ #1-1	5%	2.302	0.125	0.081	BATCH
HEMA-Ch+ #1-2	5%	2.304	0.138	0.114	BATCH
HEMA-Ch+ #1-3	5%	2.329	0.131	0.134	BATCH
HEMA-Ch+ #1-4	5%	2.357	0.143	0.102	BATCH
HEMA-Ch+ #1-5	5%	2.301	0.137	0.110	BATCH
HEMA-Ch+ #1-6	5%	2.300	0.139	0.094	BATCH

Table 3. 11: Different synthesis of HEMA-Ch+ #1 NPs. Actual weights of the reactants.

3.2.1.3.1 Reproducibility

Nanoparticles size has been investigated by DLS technique and the obtained values are reported in Table 3.12 and plotted in Figure 3.6.

	Diameter [nm]	PDI
HEMA-Ch+ #1-1	143.48	0.087
HEMA-Ch+ #1-2	91.86	0.038
HEMA-Ch+ #1-3	105.46	0.036
HEMA-Ch+ #1-4	117.60	0.048
HEMA-Ch+ #1-5	114.76	0.082
HEMA-Ch+ #1-6	143.50	0.087

Table 3. 12: Dimensional characterization of NPs through DLS measurements for HEMA-Ch+ #1 from test 1 to 6.

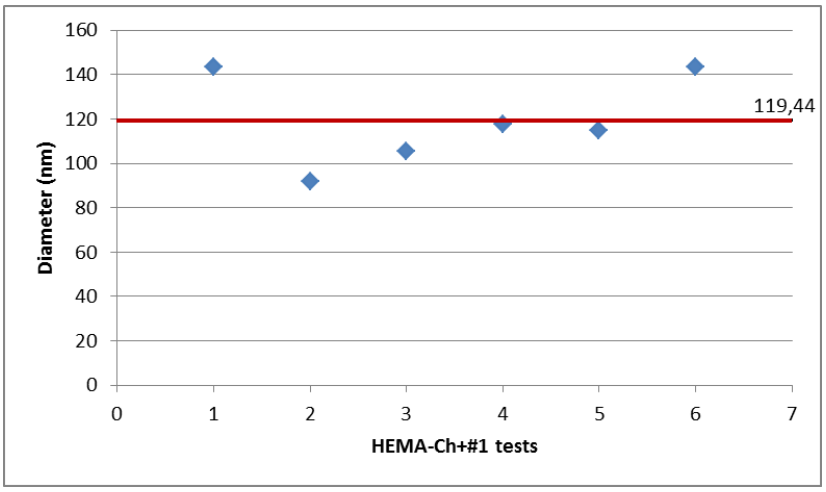

Figure 3. 6: Diameter (nm) of different HEMA-Ch+ #1 NPs and their average value. The tests are in x-axis from test 1 to 6.

For the tests made with the same composition small values of PDI have been obtained, so nanoparticles latexes are monodispersed. Moreover, Figure 3.6 shows similarity among the tests: this is an index of good reproducibility of the process. This process can be considered easily controllable and tunable.

3.2.1.3.2 Infrared spectroscopy

Infrared spectroscopy (IR) characterization has been carried on with the purpose of comparing NPs and hydrogel characteristics. Indeed, the aim of the test was not so much the characterization of the NPs, but rather to investigate on what was happening with their gelation.

Infrared analysis of HEMA-Ch+ #1 gave the spectrum in Figure 3.7.

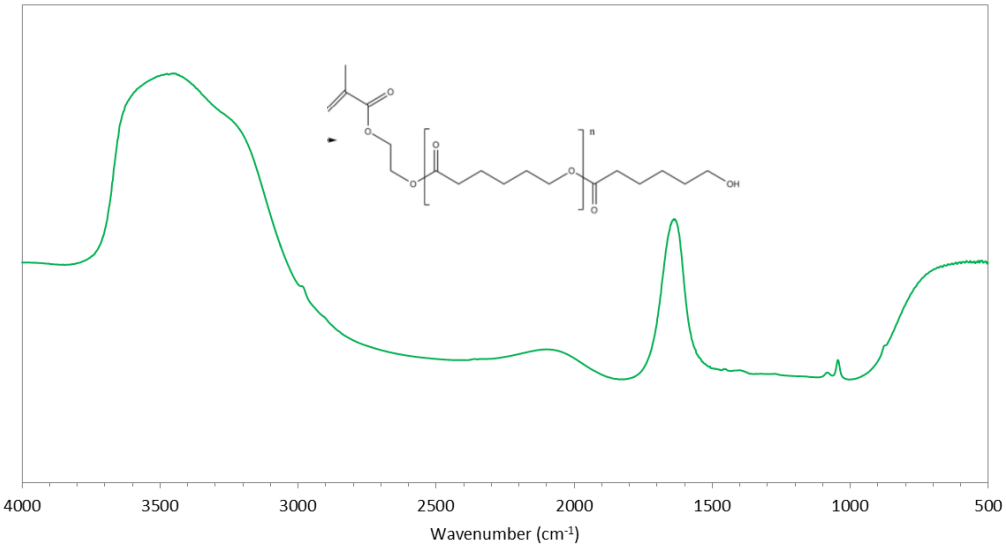

Figure 3. 7: IR spectrum of HEMA-Ch+ #1 NPs .

As explained in Chapter 2, IR spectroscopy gives information about functional groups present in the nanoparticles. The spectrum must be read from a qualitative point of view, so the magnitude of the peaks is not significant.

The wide peak between 3700 to 3000 cm^{-1} may correspond to O-H stretching vibration, while within 2960-2850 cm^{-1} there is a small peak due to C-H stretch of alkanes. The absorbance registered within 1760-1670 cm^{-1} can be attributed to C=O stretching vibration and the peak in the region 1200-1000 cm^{-1} can be due to C-O stretching vibration. All functional groups can be found in HEMA-PCL_3 structure, as indicated in the figure above.

3.2.2 Negatively charged HEMA-PCL_3-based NPs

Negatively charged nanoparticles are synthetized from HEMA-PCL_3 adding HEMA-SO_3- as stabilizing agent. HEMA-SO_3- presents a carbon double bond at the end of the chain, so it is able to co-polymerize and stabilize the nanoparticles thanks to its fixed charge. It provides negative charges on the surface of the HEMA-PCL_3-based nanoparticles, so they can easily aggregate with positively charged nanoparticles to form a macrostructure. Electrostatic interactions are the driving forces of the aggregation process.

In Table 3.13 are presented the actual weights of reactants used in the nanoparticles synthesis:

	LATEX	HEMA-SO_3- [g]	HEMA-PCL_3 [g]	Reaction procedure
HEMA-SO_3- #0	5%	0.1252	2.3790	BATCH
HEMA-SO_3- #1	5%	0.1280	2.3859	STARVED

Table 3. 13: Actual weights of reactants of HEMA-SO3- #0 and HEMA-SO_3- #1 NPs.

Two different ways of synthesis were used: at first the polymerization reaction was made in a “batch mode” but the nanoparticles obtained from this process presented a plurimodal distribution of characteristic diameter, so the “starved mode” was applied to control in a better way the dimensions of the nanoparticles. Moreover, for multimodal distribution, DLS becomes a less reliable technique. So, the obtained data are not representative of the real dimensions.

As shown in Figure 3.8, by adopting starved procedure it is possible to obtain a monodispersed latex.

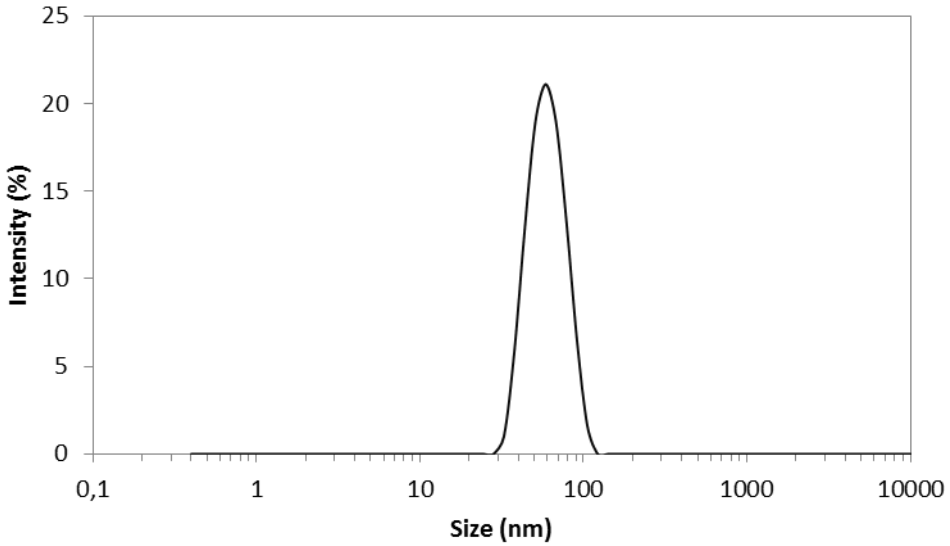

Figure 3. 8: : Size distribution from DLS analysis of HEMA-SO_3- #1. The peak intensity (y-axis) is related to the diameter (nm) in x-axis.

As mentioned for positively charged nanoparticles, MAA can be added to the starting mixture of reactants to improve swelling capability.

The combinations of HEMA-SO_3- and MAA and the actual quantities that have been tested are reported in Table 3.14.

	#	LATEX	HEMA-PCL_3 [g]	MAA [g]	HEMA-SO_3- [g]	Reaction procedure
HEMA-SO_3- #2	1	5%	2.1259	0.2662	0.1260	BATCH
	2	5%	2.133	0.256	0.1265	BATCH
HEMA-SO_3- #3	1	5%	2.1260	0.2610	0.1252	STARVED
HEMA-SO_3- #4	1	5%	2.312	0.143	0.0770	STARVED
	2	5%	2.3091	0.1304	0.0755	STARVED
	3	5%	2.3028	0.1320	0.0765	STARVED

Table 3. 14: Actual weights of reactants of HEMA-SO_3- #2, HEMA-SO_3- #3, HEMA-SO_3- #4 NPs.

The negatively charged nanoparticles latexes have been characterized by DLS technique: the obtained results are not reported because they all presented plurimodal distributions. Non-monodispersed latex could lead to non-reproducible behaviour in terms of gelation and final materials characteristics.

The presence of multiple peaks in the DLS analysis of the latex synthesized may be referred to the difficulty of polymerize HEMA-PCL_3 with both HEMA-SO_3- and MAA, indeed it led to the formation of aggregates.

The swelling properties of HEMA-PCL_3-based nanoparticles with only HEMA-SO_3 were not good enough to form a stable hydrogel with high production yield, as explained further on, so MAA was necessary in nanoparticles synthesis. Therefore, in order to overcome this issue nanoparticles composed only by HEMA-PCL_3 and MAA were synthesized; the negative charge is given by the -COOH group, which is dissociated in basic environment.

A fixed composition of MAA (10%) was used in the synthesis. Nanoparticles were synthetized by starved procedure and the diameters obtained by light scattering technique are provided in Table 3.15.

	#	Diameter [nm]	PDI
MAA #1	1	340,2	0,052
	2	325,6	0,083
	3	311	0,114

Table 3. 15: Dimensional characterization of MAA #1 NPs through DLS measurements. Diameter and PDI are reported.

Dimensional characterization has been made thanks to dynamic light scattering technique.

For MAA #1 the dimensions obtained are presented in Table 3.15. As it is possible to see in Figure 3.9, the latex was monodispersed.

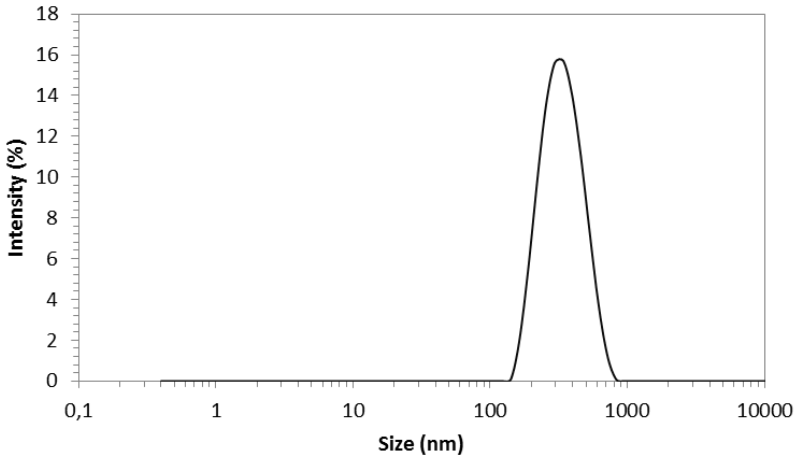

Figure 3. 9: Size distribution from DLS analysis of MAA #1. The peak intensity (y-axis) is related to the diameter (nm) in x-axis.

For the three tests made with the same composition it has been possible to obtain almost the same dimensions, as observable in Figure 3.10. This is an index of good reproducibility of the process, in order to obtain similar characteristics when the polymerization is carried out with the same parameters.

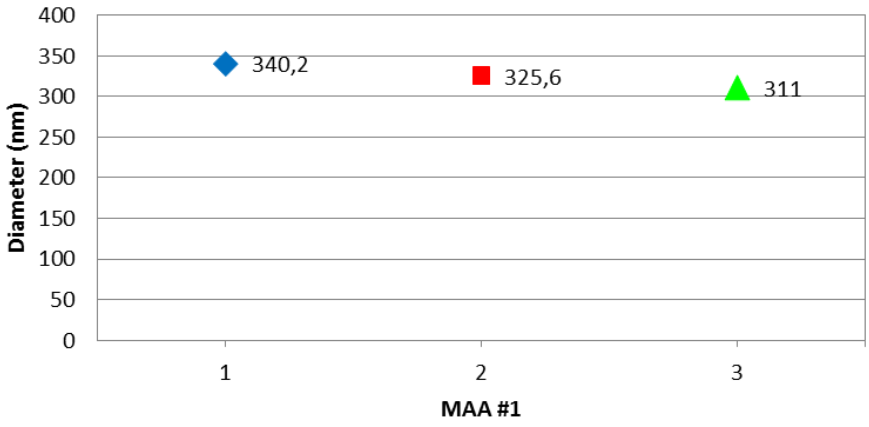

Figure 3. 10: DLS diameters for MAA #1: test 1,test 2 and test 3.

The results obtained by DLS technique shown a good reproducibility of this set of tests. The latexes of HEMA-PCL_3 with MAA are stable monodisperse colloidal dispersions and the nanoparticles present a spherical shape. The regularity of these particles is evident in the images obtained by a transmission electron microscope. The images are reported in paragraph 3.2.2.1 about TEM characterization.

The good dimensional characteristics of this formulation were not sufficient to obtain a stable hydrogel. While HEMA-SO_3- presents a fixed strong charge, MAA is negatively charged when dissociated in neutral pH solutions and this charge is probably not strong enough to form physical bonds that could resist to mechanical stress and dissolution in water or PBS.

Due to the problem of the last formulation, the work has been focused again on nanoparticles containing both MAA and HEMA-SO_3- in order to have fixed surface charge on the nanoparticles.

Tween 80, a steric tenside, non-toxic and compatible with cell, has been used to synthetize HEMA-PCL_3-based NPs with MAA and HEMA-SO_3.

The composition of the initial mixture containing also Tween 80 is shown in Table 3.16.

	LATEX	**HEMA-PCL_3 [g]**	**MAA [g]**	**HEMA-SO_3 [g]**	**Tween 80 [g]**	**Reaction procedure**
TWEEN #1	5%	2.0675	0.1486	0.0792	0.2603	STARVED

Table 3. 16: Actual weights of reactants for NPs synthesis of TWEEN #1.

Analyzing TWEEN #1 by DLS technique, a monodisperse distribution of diameters was obtained (Figure 3.11). Adding 10% of Tween 80 in the initial mixture it was possible to control the dimensions of the synthetized nanoparticles. It is cytocompatible and non-toxic for human cells, and it provides good stabilizing effect.

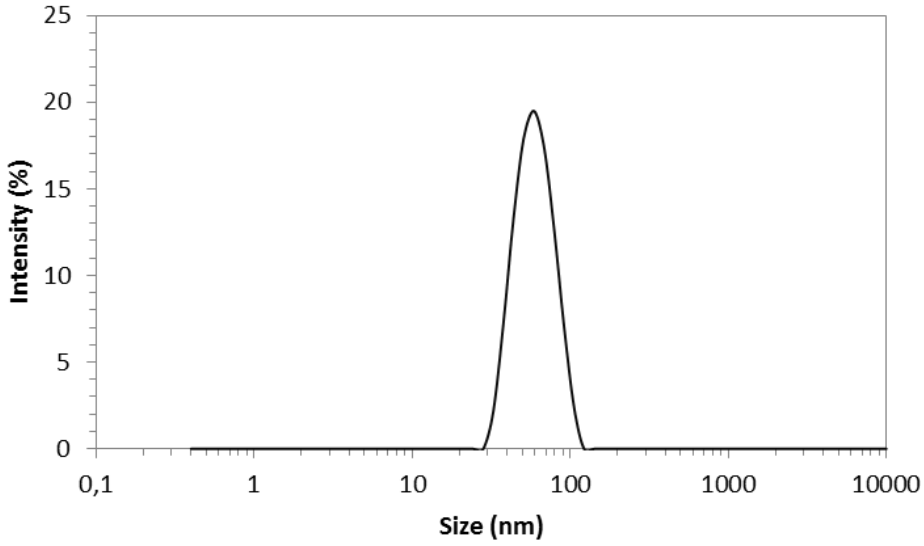

Figure 3. 11: Size distribution from DLS analysis of TWEEN #1. The peak intensity (y-axis) is related to the diameter (nm) in x-axis.

The polymeric HEMA-PCL_3-based nanoparticles composed of 3% HEMA-SO_3-, 5% of MAA and 10% of Tween 80, are the ones that shown better characteristics of stability and regularity. The hydrogel obtained by aggregation of TWEEN #1 nanoparticles and the positive ones, presented good mechanical and toxicological properties. To fully understand the choice of the nanoparticles relative to the formed hydrogel characteristics it is necessary to consult the following chapters where nanoparticles and hydrogel have been characterized.

3.2.2.1 TEM characterization

Transmission electron microscope provides information about morphology, composition and crystallographic characteristics of samples. The two-dimensional, black and white images show different darkness areas: the lighter ones are the ones where electrons can easily pass, in this case they correspond to water, the medium where nanoparticles are dispersed, while the darker ones are the dense parts of the colloidal solution, so they correspond to nanoparticles.

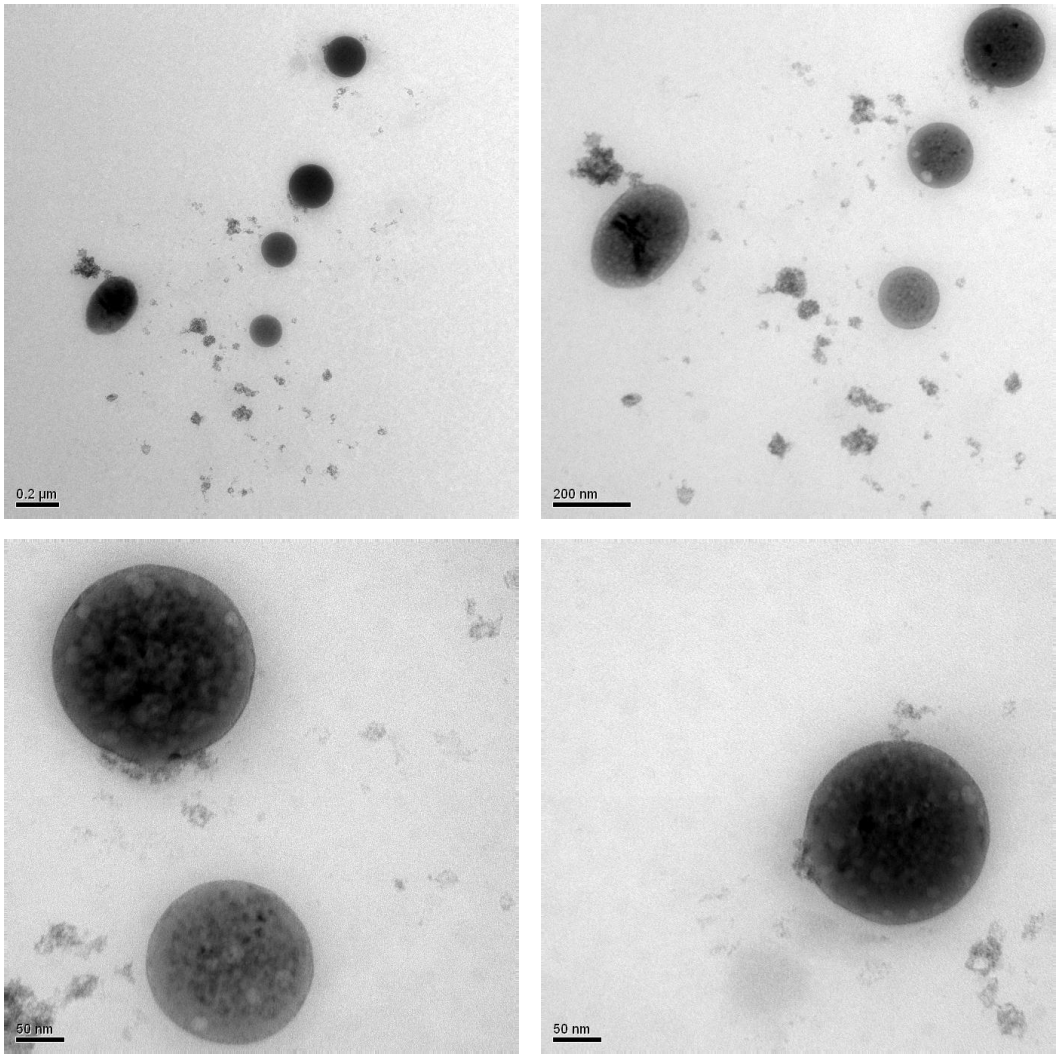

Figure 3. 12: TEM images of HEMA-SO_3- #0 . They have resolutions of 200 and 50 nm.

TEM images of HEMA-PCL_3-based nanoparticles with formulation HEMA-SO_3-#0 (Figure 3.12) show almost spherical and regular particles, the dark areas, immersed in water. In the first picture it is possible to notice that nanoparticles have different dimensions; indeed the light scattering measurements of the sample presented two peaks of different magnitude. Even HEMA-SO3- #4 nanoparticles have been analyzed by TEM (Figure 3.13).

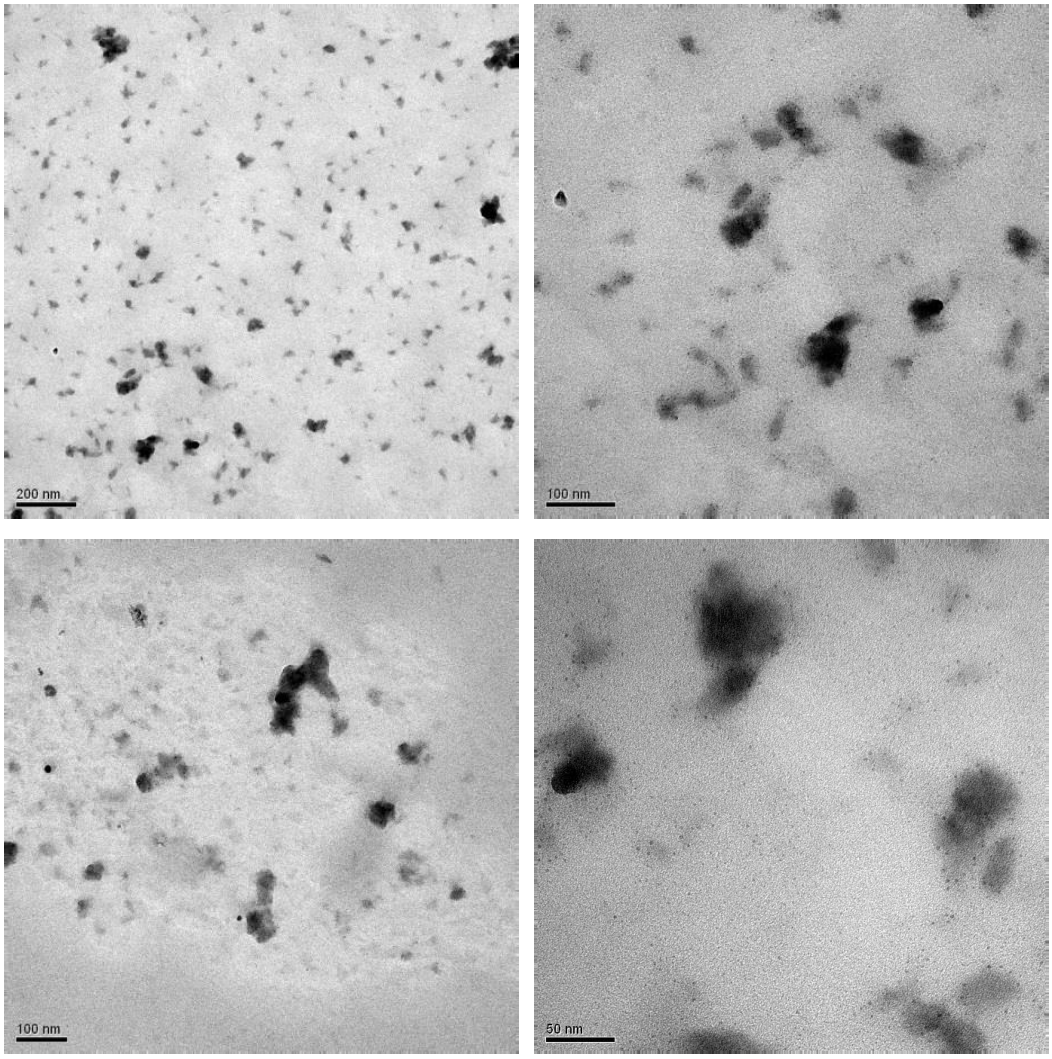

Figure 3. 13: TEM images HEMA-SO3- #4. They have resolutions of 200, 100 and 50 nm.

The images above represent in a qualitative way the light scattering measurements obtained for HEMA-SO3- #4. The latex obtained presented at least two peaks when analyzed by DLS technique, indeed, as above-mentioned this formulation shown a lot of impurities during the reaction process and a bad control of shape and dimensions of nanoparticles.

In the first image of Figure 3.13 there are agglomerates of big dimensions and also smaller and nearly spherical particles; as above-mentioned the reproducibility problem was evident and not negligible in this case. Images are not bright and clear, this can probably be referred to the difficulty of analyzing a polymeric sample with an electron beam.

On the other hand it has been possible to obtain almost spherical, regular and similar nanoparticles for MAA #1 composition (Figure 3.14).

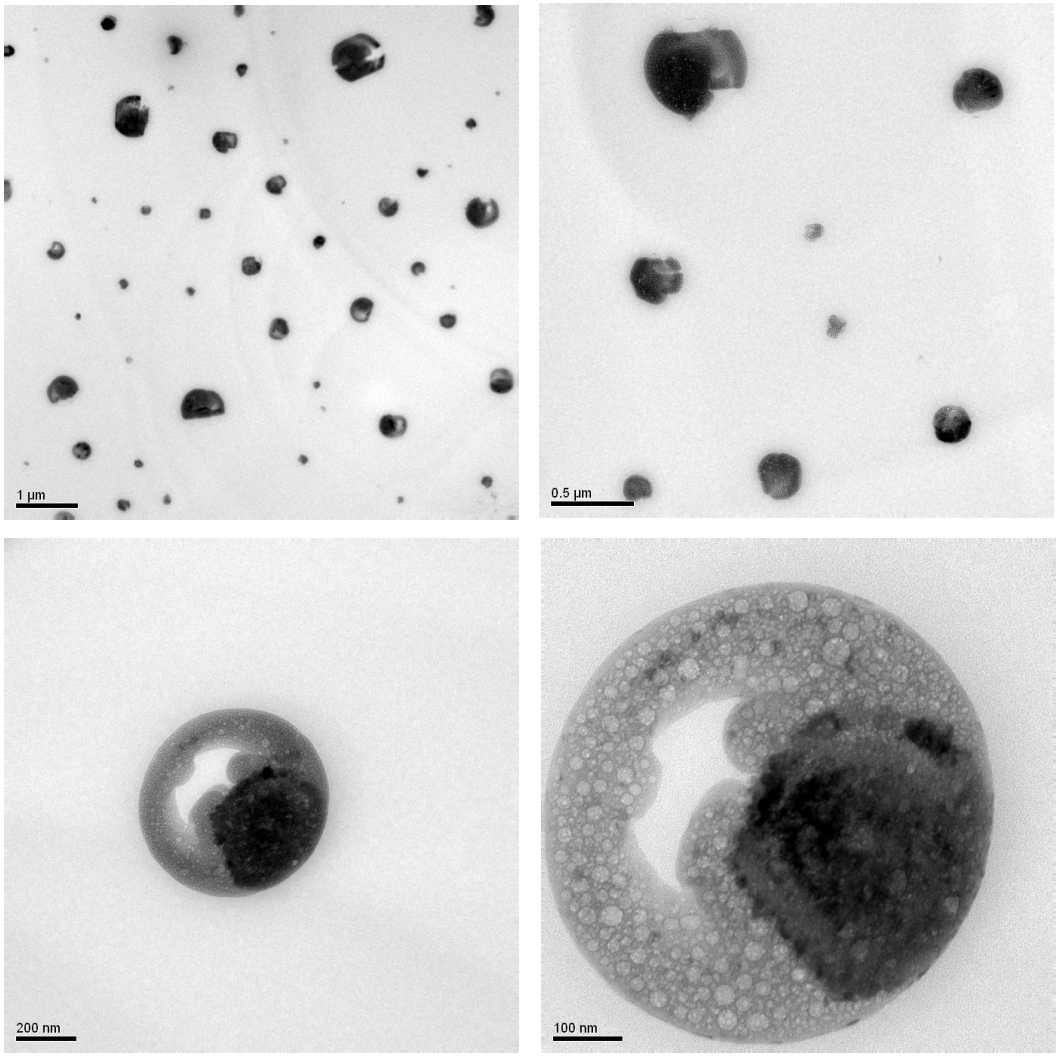

Figure 3. 14: TEM images of MAA #1. They have resolutions of 1000, 500, 200 and 100 nm.

In the last pictures is clearly visible the spherical shape of the polymeric nanoparticle.

3.2.2.2 Infrared spettroscopy

Infrared analysis of MAA #1 and TWEEN #1 gave the spectrum in figure 3.15 and 3.16, respectively.

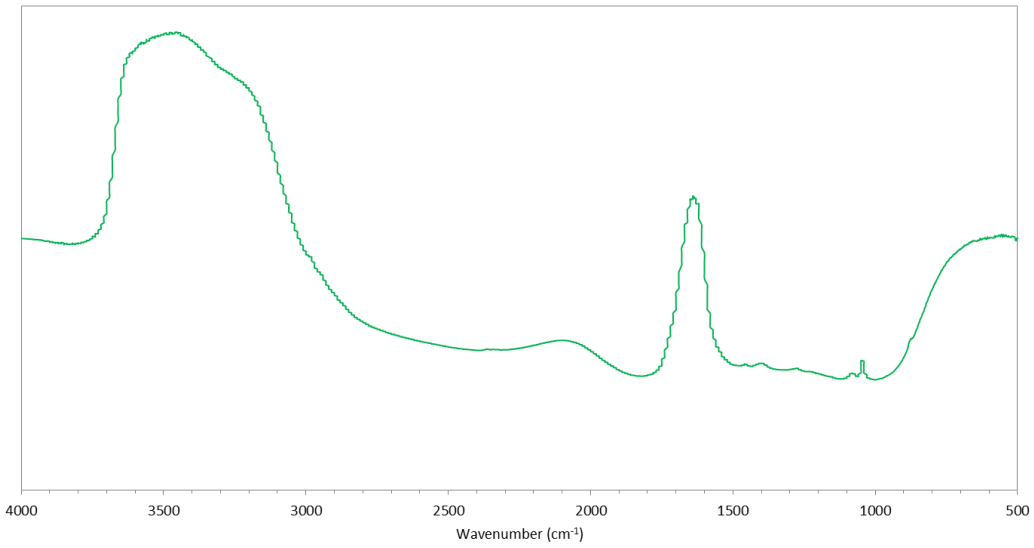

Figure 3. 15: IR spectrum of MAA #1 NPs.

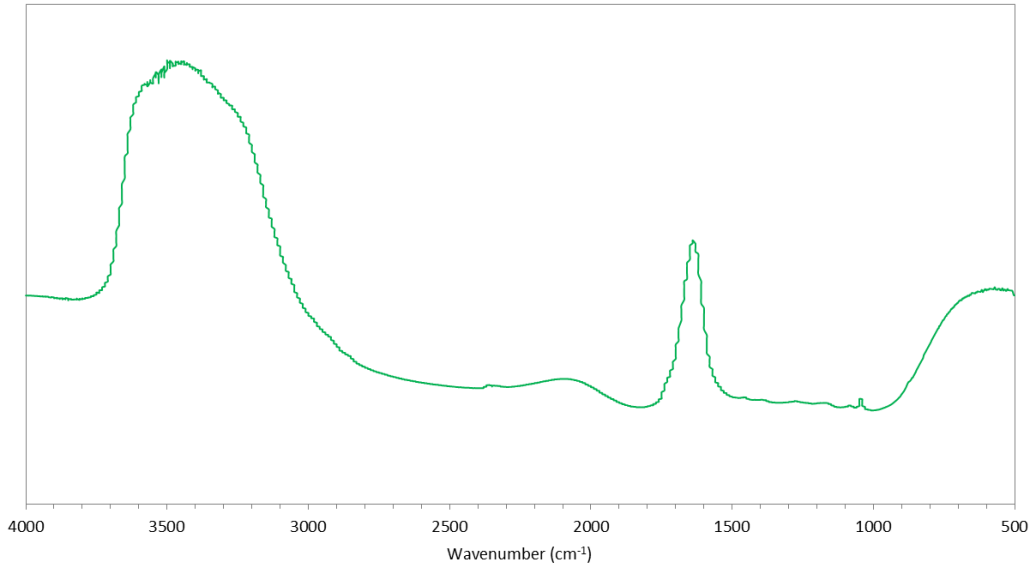

Figure 3. 16: IR spectrum of TWEEN #1 NPs.

Following the IR theoretical explanation of Chapter 2, it is possible to read the functional groups present in the synthetized polymer in the spectrum in figure. The spectrum is read from a qualitative point of view, not taking into account the magnitude of the peaks.

The wide region between 3800 and 3100 cm^{-1} corresponds to O-H stretching vibration. The first peak in the region between 1700-1600 cm^{-1} is referred to C=O bond of carboxilic acids and the second one in the region 1200-1000 cm^{-1} is due to C-O group.
Both the spectra, the first referring to MAA #1 and the second to TWEEN #1, present the same functional groups, that are the ones present in HEMA-PCL_3.

3.2.3 Discussion

The best formulation for positively charged nanoparticles consists of HEMA-Ch+ as stabilizing agent and MAA as co-monomer. Further studies about the best specific composition involve the characterization of the resulting hydrogel.

In the matter of negatively charged nanoparticles, nanoparticles synthesized with HEMA-SO_3- and MAA as co-monomer were chosen, but they need the addition of Tween 80 as stabilizing agent.

The choice is nevertheless linked to the characterization of the resulting hydrogel which will be the subject of the following paragraphs.

3.3 Hydrogel characterization

This chapter is focused on the characterization of the hydrogel obtained by HEMA-ε-Caprolactone NPs with opposite-charges aggregation technique. The first part deals with the choice of the best-performing formulation in terms of hydrogel stability. Later on, the chosen sample is characterized, as mentioned in Chapter 2, in a qualitative and quantitative way, including: IR, SEM, AFM analysis, gelation yield, swelling, degradation, drug release and cytocompatibility tests.

3.3.1. Description

The hydrogel is a white, sticky material with a quasi-spherical shape. Apparently, it presents good mechanical properties and elasticity.

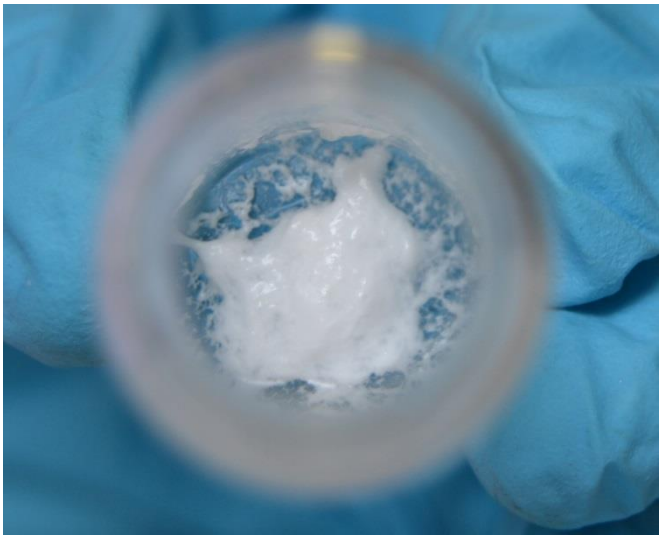

Figure 3. 17: Hydrogel.

Hydrogels have been synthesized starting from different NPs in order to analyze the influence of composition on their properties and stability. The combinations examined are pointed out in Table 3.17 together with the names that are used hereinafter to identify the hydrogel samples.

	HEMA-SO_3- #1	MAA #1	TWEEN #1
HEMA-Ch+ #1	/	HG1	HG2
HEMA-Ch+ #2	HG3	HG4	/
HEMA-Ch+ #3	/	HG5	/
HEMA-Ch+ #4	/	HG6	/
HEMA-Ch+ #5	HG7	HG8	/

Table 3. 17: Hydrogel samples.

Not all the combinations have been tested because the results obtained during the work influenced the operative choices, as it is explained in the following section.

3.3.2 Swelling test

Hydrogels capability of absorbing large amounts of water is the property that makes them potential materials for biomedical applications. Hydrogels can retain huge quantities of hydrophilic solution increasing their volume. Water entrapment in the inner empty spaces involves polymeric chains elongation thanks to their good mechanical and elastic properties.

Swelling tests have been made for both non-lyophilized and lyophilized hydrogels to analyze the different absorption capability and hydrogels stability. Hydrogels were weighed and inserted in 6 mL of deionized water or PBS 10x at room temperature. The diagrams below summarize hydrogels swelling ratio at 1, 4, 8, 24 and 120 hours. As presented in paragraph 2.4.5 swelling ratio is so defined:

$$q_{swelling} = \frac{m_s - m_i}{m_i} * 100$$

Equation 3. 1: Swelling ratio.

For non-lyophilized hydrogels m_i is the mass of the hydrogel immediately after its formation, while m_s is the wet swollen mass at certain time points. For lyophilized hydrogels m_i is the initial mass of the dry hydrogel and m_s is the wet swollen mass at certain time points.

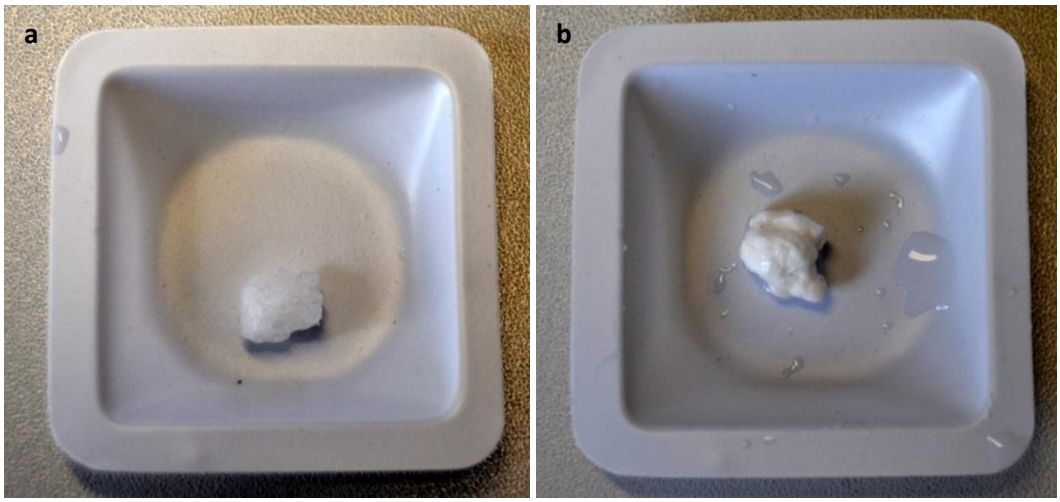

Figure 3. 18: Lyophilized hydrogel before (a) and after (b) swelling.

The initial mass of the hydrogels was usually in the range 30-60 mg in order to obtain similar results (Figure 3.18). Indeed, swelling process is probably influenced even by the ratio between hydrogels initial mass and supernatant. Samples with the same composition have been tested in parallel in order to obtain representative and reliable measurements.

Figure 3.19 presents swelling ratio in deionized water of non-lyophilized hydrogels with different composition. For the three hydrogels almost the same trends are obtained: hydrogels increase their mass in the first 24 hours, then they reach an asymptotic value (swelling equilibrium). Comparing these results with the ones of lyophilized hydrogels (Figure 3.20), it seems that lyophilized hydrogels present better swelling properties. Actually, this can be attributed to the water content already present into non-lyophilized hydrogels that decreases the amount of water they are able to absorb.

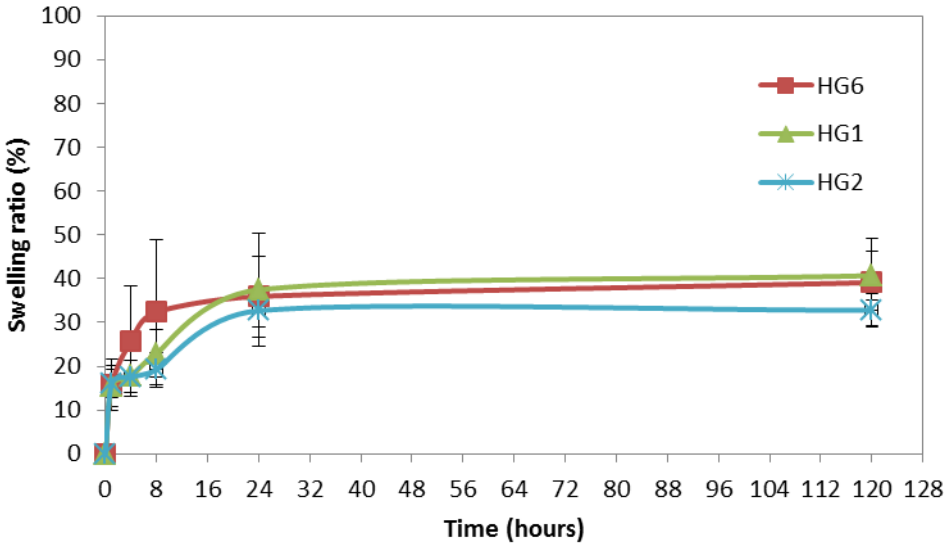

Figure 3. 19: Swelling ratio comparison of non-lyophilized hydrogels with different composition in H_2O. Error bars identify standard deviation.

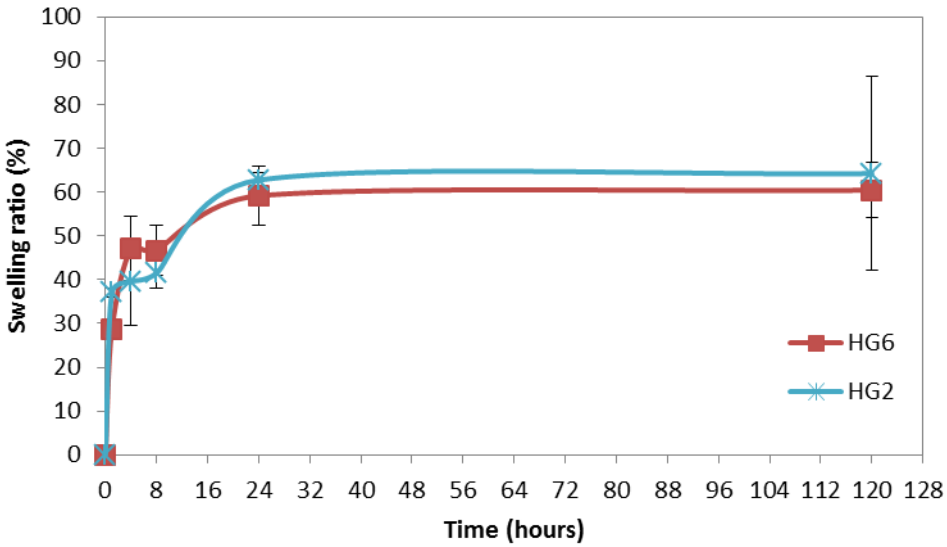

Figure 3. 20: Swelling ratio comparison of lyophilized hydrogels with different composition in H_2O. Error bars identify standard deviation.

In Figure 3.21 and 3.22, swelling ratios respectively for non-lyophilized and lyophilized hydrogels immerged in PBS 10x are shown.

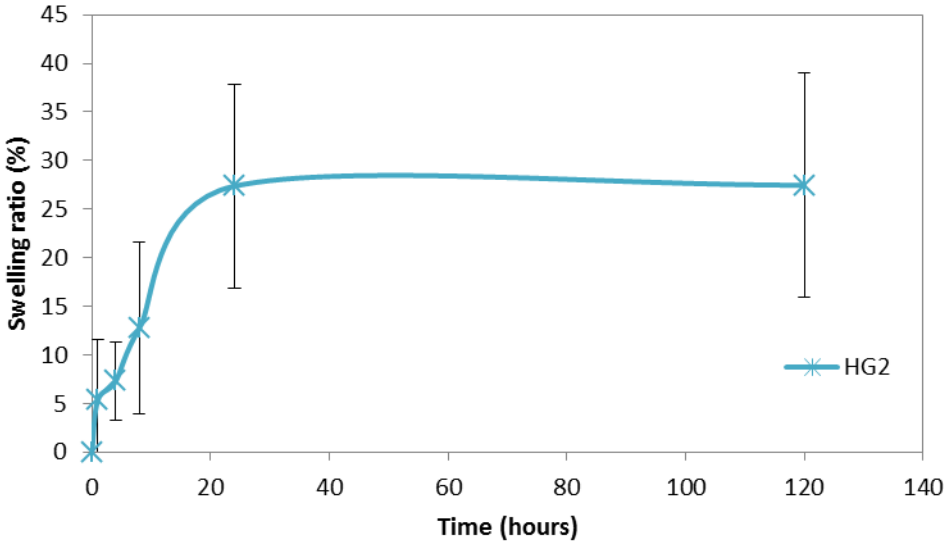

Figure 3. 21: Swelling ratio comparison of non-lyophilized hydrogels with different composition in PBS. Error bars identify standard deviation.

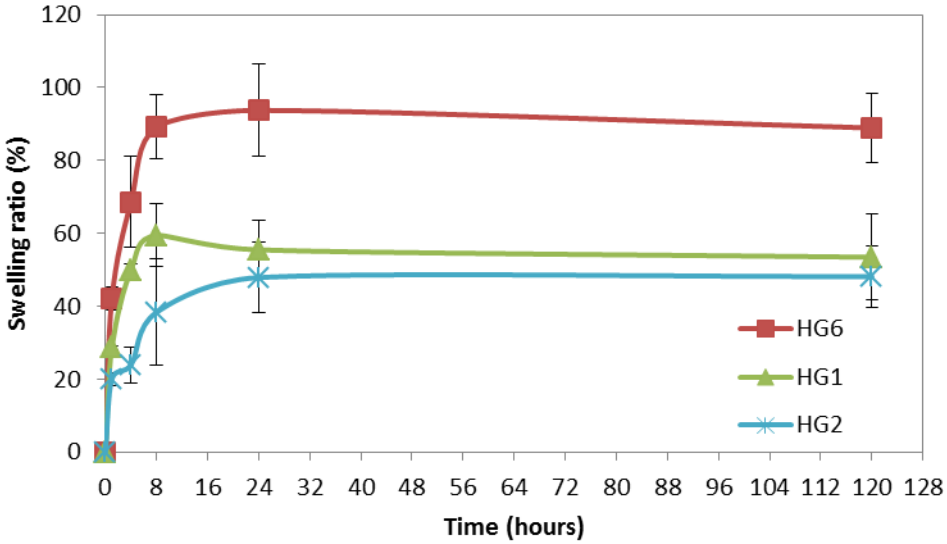

Figure 3. 22: Swelling ratio comparison of lyophilized hydrogels with different composition in PBS. Error bars identify standard deviation.

For what concerns non-lyophilized hydrogels, the results are present just for one composition, HG2, because the other tested samples were not stable. Indeed, PBS swelling tests made for hydrogels formed by negative HEMA-PCL_3-based nanoparticles containing only MAA (MAA #1) started degrading after few hours in PBS. In MAA #1 NPs, the negative charge is provided by the –COOH group, which is completely dissociated in basic environment. Apparently, the physical interaction between MAA #1 and positive NPs was not enough to resist to such ionic environment. Thus, degradation and loss of integrity occurred. The data are not reported in the graphs because it was not possible to measure the swelling due to the dissolution of the samples.

As regard lyophilized hydrogels in Figure 3.22, all the samples showed an upward trend with high swelling ratios.

Although the swelling equilibrium does not reach high values, the synthesized hydrogels can be considered superabsorbent because the equilibrium swelling is attained in small time.

All the values above present large error bars; this is due to the empirical error that inevitably affects the measures because of the sticky nature of the materials that is enhanced when immersed in a liquid medium.

Even if HG1 and HG6 showed good swelling properties, HG2 was the only one that remained stable when immerged in PBS, so it was chosen for further characterizations.

3.3.3 Hydrogel HG2 characterization

Following paragraphs deal with the characterization of the gel made with HEMA-Ch+ #3 and TWEEN #1. All the tests have been carried out to verify if the synthesized materials present the required characteristics to be applied as cell housing and drug delivery system, such as swelling capability, biodegradability, cytocompatibility and drug release.

3.3.3.1 Gelation yield

Different tests of HG2 composition show a gelation yield within the range of 60-100%. The variation interval is quite wide, it can be due to the difficulty of reaching the isoelectric point since it is almost impossible to predict the superficial charges present on the synthesized NPs. Gelation yields of each sample are reported in Figure 3.23.

The gelation yield can be computed as follows:

$$y_{hydrogel} = \frac{m_{solid}}{m_{NPs+} + m_{NPs-}}$$

Equation 3. 2: Gelation yield.

Where m_{solid} is the mass of the solid formed after lyophilization, m_{NPs+} is the actual mass of the positive nanoparticles used for aggregation, and m_{NPs-} the mass of the negative nanoparticles.

The actual mass m_{NPs+} and m_{NPs-} do not correspond to the theoretical latex concentration, so their value must be calculated with concentration tests. Concentration tests consist of evaporation of the solvent for 15 minutes at 150°C.

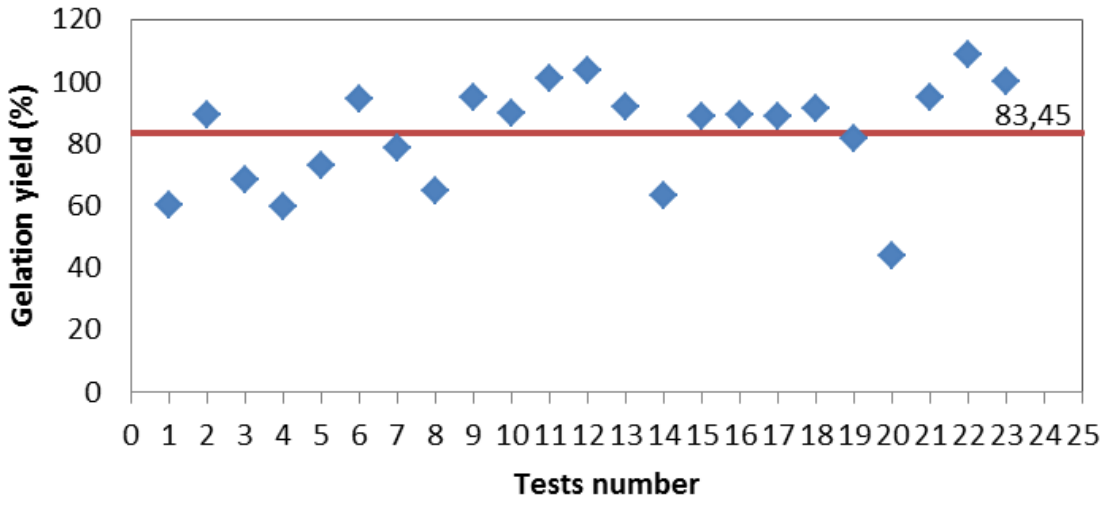

Figure 3. 23: Statistical gelation yield.

3.3.3.2 Infrared spectroscopy

As explained in Chapter 2, IR spectroscopy gives information about functional groups present in the material. The aim of this characterization is to examine whether if specific bonds are created or broken during the aggregation by comparing NPs and hydrogel spectra. The spectrum must be read from a qualitative point of view, so the magnitude of the peaks is not significant.

Referring to Figure 3.24, as well as for NPs, the wide peak between 3700 to 3000 cm^{-1} may correspond to O-H stretching vibration, while within the range of 2960-2850 cm^{-1} there is a small peak due to C-H stretch of alkanes. The absorbance registered within 1760-1670 cm^{-1} can be attributed to C=O stretching vibration and the peak in the region 1200-1000 cm^{-1} can be due to C-O stretching vibration.

In conclusion, not many changes occurred during the gelation process. This demonstrates that, as expected, no covalent bonds are created.

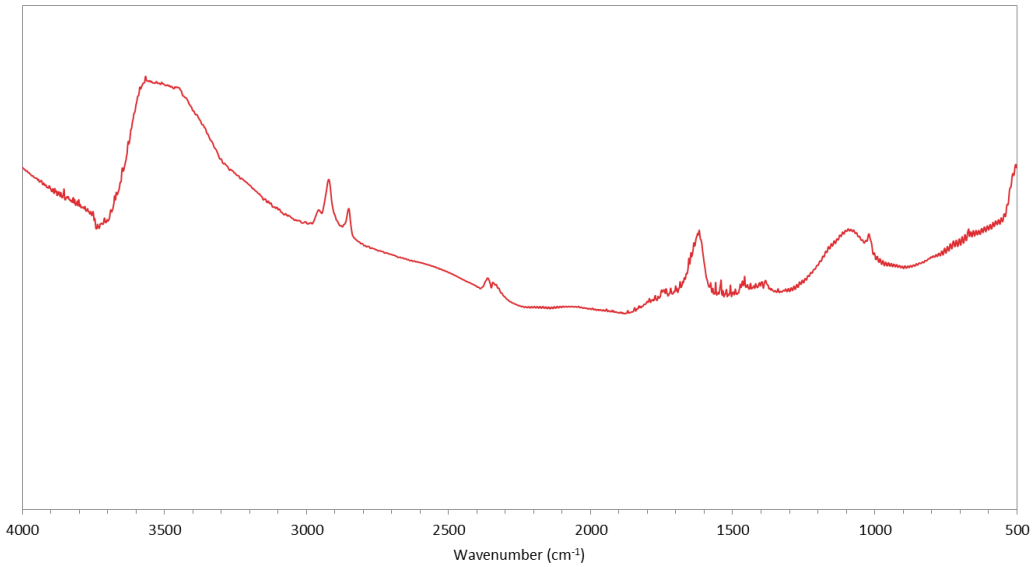

Figure 3. 24: IR hydrogel and NPs.

3.3.3.3 Qualitative characterization: SEM, AFM

A deep qualitative analysis of hydrogel structure can be done by SEM and AFM images, where its three-dimensional network is highlighted.

The following Figures 3.25, taken from SEM analysis, show hydrogel surface.

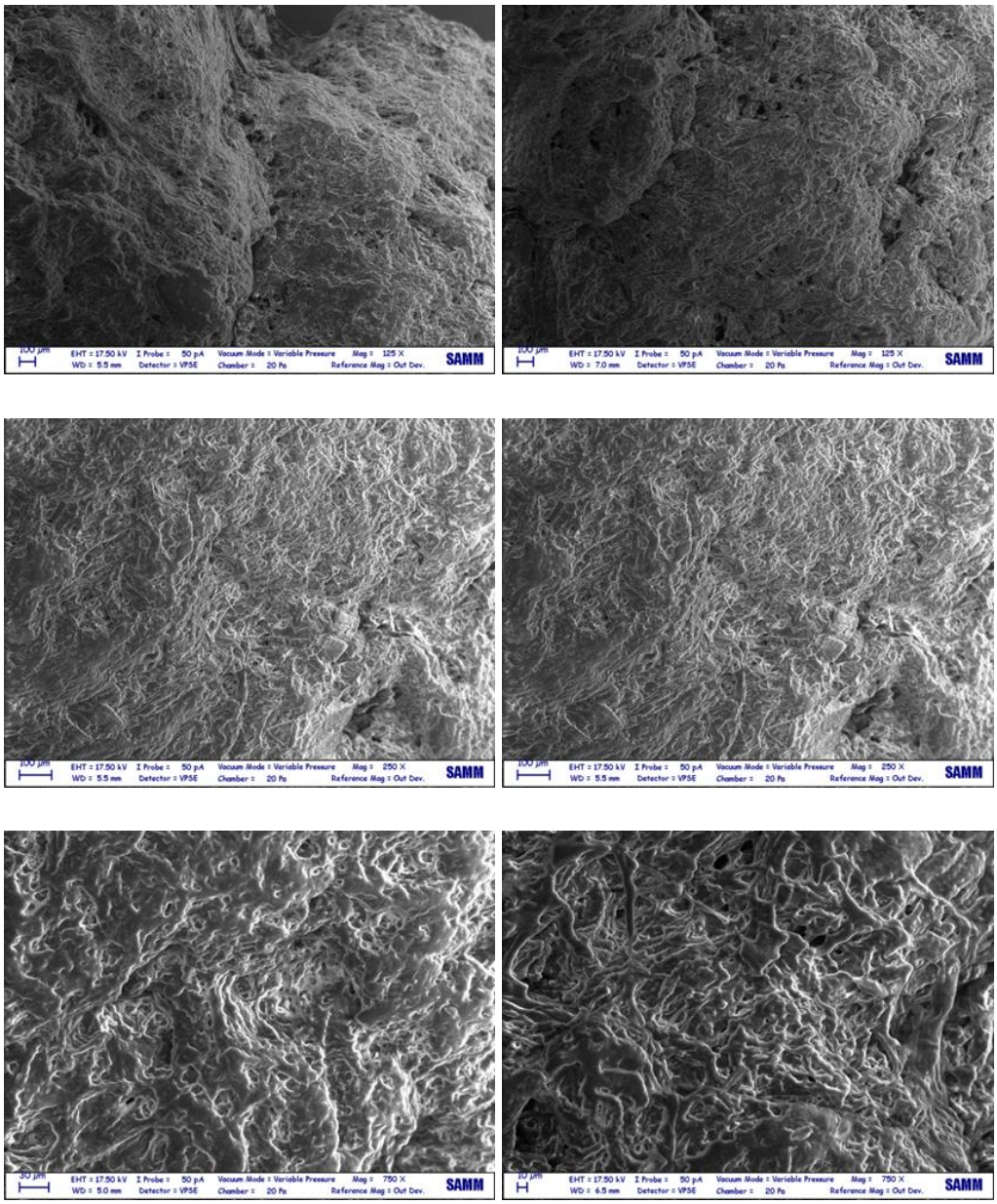

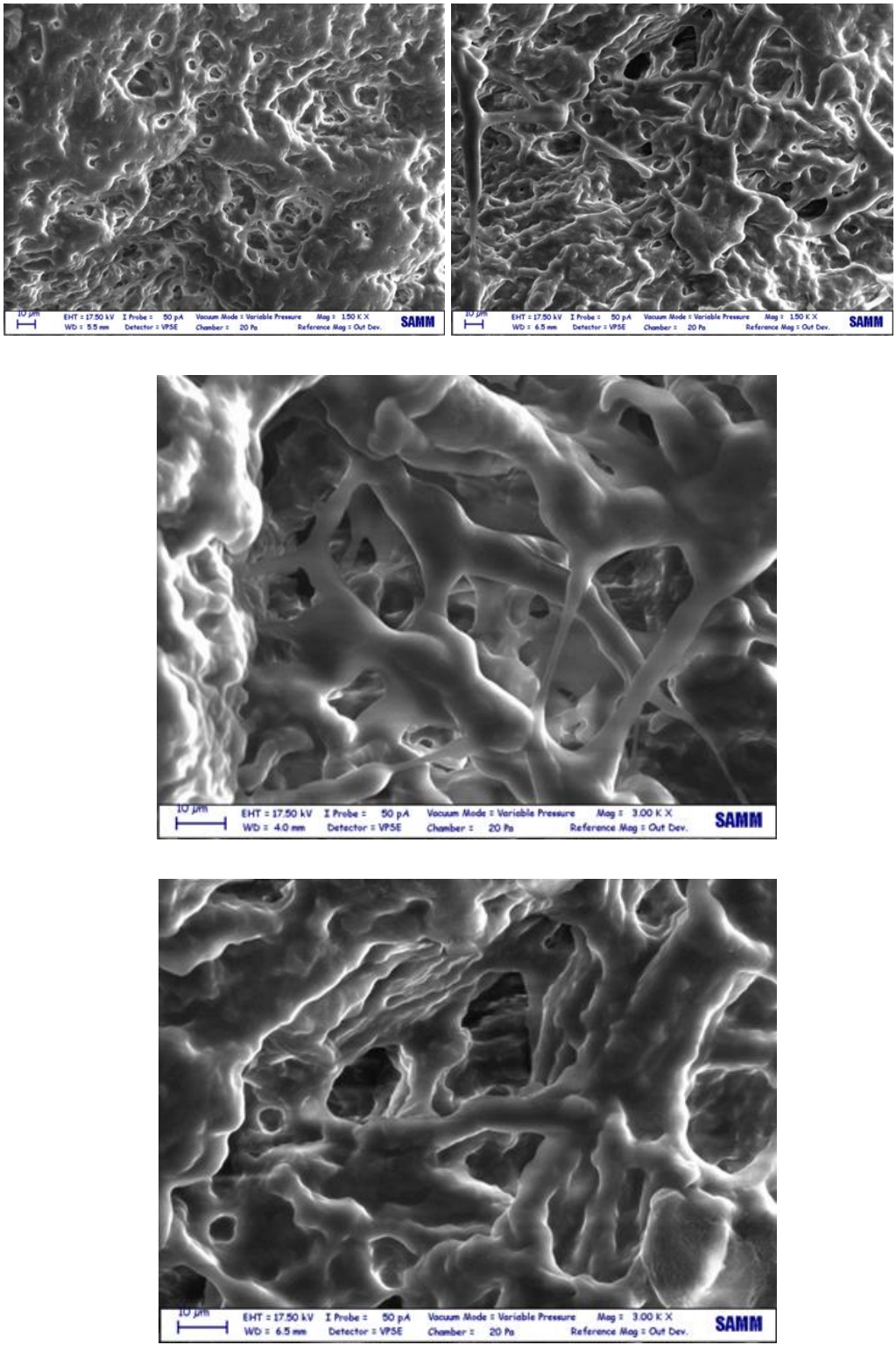

Figure 3. 25: SEM images of hydrogel structure with magnitude of 125 X, 250 X, 750 X, 1.50 K X, 3.00 K X.

Three-dimensional structure of the hydrogel is clear from the pictures above. Such reticulated structure allows hydrogels to provide support to the encapsulated cells, facilitating processes of adhesion, proliferation and migration [31]. Furthermore, the high porosity enables the matrix to retain large volumes of water and provides characteristics of hydration typical of hydrogels.

The internal view is shown in Figures 3.26.

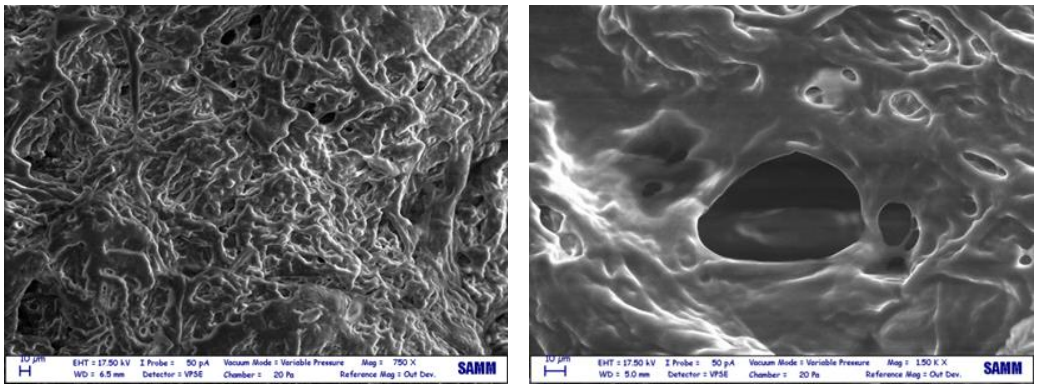

Figure 3. 26: SEM internal view at magnitude of: 250 X, 750 X, 1.50 K X.

From the internal point of view, the irregularity of canals size is stressed. Indeed, cavities dimensions can vary from about 50 μm to less than 10 μm.

Another qualitative perspective of hydrogel structure is given by AFM images (Figure 3.27).

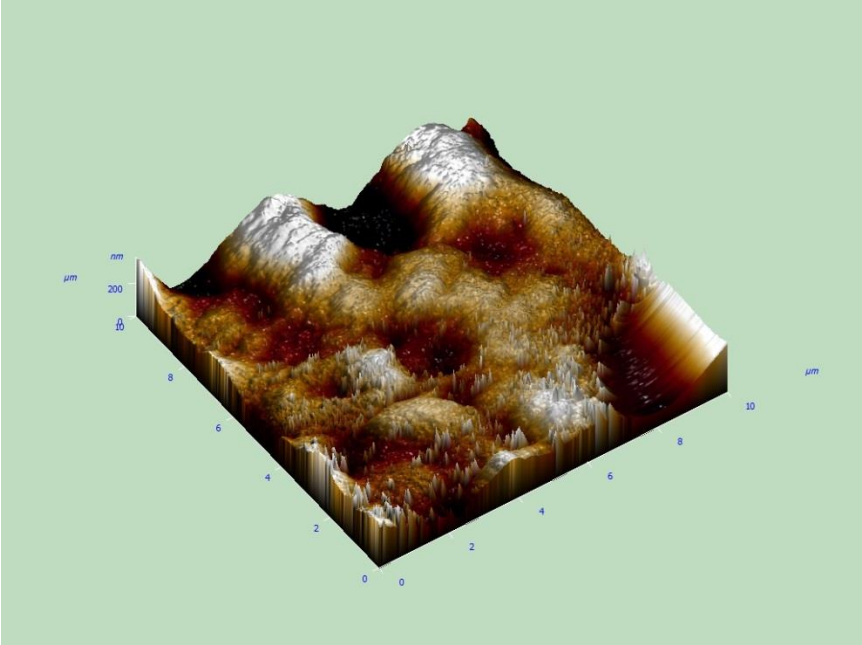

Figure 3. 27: Hydrogel by AFM.

The skeleton of hydrogel reticulum can be recognized in Figure 3.27 highlighted by white colour. Its mesh is large approximately 4 µm, so it represents a small cavity in the whole network. Small dots on the surface are superficial nanoparticles. An enlargement on the superficial nanoparticles can be observed in Figure 3.28.

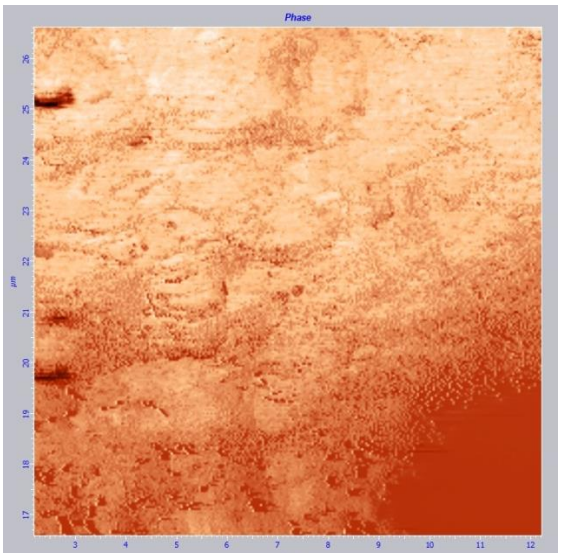

Figure 3. 28: AFM hydrogel surface.

3.3.3.4 Swelling test

In this section, swelling trends of HG2 are analyzed to compare the swelling capability between non-lyophilized and lyophilized hydrogels and the influence of water and PBS. The diagrams below summarize hydrogels swelling ratio at 1, 4, 8, 24 and 120 hours.

In Figure 3.29 swelling ratios of non-lyophilized and lyophilized hydrogels in water are compared. In Figure 3.30 the same comparison is depicted for hydrogel swollen in PBS. The swelling ratio (y-axis) is plotted for different time points (x-axis).

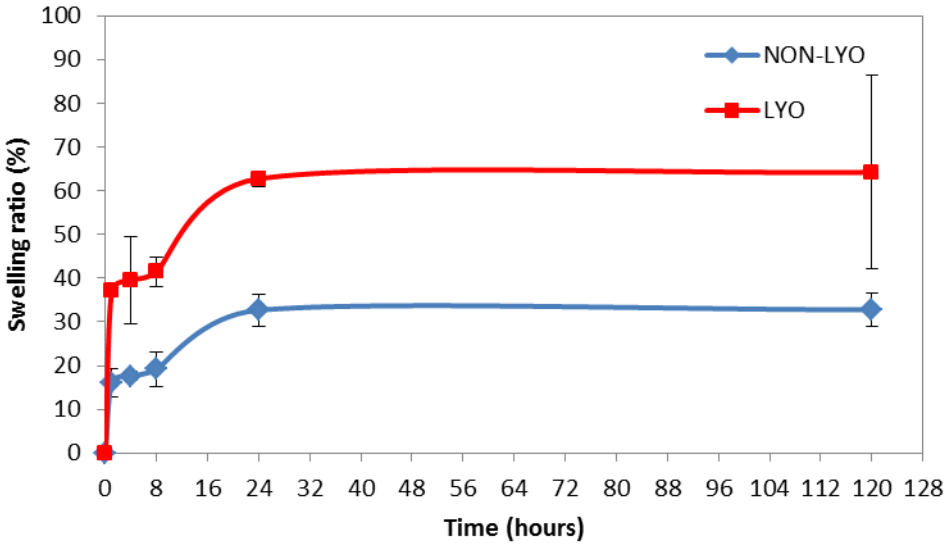

Figure 3. 29: Swelling ratio comparison between non-lyophilized (blue) and lyophilized (red) hydrogels in water. Error bars identify standard deviation.

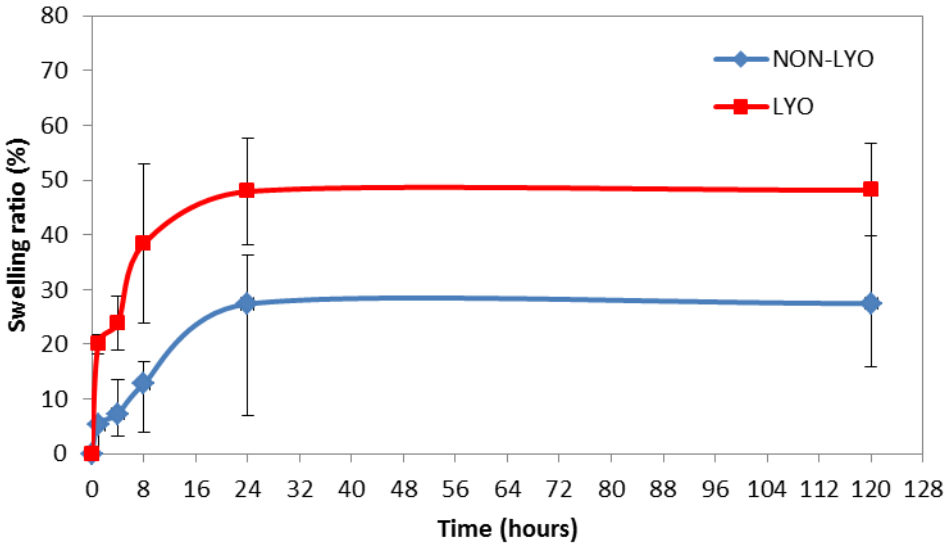

Figure 3. 30: Swelling ratio comparison between non-lyophilized (blue) and lyophilized (red) hydrogels in PBS 10x. Error bars identify standard deviation.

From both the diagrams is evident that a lyophilized hydrogel seems to swell more than a non-lyophilized one.

This trend is attributable to the fact that non-lyophilized hydrogels contain the water that has been entrapped during gelation process. For this reason the quantity of liquid they can absorb is smaller. Lyophilized hydrogels initial mass is a dry mass: the water content has been removed through freeze-drying.

It is clear that the swelling process is remarkable in the first 24 hours. Then the swelling ratio reaches a plateau and tends to an asymptotic value.

In Figure 3.31 and 3.32 the influence of water and PBS in the swelling process is depicted.

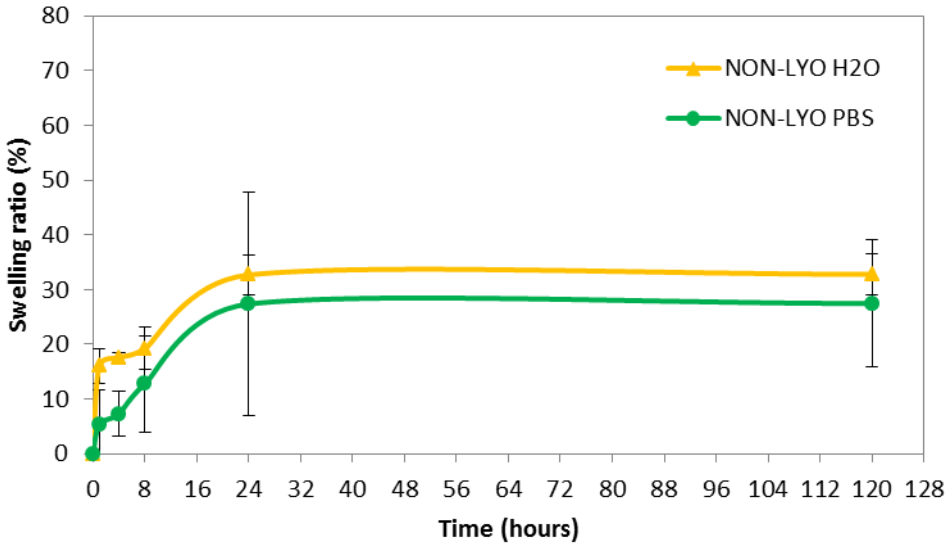

Figure 3. 31: Swelling ratio comparison of a non-lyophilized hydrogel in H_2O (yellow) or PBS (green). Error bars identify standard deviation.

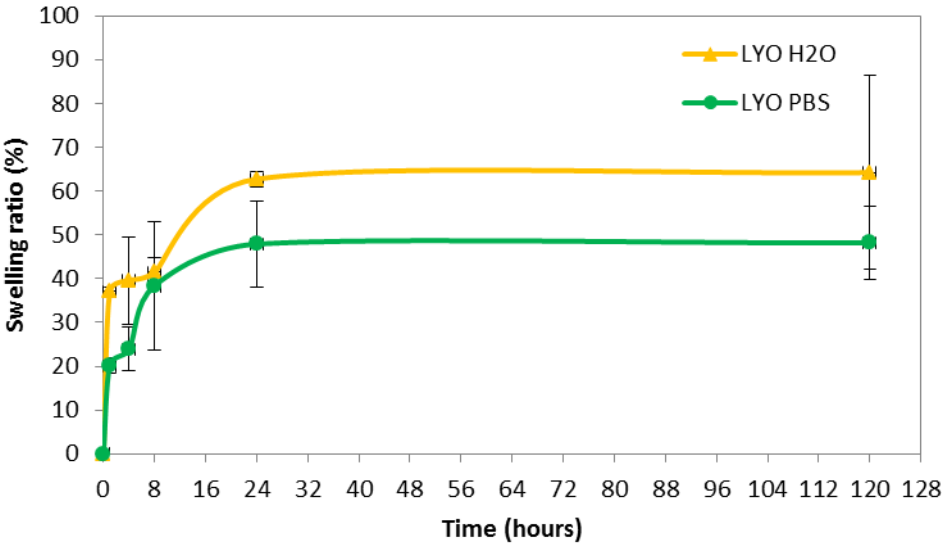

Figure 3. 32: Swelling ratio comparison of a lyophilized hydrogel in H_2O (yellow) or PBS (green). Error bars identify standard deviation.

The swelling ratio of hydrogels in PBS is smaller than in water. This can be explained by the ionic strength of PBS 10x (1.5 M) that is considerably higher than deionized water (~0 M). Due to the osmotic pressure, water tends to leave the hydrogel, decreasing final hydrogel weight and consequently the swelling ratio. In PBS the ionic strength competes with the absorption capability of hydrogels [32].

The high value of swelling ratios are an essential property of hydrogels to be applied in drug delivery or tissue engineering fields: swelling ability is fundamental in DDSs because they need to carry large amounts and a great variety of drugs and hydrophilic compounds, while, when applied in tissue engineering, this is a key property to transport nutrients for cells survival.

3.3.3.5 Degradation test

In vitro degradation tests measure the stability of hydrogels under physiological relevant conditions [32]. These tests were carried out for two sets of samples, one at 37°C and one at 50°C. For each set, three samples were prepared and everyone consisted of lyophilized hydrogels immersed in PBS solution as explained in paragraph 2.4.6.

For each time point (0, 1, 7, 14, 28, 56 days) the sample was lyophilized to remove entrapped water and weighed. Degradation ratio was calculated as the difference between the degraded mass (m_d) and the initial mass (m_i) divided by the initial mass, as reported in Equation 3.3.

$$q_{degradation} = \frac{m_d - m_i}{m_i}$$

Equation 3. 3: Degradation ratio.

Results of samples preserved at 37°C are reported in Figure 3.33, while those at 50°C in Figure 3.343 where degradation ratio trend (y-axis) is shown during time (x-axis).

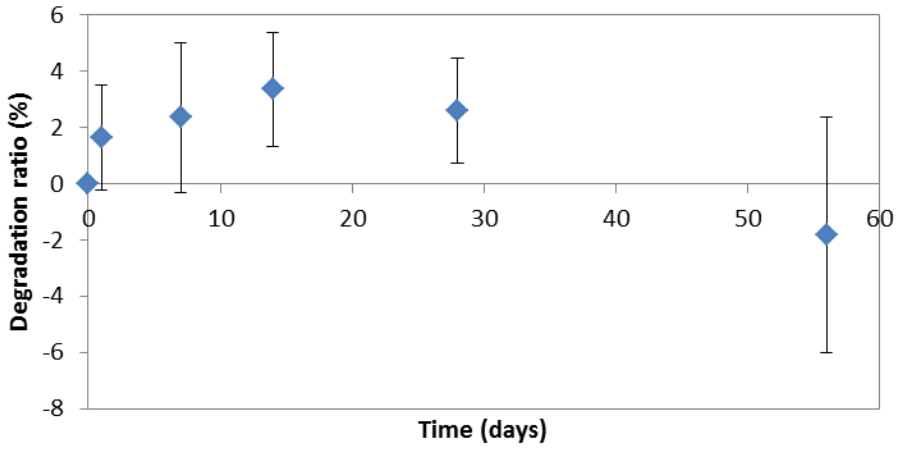

Figure 3. 33: Degradation ratio over time at 37°C. Error bars identify standard deviation.

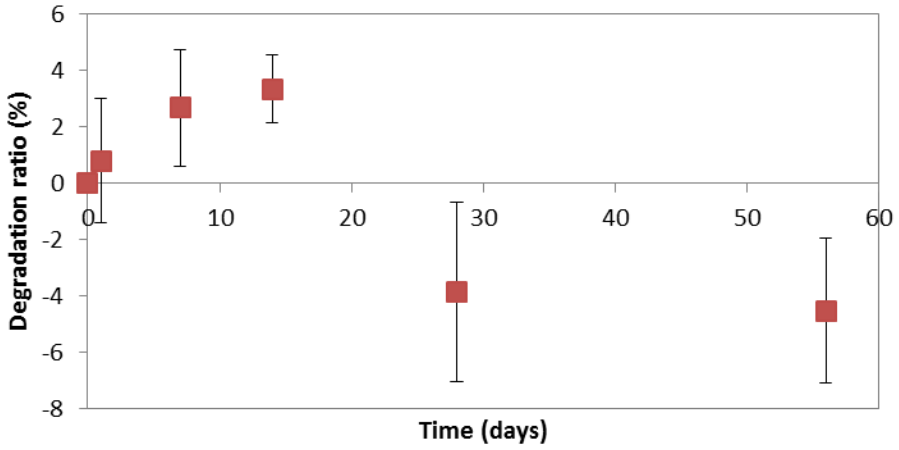

Figure 3. 34: Degradation ratio over time at 50°C. Error bars identify standard deviation.

Both degradation trends show an initial swelling behaviour. Indeed, their mass percentage grows in respect to the initial mass: PBS ionic solution enters the hydrogel network causing its enlargement and salts remain entrapped even after lyophilization. Therefore, it can be said that until the 14th day the hydrogel is stable and swelling behaviour was predominant.

Afterwards, a different trend was observed for the two temperatures. The samples at 37°C started to decrease their weight, but until 28 days they were still larger than the original mass. A real degradation could be seen only at 56 days, where a weight loss could be registered in respect to the initial mass.

For what concerns the samples at 50°C, degradation signs were shown before: at 28 days, the weight loss was registered. Degradation occurred before for the higher temperature.

The measures depicted above present large error bars. Indeed, mainly due the sticky nature of the lyophilized hydrogel samples and to the fact that the samples needed to be removed from the vial for each measure, weight measurement were likely affected by a considerable empirical error.

Biodegradability is a key-property of hydrogels for cell housing or drug delivery applications because they can be eliminated from the physiological system after the drug supply is depleted [33]. In this field, degradation time is an important parameter that should be tunable and settable. Indeed, it should proceed together with the generation of the new tissue or with the controlled release of the drug in the target area [34].

ε-caprolactone is commonly used as building block for synthetic hydrogels [31] for its hydrolytically degradation capability, and the obtained results confirmed the expectations. However, further studies must be done to define this material as biodegradable, in the sense that the degradation products must be confirmed non-toxic.

3.3.3.6 In vitro cytocompatibility test

The cytocompatibility of the hydrogel system was evaluated by treating murine fibroblast cells, as explained in paragraph 2.4.7. Cytotoxicity of hydrogels was evaluated by performing an MTS assay after 3 days of culturing and comparing the vitality of the samples with correspondent fibroblasts vitality.

The MTT assay is a well-known colorimetric assay for assessing cell viability.

Results are expressed in figure 3.35. The cross-section consisted of 24 samples.

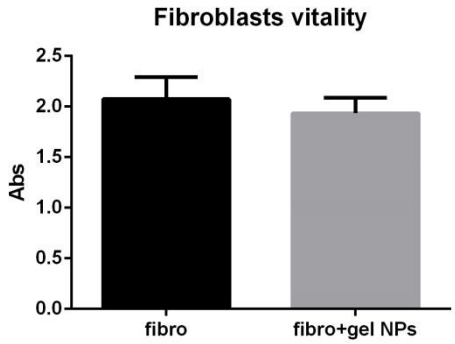

Figure 3. 35: Fibroblasts and fibroblasts+hydrogel vitality. Error bars identify standard deviation.

Almost the same value of hydrogel+fibroblasts vitality show a good hydrogel cyto-compatiblity.

Further tests will be done to load cells within the hydrogel network. During this thesis two different procedure have been applied: the first one consisted of loading by simple dripping cells suspension on the hydrogels previously lyophilized (Figure 3.36), the second one consisted of loading HEMA-SO_3--based NPs first, and the HEMA-Ch+-based ones were dripped to form the hydrogel.

Unfortunately, it was not possible to understand whether if cells were able to enter inside the hydrogel reticulum. Despite latex was only 5%-concentrated, it was still too opaque to be investigated in the inner part.

Figure 3. 36: Hydrogels loaded with cells.

Figure 3.37 shows spreading fibroblasts in cell culture plate.

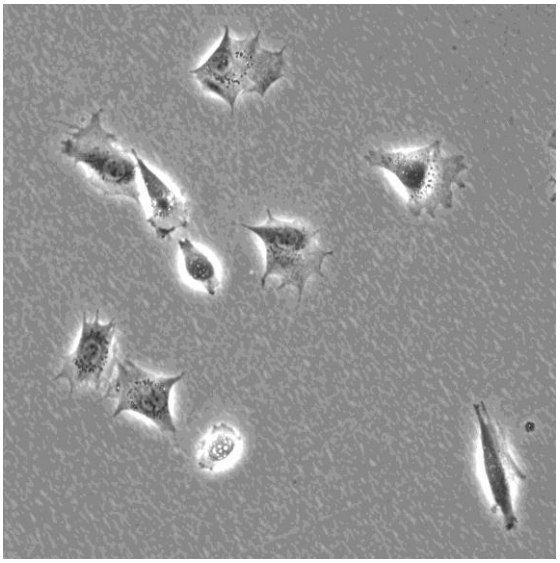

Figure 3. 37: Isolated fibroblasts.

3.3.3.7 In vitro drug delivery

To understand hydrogels ability to retain and release entrapped drugs, *in vitro* drug delivery tests have been made. Hydrogels delivery of Fluorescein and To-Pro3 has been investigated. Hydrogels, loaded with Fluorescein and To-Pro3 as explained in paragraph 2.4.4, have been immerged in 4 mL of PBS 10x and incubated at 37 °C (Figure 3.38). Small aliquots (100 µL) of supernatant were collected and replaced by fresh PBS at different time points: 1, 2, 4, 7, 14, 21 and 28 days. The amount of To-Pro3 and Fluorescein in the supernatant was fluorimetrically evaluated. The loading percentages were calculated as:

$$\%\ loading = \frac{drug\ entrapped}{initial\ amount\ loaded} * 100$$

Equation 3. 4: Dye loading percentage.

The loading percentages were 62.23% for Fluorescein and 83% for To-Pro3.

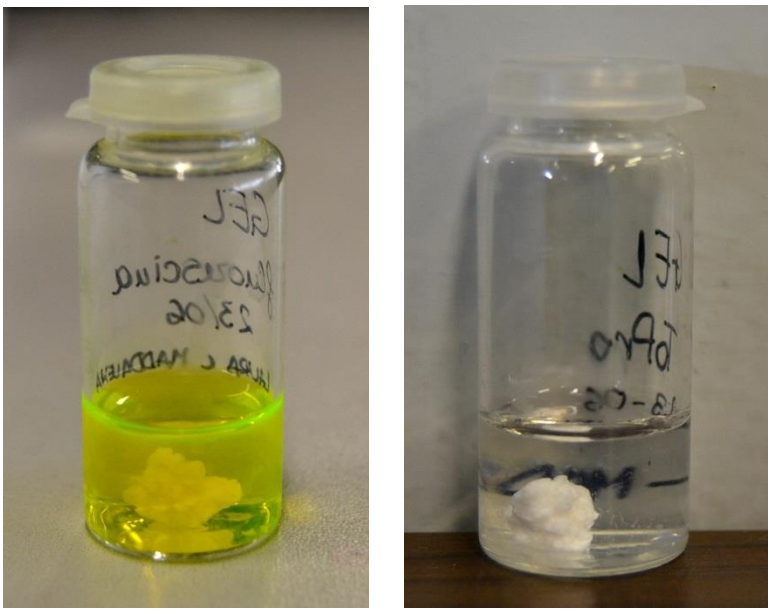

Figure 3. 38: Hydrogel loaded with Fluorescein (a) or To-Pro3 (b) immerged in 4 mL of PBS.

In Figure 3.39 Fluorescein release percentages (y-axis) are plotted as a function of time (x-axis). Fluorescein is a small hydrophilic molecule, so it can be easily loaded inside the hydrogel matrix.

The much bigger dimensions of hydrogel meshes lend high mobility to the dye molecules minimizing diffusive limitations. For this reason, the release trend presents a high slope and reaches a value of 100% after 2 days. The results obtained prove that Fluorescein molecules follow Fickian diffusion only after an initial high burst release, as it is evident from Figure 3.40 where percentages released are depicted as a function of square root time.

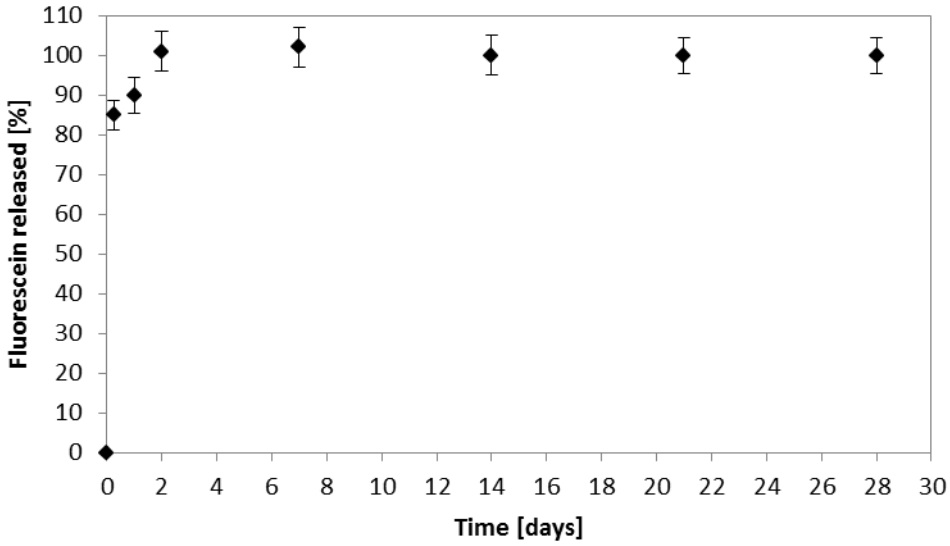

Figure 3. 39: In vitro Fluorescein release profile of the hydrogel. Error bars identify standard deviation.

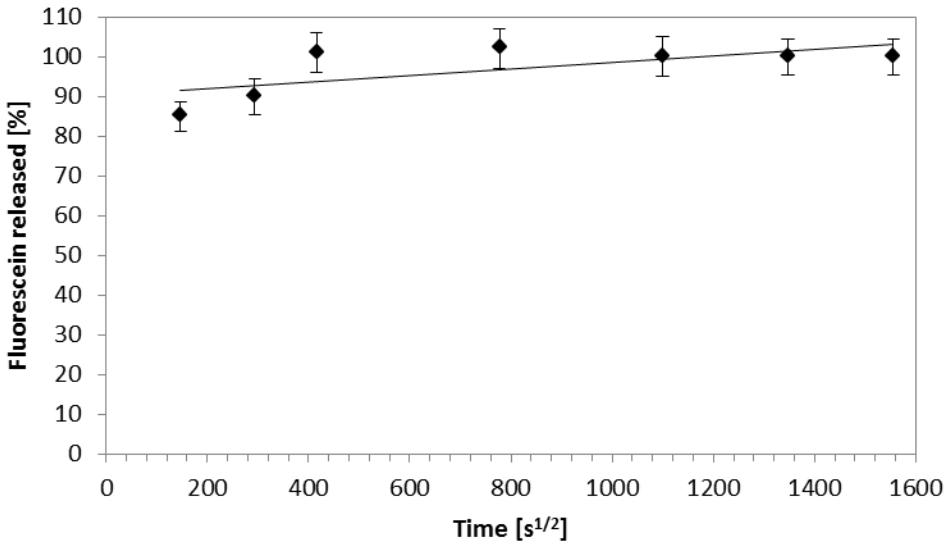

Figure 3. 40: In vitro Fluorescein release profile of the hydrogel against square root time. Error bars identify standard deviation.

In Figure 3.41 To-Pro3 release percentages (y-axis) are plotted as a function of time (x-axis). To-Pro3 is an hydrophobic molecule loaded onto the nanoparticles that form the hydrogel. In this work positive HEMA-PCL_3-based nanoparticles have been loaded with To-Pro3 and aggregate with non-loaded negative nanoparticles, as explained in paragraph 2.4.4. The percentage of To-Pro3 released after 6 h reaches a value of 30%: this initial burst can be attributed to unloaded dye and to the initial concentration gradient between nanoparticles and fresh PBS. Then, To-Pro3 release slowly increases, as a proof of Fickian diffusion release mechanism. From Figure 3.42 a linear relationship between percentage released and square root time is present, as a confirm of a To-Pro3 release regulated by Fickian diffusion.

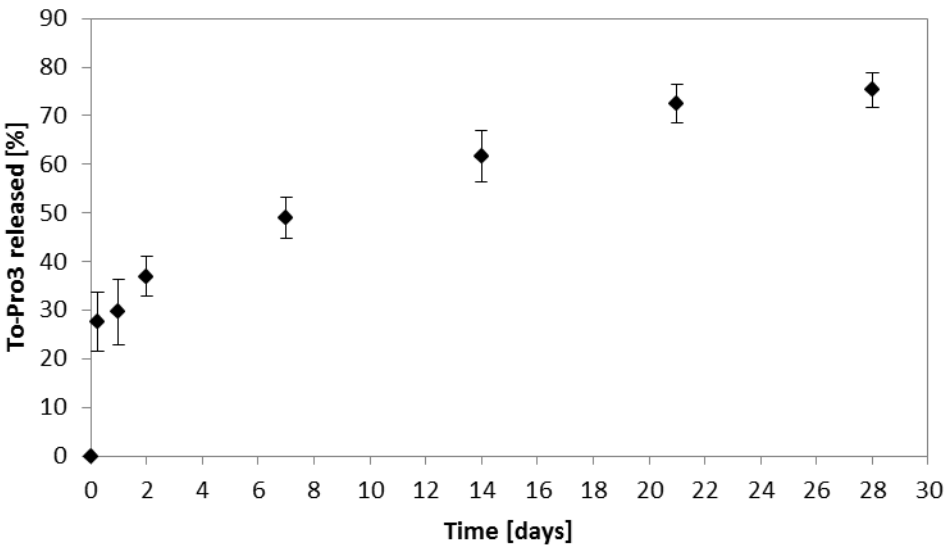

Figure 3. 41: In vitro To-Pro3 release profile of the hydrogel. Error bars identify standard deviation.

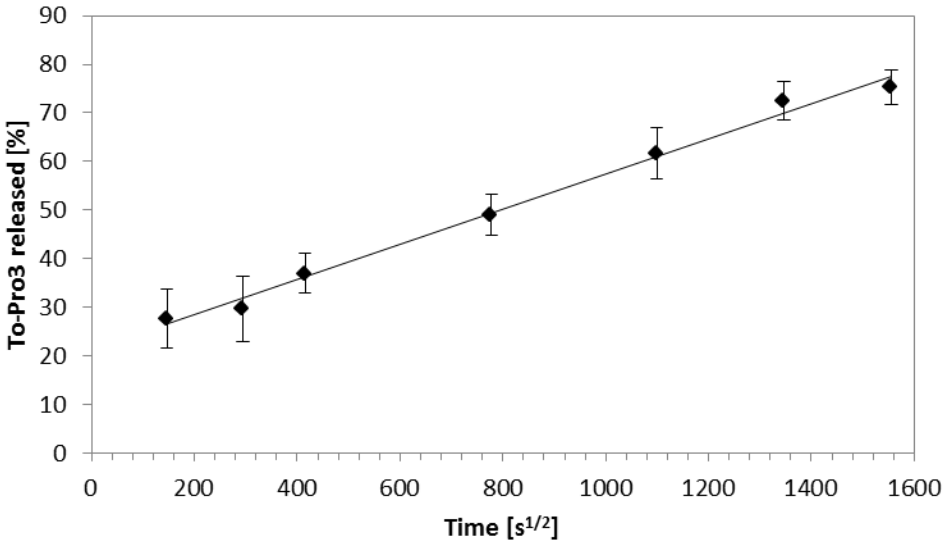

Figure 3. 42: In vitro To-Pro3 release profile of the hydrogel against square root time. Error bars identify standard deviation.

Literature data have been used to analyze To-Pro3 release from dispersed nanoparticles. Nanoparticles drug release percentages can be compared with the data obtained for hydrogels. In Figure 3.43 and 3.44 theTo-Pro3 released trend is depicted against time and square root time, respectively [35].

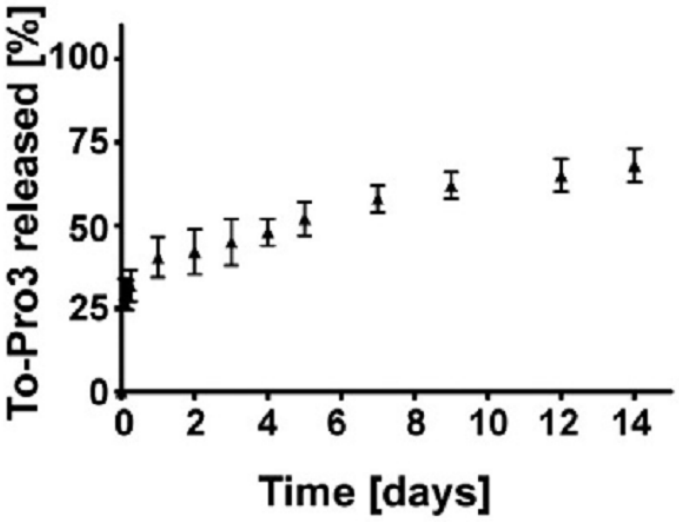

Figure 3. 43: *In vitro* To-Pro3 release profile of nanoparticles [35].

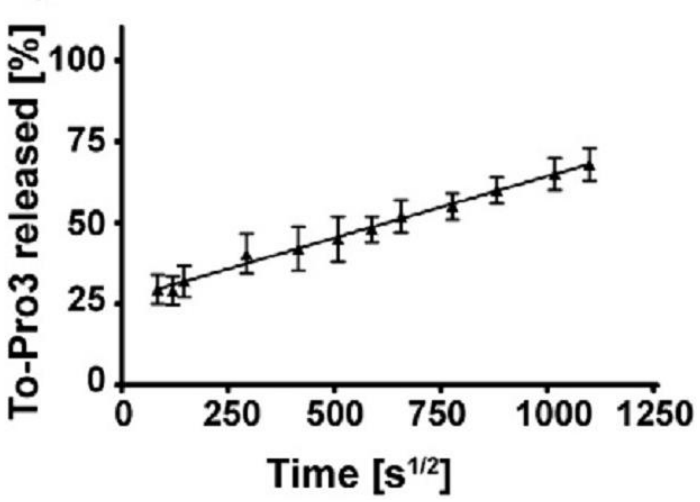

Figure 3. 44: ***In vitro*** **To-Pro3 release profile of nanoparticles versus square root time** [35].

Hydrogels release capability is comparable to the one of polymeric nanoparticles. Similar trends highlight that release mechanism is governed by nanoparticles and hydrogel matrix does not influence drug diffusion. Nanoparticles diffusion properties are preserved inside the macrostructure.

Moreover, the obtained results demonstrate the capability of hydrogels from nanoparticles aggregation to load and release both hydrophilic and lipophilic compounds. High release trends are obtained for both hydrophilic (Fluorescein) and hydrophobic (To-Pro3) dyes, as a confirm of the potentiality of these materials if implemented as DDSs. Furthermore, hydrophilic and lipophilic molecules can be loaded and released simultaneously.

Conclusions

The aim of this work was to synthesize a hydrogel from aggregation of polymeric nanoparticles of PMMA and HEMA-PCL_3 as suitable material for tissue engineering and drug delivery applications.

As regard to PMMA nanoparticles, only SDS-stabilized latex was able to form a gel structure through DLCA gelation technique, but due to the intrinsic cytotoxicity of SDS, this material did not satisfy the requirements necessary for the above-mentioned purposes.

Afterwards, the research switched to HEMA-PCL_3-based nanoparticles because of their biocompatible and biodegradable nature. Oppositely charged NPs were synthesized and then combined through electrostatic aggregation.

The best performing composition of the starting latexes was sought by analyzing the stability of the resulting hydrogels. On the one hand, positively charged NPs were composed of 3% of HEMA-Ch+ and 5% of MAA, on the other hand, negatively charged NPs' optimal composition consisted of 3% of HEMA-SO_3-, 5% of MAA and 10% of Tween 80.

With this composition it has been possible to create a three-dimensional network, evident from SEM and AFM images, without covalent cross-links, as visible from IR spectra. The so-composed hydrogel displayed good stability in PBS at room temperature, unlike all the other samples that degraded after few hours.

The selected hydrogel was then characterized in order to examine its performances and potential applications. Gelation process presented an average yield of 83.45%, which is a quite high value considering that the superficial charge density was unknown. Electrostatic aggregation seems to be a promising technique for such materials. Further studies can be focused on improving the reproducibility of this physical gelation method.

In respect to swelling capability, these materials showed a good swelling ratio trend, increasing their initial mass up to a maximum value of 64% if immersed in water and 48% in PBS.

These values are not so high for hydrogels standards, but still enough to load hydrophilic compounds dissolved in water.

This latter property, typical of hydrogels, can be combined with nanoparticles capability of loading and release hydrophobic drugs. The integrated macrostructure of hydrogel made from nanoparticles, indeed, showed good release trends for both hydrophilic (Fluorescein) and hydrophobic (To-Pro3) dyes leading to final released values respectively of 100% and 75%.

Another important issue is biodegradability: degradation tests revealed hydrogel weight loss before the 56^{th} day at 37°C and before the 28^{th} day at 50°C. The chosen time points could not give more detailed information on when and how degradation occurred. For further degradation studies, the choice of time points should rather be more representative.

Finally, cytocompatibility test was necessary to verify whether the hydrogel could be suitable as cell housing scaffold. Although the test revealed good cytocompatibility with fibroblasts, the successful entrapment of cells inside the hydrogel network could not be examined due to its opacity. Indeed, it was not possible to look into the inner structure. This latter difficulty prevented our hydrogel from potential applications in tissue engineering field.

In conclusion, hydrogels from HEMA-PCL_3 nanoparticles showed good properties as drug delivery systems, but the latexes composition should be optimized in order to investigate whether cells can be effectively entrapped inside the reticulum and find a suitable environment with whom they can dynamically and efficaciously interact.

References

[1] M. W. Tibbitt e K. S. Anseth, «Hydrogels as extracellular matrix mimics for 3D cell culture,» *Biotechnology and bioengineering,* vol. 103, n. 4, pp. 655-663, 2009.

[2] P. M. Kharkar, K. L. Kiick e A. M. Kloxin, «Designing degradable hydrogels for orthogonal control,» *Chemical society review,* vol. 42, n. 17, pp. 7335-7372, 2013.

[3] S. Peter, M. Miller, A. Yasko, M. Jaskemski e M. A.G., «Polymer concepts in tissue engineering,» *Journal of Biomedical Materials Research,* vol. 43, n. 4, pp. 422-427, 1998.

[4] U. N. f. O. Sharing, «UNOS donation data,» [Online]. Available: http://www.unos.org/donation/index.php?topic=data. [Consultato il giorno 5 september 2014].

[5] G. Perale, F. Rossi, M. Santoro, M. Peviani, S. Papa, D. Llupi, P. Torriani, E. Micotti, S. Previdi, L. Cervo, E. Sundström, M. Masi, P. Veglianese, A. Boccaccini e P. Forloni, «Multiple drug delivery hydrogel system for spinal cord injury repair strategies,» *Journal of controlled release,* vol. 59, pp. 271-280, 2012.

[6] D. Williams, «Benefit and risk in tissue engineering,» *Materials today,* pp. 24-29, 2004.

[7] R. Langer e J. Vacanti, «Tissue engineering,» *Science,* vol. 260, n. 5110, pp. 920-926, 1993.

[8] S. Kuci, Z. Kuci, H. Pupovci, D. Niethammer, R. Handgretinger, M. Schumm, G. Bruchelt, B. P e T. Klingebiel, «Adult Stem Cells as an Alternative Source of Multipotential (Pluripotential) Cells in Regenerative Medicine,» *Current Stem Cell Research & Therapy,* vol. 4, n. 2, pp. 107-117, 2009.

[9] M. V. Tibbitt e K. Anseth, «Hydrogels as extracellular matrix mimics for 3D cell culture,» *Biotechnology and Bioengineering,* vol. 4, n. 103, pp. 655-663, 2009.

[10] V. Tsang e S. Bhatia, «Three-dimensional tissue fabrication,» *Advanced Drug Delivery Reviews,* vol. 56, p. 1635 – 1647, 2004.

[11] S. I. Shen, B. R. Jasti e X. Li, Standard handbook of biomedical engineering and design, The McGraw-Hill Companies, 2003.

[12] A. Vashist e S. Ahmad, «Hydrogels: smart materials for drug delivery,» *Oriental Journal of Chemistry,* vol. 29, n. 3, 2013.

[13] C. Di Bello, Biomateriali. Introduzione allo studio dei materiali per uso biomedico., Pàtron Editore, 2004.

[14] M. Hamidi, A. Azedi e P. Rafiei, «Hydrogel nanoparticles in drug delivery,» *Advanced Drug Delivery Reviews,* pp. 1638-1649, 2008.

[15] T. R. Hoarea e D. S. Kohaneb, «Hydrogels in drug delivery: Progress and challenges,» *Polymer,* vol. 49, p. 1993–2007, 2008.

[16] W. H. De Jong e P. J. Borm, «Drug delivery and nanoparticles: Applications and hazards,» *International Journal of Nanomedicine,* pp. 133-149, 2008.

[17] L. Xu, W. Ma, L. Wang, C. Xu, H. Kuang e N. A. Kotov, «Nanoparticle assemblies: dimensional transformation of nanomaterials and scalability.,» *Chem. Soc. Rev.,* vol. 42, pp. 3114-3126, 2013.

[18] C. Murray, C. Kagan e M. Bawendi, «Selforganization of CdSe nanocrystallytes into three-dimensional quantum-dot superlattices.,» *Science 270,* pp. 1335-1338, 1995.

[19] M. S. Wong, J. N. Cha, K. S. Choi, T. J. Deming e G. D. Stucky, «Assembly of nanoparticles into hollow spheres using block copolypeptides.,» *Nano Letters 2,* pp. 583-587, 2002.

[20] R. Shenhar, T. Norsten e V. Rotello, «Polymer-mediated nanoparticle assembly: structural control and applications,» *Adv.Mater.,* vol. 17, n. 6, 2005.

[21] B. Jia, W. Zhang, N. Yuan, J. Ding, Y. Ren e F. Chu, «A new oil/water interfacial assembly of sulphonated graphene into ultrathin films.,» *RSC Adv.,* vol. 4, pp. 34566-34571, 2014.

[22] N. Kotov, «Practical aspects of self-organization of nanoparticles: experimental guide and future applications,» *Journal of Materials Chemistry,* vol. 21, pp. 16673-16674, 2011.

[23] S. W. Morton, Z. Poon e P. Hammond, «The architecture and biological performance of drug-loaded LbL nanoparticles.,» *Biomaterials,* vol. 34, pp. 5328-5335, 2013.

[24] M. Y. Lin, H. Lindsay, D. Weitz, R. Ball, R. Klein e P. Meakin, «Universality in colloid aggragation,» *Nature,* vol. 339, pp. 360-362, 1989.

[25] H. Wu e M. Morbidelli, «Gelation of polymeric nanoparticles,» *Particuology,* vol. 14, pp. 1-11, 2014.

[26] H. Wyss, J. Innerlohinger, L. Meier, L. Gauckler e O. Glatter, «Small-angle static light scattering of concentrated silica suspensions during in situ destabilization,» *Journal of Colloid and Interface Science,* vol. 271, pp. 388-399, 2004.

[27] M. Lattuada, H. Wu e M. Morbidelli, «Experimental investigation of colloidal gel structures,» *Langmuir,* vol. 20, pp. 4355-4362, 2004.

[28] F. Ferrari, Y. Yu e M. Morbidelli, «epsilon-caprolactone-based macromonomers suitable for biodegradable nanoparticles synthesis through free radical polymerization,» *Macromolecules,* vol. 44, pp. 9205-9212, 2011.

[29] F. Rocci e M. Bascialla, *Sintesi di aggregati porosi di nanoparticelle polimeriche per cell housing,* 2010-2011.

[30] «1 Final Report on the Safety Assessment of Polysorbates 20, 21, 40, 60, 61, 65, 80, 81, and 85,» *International Journal of Toxicology,* vol. 3, pp. 1-82, 1984.

[31] H. Geckil, «Engineering hydrogels as extracellular matrix mimics.,» *Nanomedicine,* vol. 5, pp. 469-484, 2010.

[32] Q. Xing, K. Yates, C. Vogt, Z. Qian, M. C. Frost e F. Zhao, «Increasing mechanical strenght og gelation hydrogels by divalent metal ion removal,» *Scientific Reports,* 2014.

[33] K. Pal, A. Banthia e D. Majumdar, «Polymeric hydrogels: Characterization and Biomedical Applications- A mini review,» *Designed monomers and polymers,* vol. 12, pp. 197-220, 2009.

[34] E. Carletti, A. Motta e C. Migliaresi, «Scaffolds for tissue engineering and 3D cell,» *Methods in molecular biology,* vol. 695, pp. 17-39, 2011.

[35] S. Papa, R. Ferrari, M. De Paola, F. Rossi, A. Mariani, I. Caron, E. Sammali, M. Peviani, V. Dell'Oro, C. M. M. Colombo, G. Forloni, G. Perale, D. Moscatelli e P. Veglianese, «Polymeric nanoparticle system to target activated microglia/marophages in spinal cord injury,» *Journal of controlled release,* vol. 174, pp. 15-26, 2014.